

Winter 2009

Fabrication and tribology of composite coatings incorporating solid lubricant micro-reservoirs

Canan Gamze Guleryuz
University of New Hampshire, Durham

Follow this and additional works at: <https://scholars.unh.edu/dissertation>

Recommended Citation

Guleryuz, Canan Gamze, "Fabrication and tribology of composite coatings incorporating solid lubricant micro-reservoirs" (2009).
Doctoral Dissertations. 512.
<https://scholars.unh.edu/dissertation/512>

This Dissertation is brought to you for free and open access by the Student Scholarship at University of New Hampshire Scholars' Repository. It has been accepted for inclusion in Doctoral Dissertations by an authorized administrator of University of New Hampshire Scholars' Repository. For more information, please contact nicole.hentz@unh.edu.

**FABRICATION and TRIBOLOGY of COMPOSITE COATINGS
INCORPORATING SOLID LUBRICANT MICRO-RESERVOIRS**

by

CANAN GAMZE GULERYUZ

B.Sc., Istanbul Technical University, 1997

M.Sc., Istanbul Technical University, 2001

DISSERTATION

Submitted to the University of New Hampshire

in Partial Fulfillment of

the Requirements for the Degree of

Doctor of Philosophy

in

Mechanical Engineering

December 2009

UMI Number: 3400338

All rights reserved

INFORMATION TO ALL USERS

The quality of this reproduction is dependent upon the quality of the copy submitted.

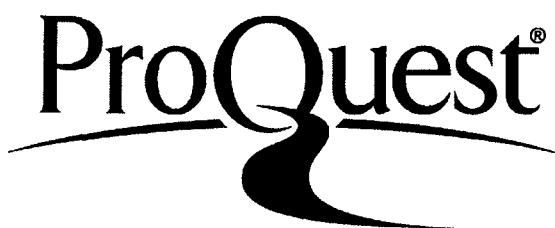
In the unlikely event that the author did not send a complete manuscript and there are missing pages, these will be noted. Also, if material had to be removed, a note will indicate the deletion.



UMI 3400338


Copyright 2010 by ProQuest LLC.

All rights reserved. This edition of the work is protected against unauthorized copying under Title 17, United States Code.

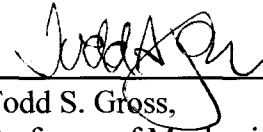


ProQuest LLC
789 East Eisenhower Parkway
P.O. Box 1346
Ann Arbor, MI 48106-1346

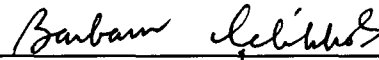
This dissertation has been examined and approved.



Dissertation Director, James E. Krzanowski,
Professor of Mechanical Engineering



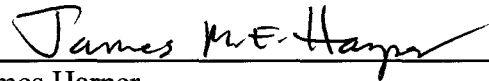
Todd S. Gross,
Professor of Mechanical Engineering



Barbaros Celikkol,
Professor of Mechanical Engineering



Barry Fussell,
Professor of Mechanical Engineering



James Harper,
Professor of Physics

1/04/2010
Date

DEDICATION

This thesis is dedicated to my parents, Sema and Veysel Guleryuz, who dedicated their lives to me and to my brother, Can Halit Guleryuz. This thesis is also dedicated to my husband, Sunal Ahmet Parasiz, who supported me through my study.

ACKNOWLEDGEMENT

I gratefully acknowledge my advisor, Prof. James E. Krzanowski, for his guidance through my study and his setting a very good example of a scientist and an academician. He was always there with me during my experiments and writings. He shared his endless practical and scientific knowledge on thin film science, technology and tribology.

I would like to thank to our collaborators at McMaster University in Canada, Prof. German Fox-Rabinovich and Prof. Stephen Veldhuis for conducting machining experiments.

I would like to thank Prof. Igor Tsukrov for both his guidance on finite element study and his support as a Graduate Advisor.

Prof. Todd Gross is also gratefully acknowledged for his kind support as Mechanical Engineering Department Chair.

I would like to thank Prof. Barbaros Celikkol for encouraging me to apply for Ph.D. study at University of New Hampshire.

Dean Prof. Taner Derbentli and all other faculty at Mechanical Engineering Department in Istanbul Technical University are gratefully acknowledged for their support through my Ph.D. study.

I would like to thank my colleague at Mechanical Engineering Department, Andrew Drach, for his technical support and prompt help through my finite element study. I also would like to thank to my colleagues at the laboratory, Dyumani Nunna, John H. Zimmerman, Margaret Nowicki and Dale Delisle for their help and sharing.

Samuel Lightner and Raphael Low-Weiner are also acknowledged for their help in coating depositions.

Finally, research funding provided by National Science Foundation-Division of Manufacturing Industrial Innovation Grant #0423329 is gratefully acknowledged.

TABLE OF CONTENTS

DEDICATION.....	iii
ACKNOWLEDGEMENTS	iv
LIST OF TABLES.....	ix
LIST OF FIGURES.....	xi
ABSTRACT.....	xviii

CHAPTER	PAGE
I. INTRODUCTION AND LITERATURE REVIEW.....	1
II. EXPERIMENTAL METHODOLOGY.....	24
II.1. Microbeading Technique.....	24
II.2. The Coating Depositions.....	30
II.3. The Friction-Wear Tests.....	33
II.4. Microscopic Inspections.....	35
II.5. Machining Tests.....	36
II.6. Machining Simulation Tests.....	38
II.7. X-Ray Photoelectron Spectroscopy (XPS).....	39
II.8. Other Techniques.....	40
III. FABRICATION OF THE TRIBOLOGICAL COATINGS WITH EMBEDDED SOLID LUBRICANTS BY MICROBEADING METHOD.....	41
III.1. The Micro-beading Method and Agglomeration Effects.....	41
III.2. Results and Discussion.....	44
III.2.1. The Results for Specimens without Reservoirs.....	44
III. 2.2. Results for the Tests with Graphite Lubrication and Various Reservoir Sizes.....	46
III.2.2.1. Area Coverage Increase Study on 10 μ m Reservoirs....	48
III.2.3. Results for the Specimens with Sputter-deposited Carbon.....	49

III.2.4. Results for the Pin-on-Disk Tests with Aluminum Ball.....	50
III.2.5. Examination of the Wear Tracks.....	53
III.3. Discussion.....	55
III.4. Finite Element Model for Surface Interaction between Composite coating and a Pin.....	60
III.4.1. Geometry of the Model Coatings with Reservoirs.....	62
III.4.2. Modeling of the Contact between Coating and the Counterface-Ball.....	65
III.4.3. Material Properties Selected for Modeling.....	65
III.4.4. Boundary Conditions, Surface Interaction, Evaluations.....	66
III.4.5. Results and Discussion.....	67
III.5. Conclusions.....	72
IV. INVESTIGATIONS ON PATTERNED SILICON SAMPLES.....	75
IV.1. Experimental Method.....	75
IV.1.1. Preliminary Samples.....	76
IV.1.2. Tests on Additional Patterned Specimens.....	77
IV.2. Results and Discussion.....	82
IV.2.1. Preliminary Tests on Previously Fabricated Patterned Si Samples.....	82
IV.2.2. Results for Additional Fabricated Patterned Si Samples (Second Batch).....	84
IV.2.2.1. Pin-on-disk Tests against Alumina Ball (First Group).....	84
IV.2.2.1.1. Evaluation of the First Group Friction-Wear Tracks by Optical Microscopy.....	90
IV.2.2.2. Pin-on-disk Tests against Alumina Ball for the Second Group (Lower Speed and Weight) and Optical Microscopic Evaluations of the Wear Tracks.....	94
IV.2.2.3. Pin-on-disk tests against Steel ball.....	100
IV.3. Discussion.....	103
IV.4. Conclusion.....	104
V. MACHINING PERFORMANCE OF TIN COATINGS INCORPORATING INDIUM AS A SOLID LUBRICANT.....	105

V.1. Experimental.....	105
V.2. Results and Discussion.....	108
V.2.1.Pin-on-disk friction tests.....	108
V.2.2.Turning Tests.....	109
V.2.3.Tribological Simulation of the Machining Operation.....	114
V.2.4. XPS Analyses on Tool Inserts.....	115
V.3. Conclusion.....	119
VI. CONCLUSION.....	120
VII. FUTURE WORK.....	123
REFERENCES.....	125

LIST OF TABLES

Table 2.1. Samples and Deposition Conditions used in the scope of this thesis.....	33
Table 3.1. Finite element models and their area densities.....	61
Table 3.2. Geometrical parameters defining holes designed in the model coatings.....	64
Table 3.3. Applied material properties in modeling.....	66
Table 4.1. Properties of the patterned samples.....	76
Table 4.2. Cleaning procedure [44].....	80
Table 5.1. Cutting insert samples tested at turning operation.....	107

LIST OF FIGURES

Figure 1.1. Various approaches for achieving tribological composite coatings [reproduced after 8 and 13].....	3
Figure 1.2. Friction test results under vacuum conditions against steel ball: (a) WC-Ag films, (b) TiC-Ag films [14].....	4
Figure 1.3. Scanning electron micrograph of the TiC-Ag film with 51% Ag content (a) after 10,000 cycles, (b) after 33,000 cycles [14].....	5
Figure 1.4. Friction results for TiC-Ag composite films with various silver contents [15].....	5
Figure 1.5. SEM pictures that shows A: dispersed Ag phases in hard coating and B: smeared Ag on hard coating in pin-on-disk test [15].....	6
Figure 1.6. (a)-(c): Steps of surface texturing and the appearance of the specimen surface after each step given on the right. (d) Ball-on-disk test and the wear track after 1,600,000 cycles with 1 GPa contact pressure [7].....	7
Figure 1.7. Ball-on-disk test friction results performed against 440C steel at 50% RH environment: (a) only MoS ₂ layer on steel substrate, (b) Ti-TiC-TiC/DLC coating on steel substrate, (c) MoS ₂ coating on Ti-TiC-TiC/DLC coating, (d) MoS ₂ coating on 3-D Ti-TiC-TiC/DLC coating (with grooves) [7].....	9
Figure 1.8. Ball-on-disk test results representing environmental adaptation of MoS ₂ coating on 3D structured Ti-TiC-TiC/DLC coating. Lower graph shows the humidity level change [7].....	10
Figure 1.9. Example pictures of laser drilled 20 μm sized holes in TiCN hard coatings: (a) 1% area coverage, (b) 8% area coverage [17].....	11
Figure 1.10. Inverted, upside-down profile of a laser drilled reservoir. z-axis scale is different from x-and y-axes [17].....	11
Figure 1.11. Wear cycles before failure occurs for 10 and 20 μm reservoirs filled with MoS ₂ : (a) Wear life versus relative area coverage of the lubricant, (b) Wear life versus spacing between reservoirs (or dimples) [17].....	12
Figure 1.12. Wear life results given against various dimple densities achieved on steel surface [18].....	13
Figure 1.13. Appearance of the surface dimples on the surface with (a) 10% area coverage, (b) 42% area coverage [18].....	13
Figure 1.14. Schematic profile of laser drilled reservoirs [modified after 18 to emphasize the appearance the bulges circling reservoirs].....	14
Figure 1.15. Rectangular reservoirs created by reactive ion etching [19].....	14
Figure 1.16. Pin-on-disk friction-wear tests performed with MoS ₂ as a solid lubricant (SL) under dry air [19].....	15

Figure 1.17. Steps of photolithography and coating processes to obtain a hard coating containing reservoirs [13].....	16
Figure 1.18. SEM picture of pattern prepared on silicon samples by photolithography [20].....	16
Figure 1.19. SEM images of the patterned silicon samples after Cr-coated by magnetron sputtering process, on the left before cleaning of the mask, on the right after some cleaning process applied [20].....	17
Figure 1.20. Scanning electron micrograph of TiC-MoS ₂ composite coating: (a) View after cleaning of mask a few remaining), before MoS ₂ coating. (b) View after MoS ₂ coating. (c) Appearance of a wear track after pin-on-disk test. (d) Closer view of the wear track showing MoS ₂ filled reservoirs.....	17
Figure 1.21. Detailed picture of a laser drilled 10 μm sized reservoir [18].....	19
Figure 1.22. Profile of laser processed steel surface with area coverage of 26% [19].....	19
Figure 1.23. Mutual solubility of metals based on the binary phase diagrams, I is good mutual solubility, IV is low mutual solubility [24].....	22
Figure 2.1. Schematic view of the bead spraying technique with an optical picture of 10 μm sized beads on the specimen surface.....	25
Figure 2.2. Schematic view of the magnetron sputtering process on the micro-particles-sprayed surface. Micro-sphere size used for this sample is 1.5 μm.....	26
Figure 2.3. Schematic view of the micro-particle cleaning process.....	27
Figure 2.4. SE micrograph of reservoirs with 5 μm diameter on the coating surface.....	27
Figure 2.5. Scanning electron micrographs of reservoirs with 10 μm diameters on coating surface.....	27
Figure 2.6. Appearance of the sprayed graphite flakes on the specimen surface.....	28
Figure 2.7. Filled reservoirs (with graphite) after sprayed graphite particles forced into the reservoirs (on the left) and graphite sprayed steel sample with wear tracks (on the right).....	29
Figure 2.8. Schematic explanation of the “ <i>Dipping Technique</i> ”.....	30
Figure 2.9. Magnetron sputtering system.....	31
Figure 2.10. Magnetron sputtering chamber with front and side views during deposition.....	32
Figure 2.11. Substrate holder of the magnetron sputtering system with two of the 440C stainless steel and a silicon sample after TiN coating.....	33
Figure 2.12. Schematic view of the pin-on-disk friction-wear tester.....	34
Figure 2.13. Friction-wear testing chamber.....	35
Figure 2.14. Schematic view of the turning insert while machining, on the left; a SE micrograph example of a worn tool insert from this project, on the right.....	37

Figure 2.15. (a) Sample flank wear graph showing important stages of the tool wear from Ref.[32], (b) schematic representation of the flank wear on a tool from Ref. [33].....	37
Figure 2.16. Schematic view of the equipment used to simulate adhesive conditions at machining (1: Workpiece material, 2: Sample made of tool material, 3: driving rope, 4: driving disc, 5: electrical contact wires, 6: isolation system (Ref. [34,35])).....	39
Figure 3.1. SEM pictures showing the agglomeration on a 1.5 μm sized particles sprayed sample (after TiN coating).....	42
Figure 3.2. Optical micrographs showing agglomeration for a: 1.5 μm beads-, b: 5 μm beads-, c: 10 μm beads-sprayed sample. Pictures were taken after beads removed from coating.....	43
Figure 3.3. Reference pin-on-disk tests performed on the plain stainless steel substrate, TiN coating without any reservoirs or lubricant, and with graphite lubrication.....	45
Figure 3.4. Optical micrograph of the wear track after the test on TiN with graphite lubrication. Coating failures can behave as reservoirs that store and replenish graphite.....	45
Figure 3.5. Pin-on-disk results for various sizes of the reservoirs: highest curve belongs to dry test (no graphite) others are all with the graphite application.....	46
Figure 3.6. Optical image of the wear tracks after POD test on coatings with (a) 1.5 μm , (b) 5 μm , (c) 10 μm reservoirs. In (a) there are still filled holes despite the damages, in (b) filled holes (A) in the track and the empty holes (B) at the edge of the track are marked.....	47
Figure 3.7. POD friction-wear test results for two 10 μm samples having two different area coverage and agglomeration levels (The unmarked dry test belongs to sample that has lower area coverage with less agglomeration).....	49
Figure 3.8. Pin-on-disk test results of a sample with 10 μm reservoirs with and without carbon coating.....	50
Figure 3.9. Pin-on-disk test results on a sample with no reservoirs (dry or lubricated with 2% graphite) and 10 μm reservoir sample with 2% graphite lubrication.....	51
Figure 3.10. Pin-on-disk experiment results on no reservoir in dry and lubricated with carbon sputtering and 10 μm reservoirs coating with lubrication with carbon sputtering.....	51
Figure 3.11. Detail of first 500 cycles of POD experiment results on no reservoir in dry and lubricated with carbon sputtering and 10 μm reservoirs coating with lubrication with carbon sputtering (Detail of the graph given in Figure 3.10).....	52
Figure 3.12. Optical views of the wear tracks of the POD experiments with aluminum ball and sputtered carbon coating lubrication after 2000 cycles (on the left), and 8500 cycles (on the right). The carbon coating around the holes was completely worn on the track after 8500 cycles.....	55

Figure 3.13. Optical views of the wear tracks of the tests performed with aluminum ball on the samples with 10 μm reservoirs and carbon coating (These views are from the same tracks in Figure 3.12, left track is the left one and right track is the right one).....	55
Figure 3.14. Applied bead size vs. average friction coefficient data for unlubricated and lubrication with graphite samples.....	57
Figure 3.15. General view of model with: (a) 10 μm reservoirs, (b) 5 μm reservoirs, (c) 2 μm reservoirs (Views were taken from MSC.Marc Mentat).....	61
Figure 3.16. Geometry of the reservoirs in our models (on the right) designed according to the actual coating (SE micrograph is on the left).....	62
Figure 3.17. Geometry of the 10 μm reservoirs and calculation of the virtual bead diameter.....	63
Figure 3.18. Calculations of the necessary angles used for 10 μm model.....	63
Figure 3.19. A view of the model with 10 μm reservoir diameter.....	64
Figure 3.20. Profile of a hole for: (a) 5 μm -sized-hole (b) 2 μm -sized-hole.....	64
Figure 3.21. Geometry of the counterface-ball-in the models.....	65
Figure 3.22. Symmetry axes and distributed load applied are shown on the model with 10 μm holes.....	66
Figure 3.23. Location of stresses followed on a hole (with 2 μm opening size).....	67
Figure 3.24. Shear stresses (σ_{12}) at bottom of holes while ball interacts with this hole...	68
Figure 3.25. Average shear stress values (σ_{12}) with upper and lower limits during ball-hole interaction.....	69
Figure 3.26. Average σ_{11} stress values with upper and lower limits during ball-hole interaction (values are negative, i.e. stresses are compressive).....	69
Figure 3.27. Average σ_{22} values with upper and lower limits during ball-hole interaction (values are negative, i.e. stresses are compressive).....	70
Figure 3.28. Calculated work vs. hole size curve based on shear stresses.....	71
Figure 3.29. Calculated work vs. hole size curve based on σ_{11} stresses.....	71
Figure 3.30. Calculated work vs. hole size curve based on σ_{22} stresses.....	72
Figure 4.1. Schematic view of surface layers applied to form reservoirs [42].....	77
Figure 4.2.(a) SEM images of the 4-25 type silicon samples.....	78
Figure 4.2. Images of 4-11 type silicon samples in (b) and images of 9-11 type of silicon samples in (c).....	79
Figure 4.3. Scanning electron microscope images of the 4-25 sample after coating: upper corner is before cleaning pattern mask, others after cleaning the mask.....	80
Figure 4.4. Scanning electron microscope images of the 4-11 sample after coating and cleaning of the mask.....	80

Figure 4.5. Scanning electron microscope images of the 9-25 samples after coating and after cleaning of the mask.....	81
Figure 4.6. FC graphs for pin-on-disk test of TiN coatings and silicon substrate with (a) 1 N normal load and (b) 2.2 normal load.....	83
Figure 4.7. Optical micrograph of the coating after full term of pin-on-disk test with 1 N normal load. Graphite smeared areas are the edges of the wear track.....	83
Figure 4.8. Friction-wear tests on two 4-25 on silicon patterned samples. Results of one sample are shown with green color: dry test is marked with dark green, one lubricant test is bright green and other lubricant test is light green. For the second sample, dry test is marked with brown; three lubricant tests are marked with orange and yellow. Lower graph shows the detail of first 500 cycles of only the tests performed with lubrication...	85
Figure 4.9. Friction-wear tests on 4-11 on silicon patterned samples. Results of one sample are shown with blue color: dry test is marked with dark blue, lubricant test is light blue For the second sample, dry test is marked with red color; three lubricant tests are marked with dark or light pink. Lower graph shows the detail of first 500 cycles of only the tests performed with lubrication.....	86
Figure 4.10. Friction-wear tests on 9-25 on silicon patterned samples. Results of one sample are shown with blue color: dry test is marked with dark blue, lubricant test is greenish blue. For the second sample, dry test is marked with brown; lubricant test is marked with red. Lower graph shows the detail of first 500 cycles of only the tests performed with lubrication.....	87
Figure 4.11. Average percent standard deviation values for each specimen type.....	89
Figure 4.12. Optical micrographs of wear tracks of two 4-25 samples showing details of the reservoirs (the tests performed with higher speed and weight).....	92
Figure 4.13. Optical micrographs of wear track on two of the 4-11 samples belong to the tests performed with higher speed and dead weight.....	93
Figure 4.14. Optical micrographs of wear track on the 9-25 samples belong to the tests performed with higher speed and dead weight.....	93
Figure 4.15. Schematic view of a single reservoir-counterface interaction: Scheme on the left, (a), shows how the counterface (ball) would transport graphite from the reservoirs and how the graphite smears on TiN surface. Scheme on the right, (b), shows that smearing area would be larger for each bigger-sized-reservoir.....	94
Figure 4.16. Pin-on-disk lubricated friction test results obtained under lower load and speed conditions.....	95
Figure 4.17. Pin-on-disk lubricated friction test results obtained under lower load and speed conditions.....	96
Figure 4.18. Pin-on-disk lubricated friction test results obtained under lower load and speed conditions. These tests are repeats of the tests shown in Figure 4.15.....	97
Figure 4.19. Optical micrographs of wear tracks of 4-25 samples belong to the tests performed with lower speed and dead weight (2000 cycles).....	98

Figure 4.20. Optical appearance of the wear track of 4-11 sample after the test with lower speed and dead weight (2000 cycles).....	98
Figure 4.21. Optical appearance of the wear track of 9-25 sample after the test with lower speed and dead weight (2000 cycles).....	98
Figure 4.22. FC data recorded for the tests against 440C steel ball: Full range of the tests were shown on the left, only first 500 cycles were shown below.....	101
Figure 4.23. Optical micrographs of the tracks after friction tests of (a) 4-11 specimen after wear test, (b) 9-25 specimen after wear test.....	102
Figure 4.24. Optical micrographs of the tracks taken after friction test kept going until about 12,000 cycles for one of the 9-25 specimens.....	102
Figure 5.1. Position of rake and flank surfaces when TiN and In deposited.....	106
Figure 5.2. Pictures of rake face of the insert specimens after cleaning the micro-beads from the surface; micro-beads left the empty reservoirs behind.....	107
Figure 5.3. Friction coefficient graphs during pin-on-disk tests for the TiN coating without reservoirs; TiN coating with 5 μm reservoirs and TiN coating with 10 μm reservoirs.....	108
Figure 5.4. Optical micrographs of the wear tracks on indium coated inserts (a) with no reservoirs, (b) with 5 μm reservoirs and (c) with 10 μm reservoirs.....	109
Figure 5.5. The progress of the wear during machining tests performed in the presence of cutting fluids on various coatings: TiN coating without any embedded lubricants (TiN), indium film on TiN coating without any reservoirs (TiN-In) and TiN coatings with lower or higher density of the 5 or 10 μm -sized-reservoirs and embedded lubricants in them (TiN-In5L, TiN-In5H or TiN-In10L and TiN-In10H).....	111
Figure 5.6. Flank wear results of dry machining experiments performed on three samples: tool insert with just TiN coating (TiN), tool insert with indium on TiN without any reservoirs (TiN-In) and tool insert with indium on TiN with high density of 5 μm reservoirs (TiN-In5H).....	112
Figure 5.7. Rake surface appearance of the turning inserts after machining experiments: (a) Only TiN coated insert, (b) Insert with indium on TiN with 5 μm reservoirs.....	113
Figure 5.8. SEM micrographs of the collected chips for (a) the tool with plain TiN coating and (b) for the tool with indium layer on TiN with 5 μm reservoirs.....	114
Figure 5.9. Friction coefficient values obtained from the tests conducted at various temperatures for Pin sample coated with indium film on top of TiN with 5 μm reservoirs, and for Plain TiN coated pin sample [45].....	115
Figure 5.10. XPS outputs from a region near cutting edge of tool insert that were tested in dry machining: (I) is after 4 min. etching, (II) is after 14 min. etching.....	117
Figure 5.11. Atomic concentration changes through depth of surface layers of dry machined insert coated by indium layer on TiN with 5 μm reservoirs.....	117

ABSTRACT

FABRICATION AND TRIBOLOGY OF COMPOSITE COATINGS
INCORPORATING SOLID LUBRICANT MICRO-RESERVOIRS

by

Canan Gamze GULERYUZ

University of New Hampshire, December, 2009

The tribological behavior of composite coating incorporating solid lubricant reservoirs has been investigated in this study. A new method, termed “*microbeading*” was devised to create microscopic reservoirs on the surface of sputter-deposited hard coatings. Pin-on-disk tests were used to evaluate the lubricating performance of these newly devised composite coatings. Three sizes of the reservoirs were investigated: 1.5, 5 and 10 μm . The 10 μm -sized-reservoirs performed better in terms of reducing friction and extending wear life. These coatings were also evaluated with finite element models. It was found that during ball-coating surface interaction, the lowest stresses and calculated work done were obtained at a critical location at the bottom of hole on the coating with 10 μm holes.

Further investigations were conducted using photolithography to fabricate the coatings, which allows a more controlled reservoir distribution on the surface. For these tests, silicon wafer substrates were used with masks prepared by photolithography. Reservoir diameter (4 and 9 μm) and area coverage (2% and 10%) were the primary variables, and it was found that the larger diameter reservoirs (9 μm) and higher area coverage values (10%) were more beneficial in providing lubricant storage and

replenishment in the wear track. These results were correlated with observations of wear tracks after the tribological tests, particularly the aspects of microreservoir filling and spreading on the track.

The microbeading coating method was also applied on machining tool inserts and their performance was investigated by lathe turning tests. Indium was chosen as the solid lubricant for this test, and hardened 4340 steel was used as the workpiece. All coatings with indium (with or without reservoirs) showed substantially better wear lives than TiN alone under wet cutting test conditions, and slightly higher wear life under dry cutting conditions. Further research was conducted with machining simulation tests and it was found that the frictional lubricity of the indium coating was lost at high temperatures (above 600°C). X-ray photoelectron spectroscopy (XPS) was conducted on the surfaces of the tool inserts after dry cutting, and it was found that some indium was still present. Based on these results, indium has been demonstrated to be capable of providing increased lubricity when cutting under lubricated conditions.

CHAPTER I

INTRODUCTION AND LITERATURE REVIEW

Wear, friction and corrosion are materials degradation processes that begin at surfaces. Failure to control these processes can have a high economic cost, use excessive energy resources, and even lead to great human catastrophes [1-6]. The goal of our research is to develop, through the use of coatings, a new technological foundation for reducing friction and wear at interacting surfaces in engineered components. To help meet this goal, we have developed and investigated a new method for fabricating composite coatings incorporating one hard and one soft (lubricious) phase. We expect hard phase will strengthen the coating, while the soft phase will decrease friction and reduce wear. We have demonstrated the potential of this new coating method by applying it to cutting tools for dry machining processes.

Coatings for cutting tools, and other applications requiring good wear resistance and low friction, have observed steady advances for the last several decades. Intensive research has resulted in a transition from single layer/single phase coatings to multiconstituent, multilayer/multiphase, gradient, superlattice and composite coatings [7-9].

Composite coatings are multiphase/multiconstituent coatings that are tailored to combine the advantageous properties of several phases, such as combining a hard phase with a tough phase [7]. The motivation for composite coatings has often been one or

several of the following: to improve adhesion of the coating to the substrate, to decrease residual stress of the overall coating, to increase the crack arresting capability of coating structure or to extend the application area of the coating [8,10]. Among composite coatings, some consists of a hard phase and a soft phase, specifically developed for tribological applications. While the function of the hard phase is to give the coating necessary strength and long wear life, the soft phase provides low friction [11,12]. Several different approaches have been used to achieve the aforementioned multiconstituent/ multiphase/multilayer tribological coatings, which followed the historical improvements in the general coatings area as summarized in Figure 1.1. [8,13]:

- *Multilayered coatings* consisting of a soft and a hard phase stacked sequentially;
- *Multiconstituent/Multiphase coatings* designed as a matrix incorporating a dispersed soft constituent/phase or vice versa. These phases are generally formed by natural phase separation during deposition of the film.
- *Three-dimensionally designed coating structures* with an intention to improve tribological performances for different applications. These coatings are engineered to create the 3-D structure by some method of surface patterning.

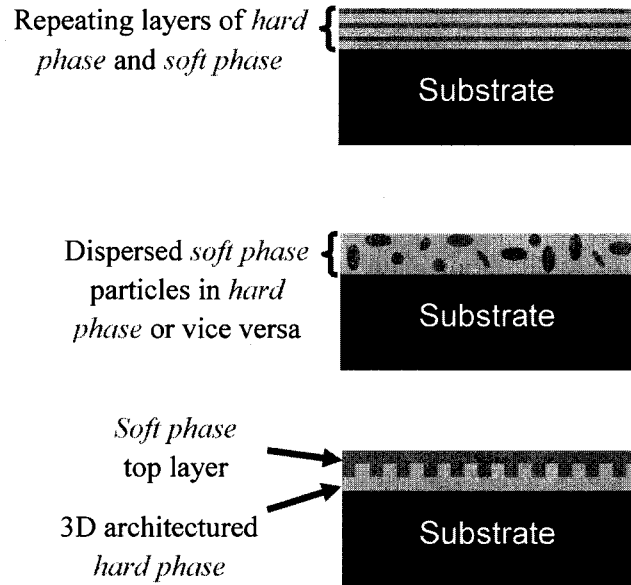


Figure 1.1. Various approaches for achieving tribological composite coatings [reproduced after 8 and 13].

In one study done by Endrino et.al. [14], WC or TiC and Ag were co-deposited by magnetron sputtering. Both films exhibited composite structures with separate lubricant Ag phases in hard WC or TiC phase. Friction tests performed and the results are given in Figure 1.2. Endrino et.al. showed that it is possible to decrease the friction coefficient with addition of silver. Significant decreases in friction coefficient were achieved for WC-Ag films at 21% and 39% Ag containing films, whereas for TiC-Ag films at 51% and 86% Ag containing films were optimal. The lowest average friction coefficient was 0.25 for WC-Ag composite film with 21% Ag and 0.26 for TiC-Ag composite film with 51% Ag.

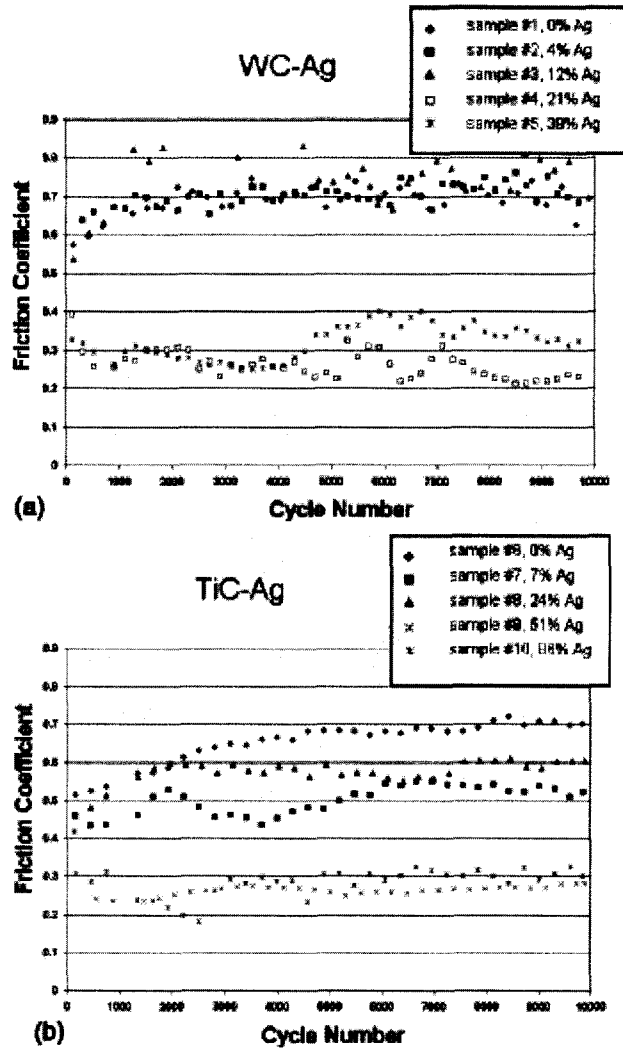


Figure 1.2. Friction test results under vacuum conditions against a steel ball: (a) WC-Ag films, (b) TiC-Ag films [14].

The silver phase can be observed as bright particles using scanning electron microscopy (SEM) to examine the wear track. The TiC-Ag film with 51% Ag after 10,000 cycles is shown in Figure 1.3.(a). For this particular film, the friction test was repeated until failure and the low values of friction coefficient lasted for 33,000 cycles. In Figure 1.3.(b), elongated silver stripes can be observed on the track exhibiting the lubricating effect of this phase.

Further investigations on TiC-Ag composite coating system were also performed by Endrino et.al. [15] where the coating was deposited using a combined magnetron

sputtering-pulsed laser deposition (MSPLD) process. The silver content in the coatings was varied from 6 to 46 atomic%. Phase separation was confirmed by XRD analyses. A nano-crystalline structure for silver was observed. With increasing silver contents (15.4 atomic% and more) larger crystals (about 50-200 nm) on the surface accompanied the nano-crystalline structure. Pin-on-disk friction and wear test were performed against steel balls for these samples, and the coefficient of friction versus number of cycles curves are given in Figure 1.4. for various silver contents. The lowest friction coefficient (about 0.2) was obtained for the 15.4 atomic% silver content; lower or higher amounts gave higher friction coefficients. Also for this composition, the coating had the lowest wear value among the coatings tested.

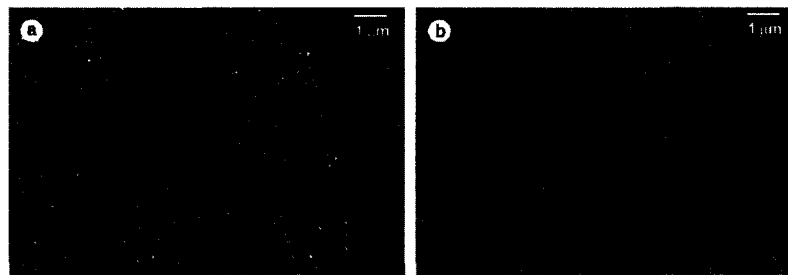


Figure 1.3. Scanning electron micrograph of the TiC-Ag film with 51% Ag content (a) after 10,000 cycles, (b) after 33,000 cycles [14].

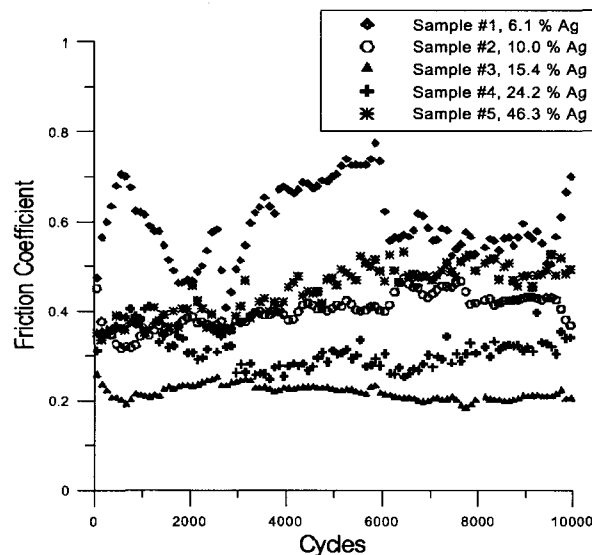


Figure 1.4. Friction results for TiC-Ag composite films with various silver contents [15].

The appearance of the coating surface for this specific composition (15.4 at.% Ag in TiC) is shown in Figure 1.5(a). A non-homogeneous size dispersion was observed for the silver phases. SEM image of the wear track after 10,000 cycles (Figure 1.5B) showed extensive silver smearing on the wear track proving the lubricating effect of this phase.

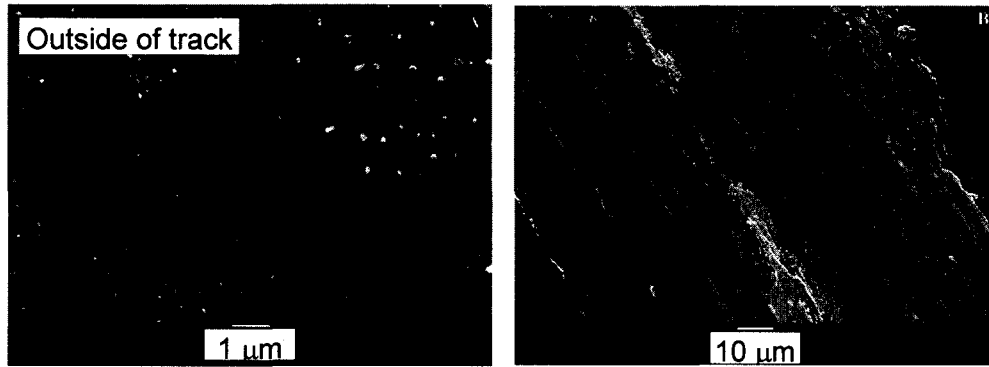


Figure 1.5. SEM pictures that shows A: dispersed Ag phases in hard coating and B: smeared Ag on hard coating in pin-on-disk test [15].

More recently, Mulligan et. al. [16] investigated the effect of growth temperature on the microstructure of CrN-Ag nanocomposite coatings with 22 at.% Ag. Film depositions were performed with dual reactive magnetron sputtering in a nitrogen environment. XRD and cross-section inspections showed that the average silver particle size increased from <25 nm to about $300 \times 300 \times 100$ nm³ and to about $600 \times 600 \times 200$ nm³, as the temperature increases from 500 to 600 and 600 to 700°C, respectively. Higher temperatures caused silver to form lamellar phases. The presence of silver phase changes the texture of CrN which was (002) for pure CrN. When Ag was added at 500°C, the (111) texture was also observed together with (002) texture. The reason behind this behavior was reported to be that the silver phases on the surface are convenient places for re-nucleation for CrN. When the temperature increased, (111)-texture for both Ag and CrN phases becomes stronger, which is related with increasing adatom mobility of the silver. Microhardness measurements show that as the deposition temperature increases,

the overall hardness of the film increases. As the silver content of the film decreases, the silver segregation to surface increases with increasing temperature, which causes a hardness decrease of the film. Also, with increasing temperature, the inhomogeneity of the film increases as observed from more scattering hardness results.

Recent studies have reported attempts to create three dimensionally structured coatings, i.e. coating properties are changing not only in the cross-section, but also on the sliding plane [7]. For instance, Voevodin et.al. [7] cut a circular groove (using and IR laser) matching the center of the track of the counterface-ball in a functional gradient Ti-TiC-DLC coating, and then sputter-deposited MoS₂ in this groove and on surface (Figure 1.6).

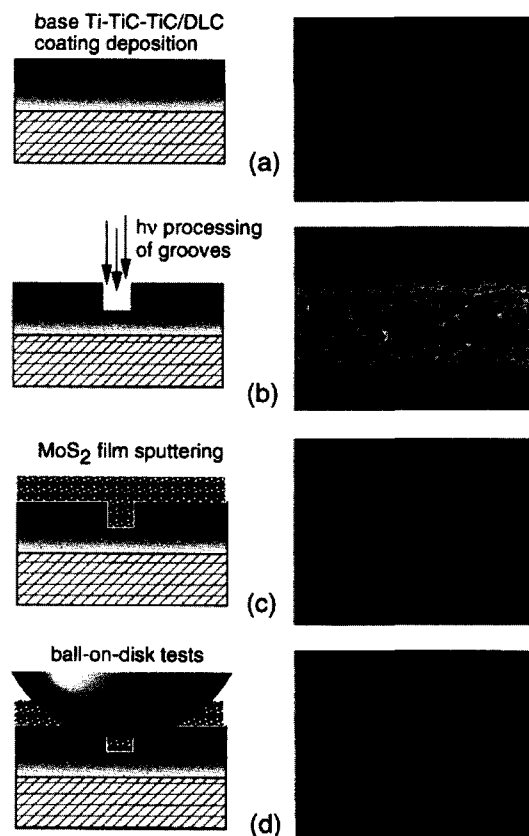


Figure 1.6. (a)-(c): Steps of surface texturing and the appearance of the specimen surface after each step given on the right. (d) Ball-on-disk test and the wear track after 1,600,000 cycles with 1 GPa contact pressure [7].

The aim in the grooving process was to aid in the storage and replenishment of the solid lubricant. This coating was reported to have a longer wear life against a steel ball than both the plain MoS₂ coating on steel and on Ti-TiC-DLC coatings in a 50% humidity environment. This behavior can be followed in Figure 1.7. In Figure 1.7 (a) a friction test is performed on only a layer of MoS₂ on steel substrate. The failure level defined for these tests is a friction coefficient of 0.4 which corresponds to steel on steel friction and shows the coating is not functioning any more. The wear life of just a MoS₂ coating on steel substrate is about 20,000 cycles. When only the functional hard coating (Ti-TiC-TiC/DLC) was applied on the substrate (Figure 1.7.(b)), the wear life was about 40,000 cycles. After 10,000 cycles, steel material transfer was observed and the coating failed earlier because of this steel-steel interaction. When MoS₂ was deposited on the functional hard coating (Figure 1.7.(c)), low friction values of about 0.08 sustained for 30,000 cycles and the coefficient of friction (CoF) gradually increased afterwards. The authors claimed that the MoS₂ layer worn through after 30,000 cycles and the lower friction was provided by the remaining MoS₂ at the edges of the ball. When this supply finished at about 160,000 cycles; steel on steel contact condition occurred with CoF values of about 0.4. In Figure 1.7.(d) we see the friction response of the grooved functional gradient coating with MoS₂ on top. Lower CoF values of about 0.15 persisted for more than 1,000,000 cycles. The authors also claimed that the saw-tooth behavior shown in the insert of Figure 1.7.(d) was because of the new lubricant provided from the groove.

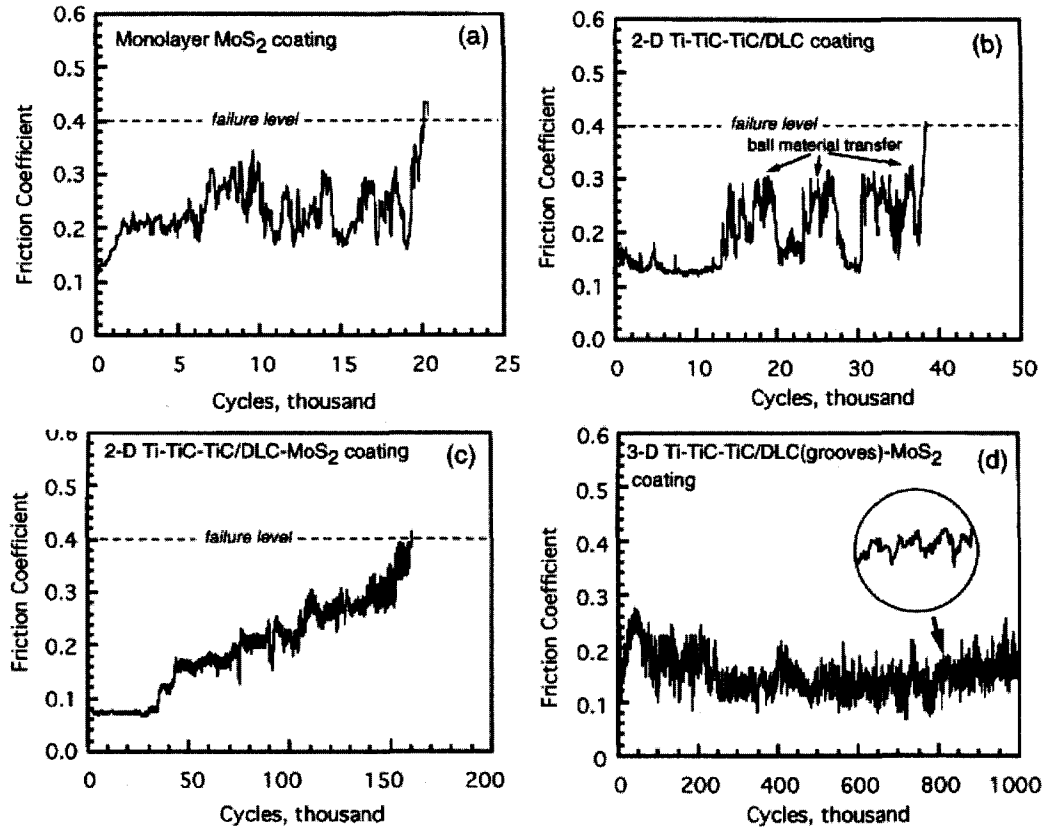


Figure 1.7. Ball-on-disk test friction results performed against 440C steel at 50% RH environment: (a) only MoS₂ layer on steel substrate, (b) Ti-TiC-TiC/DLC coating on steel substrate, (c) MoS₂ coating on Ti-TiC-TiC/DLC coating, (d) MoS₂ coating on 3-D Ti-TiC-TiC/DLC coating (with grooves) [7].

The other aim of their study was to investigate the potential of the reservoirs to help the coating to adapt different environments in terms of humidity level. Good tribological performance is often needed in both in humid and dry environments, such as space shuttles. There is no solid lubricant that performs well at all levels of humidity, providing low friction with high durability. Therefore, mixtures of the various solid lubricants with good properties at different environments could be a solution. But each solid lubricant should be kept in a fresh state (not affected by the unfavorable humidity of the environment). The reservoirs in the coating could potentially store the solid lubricants and protect them from environments not appropriate to their use. MoS₂ provides low

coefficients of friction and has the potential to increase the wear life of the surfaces, but high humidity environments cause MoS₂ to oxidize and deteriorate rapidly. On the other hand, graphite is good for the higher humidity environments; but can not provide low frictions under dry conditions. With this perspective, Voevodin et.al. thought that the groove would help to keep MoS₂ in a fresh state while graphite-like phases provided from functional gradient coating lubricate the surface under humid environments. When the humidity decreases MoS₂ would become active (Figure 1.6.). The following figure (1.8) shows humidity cyclic wear tests done on this type of coating; it shows the characteristic coefficient of frictions provided by graphite under humid air (about 0.15) and by MoS₂ under dry conditions (about 0.02).

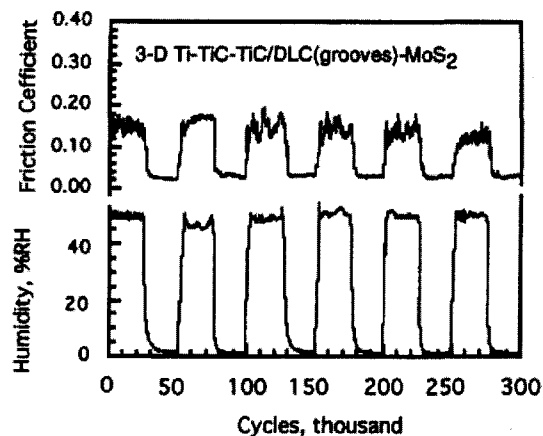


Figure 1.8. Ball-on-disk test results representing environmental adaptation of MoS₂ coating on 3D structured Ti-TiC-TiC/DLC coating. Lower graph shows the humidity level change [7].

In their more recent work, with the help of improving laser technology, Voevodin and Zabinski [17] used a UV laser to drill micrometer-sized reservoirs (with 10 or 20 μm diameter and 3-5 μm depth) in a TiCN hard coating. The hole size is defined as the diameter measured at the middle cross-section of the hole. (Figure 1.9., Figure1.10.). They applied MoS₂ on top of the hard coating after laser processing either by burnishing or magnetron sputtering; and performed sliding tests against a steel ball under humid air

and dry nitrogen environments. They changed the area coverage (in the range of 0.5%-50%) to determine the optimum structure for providing longest wear life.

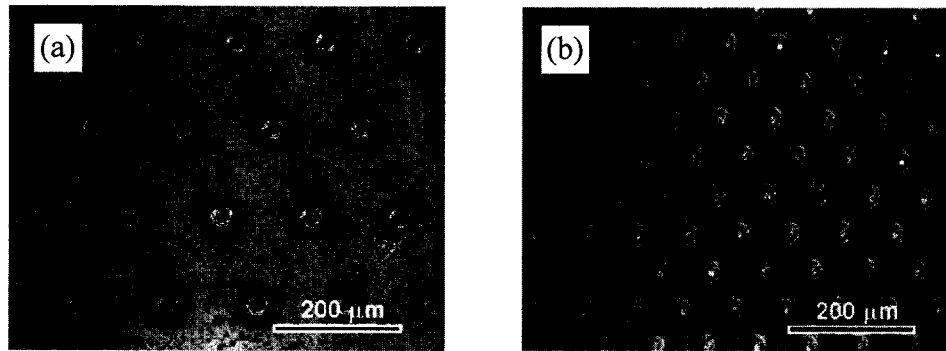


Figure 1.9. Example pictures of laser drilled 20 μm sized holes in TiCN hard coatings: (a) 1% area coverage, (b) 8% area coverage [17].

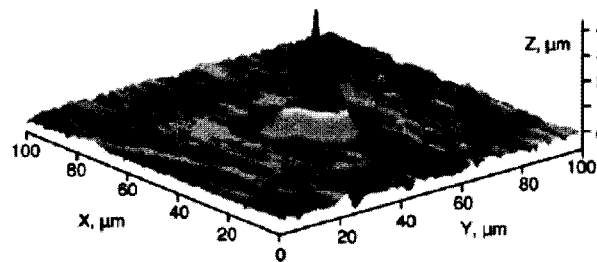


Figure 1.10. Inverted, upside-down profile of a laser drilled reservoir. z-axis scale is different from x-and y-axes [17].

Voevodin and Zabinski claimed that the reservoirs helped to improve the wear life of the solid lubricant up to one order of magnitude compared to the samples with no reservoirs. They also found that 10% was optimum area coverage for 10 μm reservoir size and 15% for 20 μm reservoirs size (Figure 1.11.(a)). More interestingly, they proposed that for optimal results a 50 μm spacing reservoirs on the surface should be used independent of reservoir size (10 or 20 μm) (Figure 1.11. (b)). As another aspect of this research, they investigated the effect of reservoirs on environmental adaptation of the burnished coating with a mixture of MoS_2 /graphite/ Sb_2O_3 as a solid lubricant, which they named a “*chameleon*” type of coating. Because the reservoirs keep the solid lubricant in

a fresh state, as in their previous study, the overall coating showed successful adaptation to both humid and non-humid environments.

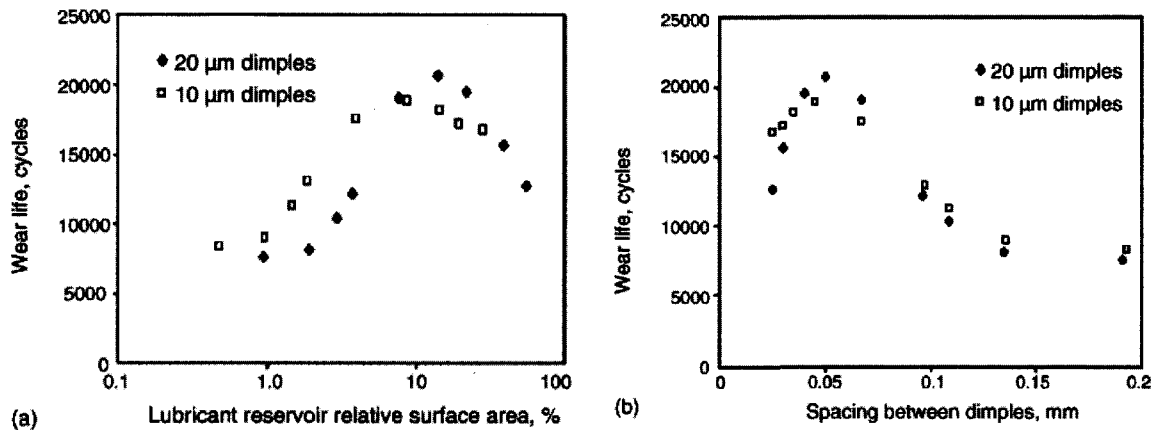


Figure 1.11. Wear cycles before failure occurs for 10 and 20 μm reservoirs filled with MoS₂: (a) Wear life versus relative area coverage of the lubricant, (b) Wear life versus spacing between reservoirs (or dimples) [17].

Rapoport et.al. [18] recently published a study reporting their research on the effect of laser texturing substrate surfaces on the friction and wear of MoS₂ as solid lubricant. This study does not include any hard coating application. Surface hardened steel surfaces were first textured by a laser technique. 65±15 μm sized shallow (1 or 2 μm-deep) reservoirs were obtained after laser processing. MoS₂ particles with sizes smaller than 2 μm were applied on the substrate surface by cloth burnishing. They changed the area coverage of the reservoirs in the range of 10-60%. They tested these samples with ball-on-flat method with increasing load under an environment of 45% relative humidity. Wear life was defined as the time period past to reach a coefficient of friction of 0.3. They recorded the wear life of samples with different area coverage and they reported a significant benefit in increasing area coverage until about 40% (Figure 1.12).

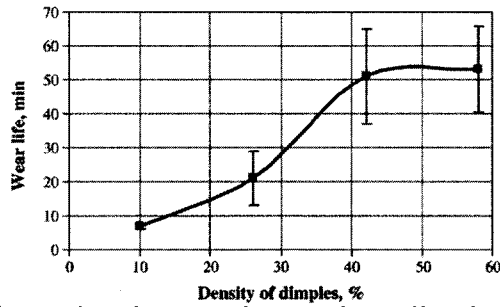


Figure 1.12. Wear life results given against various dimple densities achieved on steel surface [18].

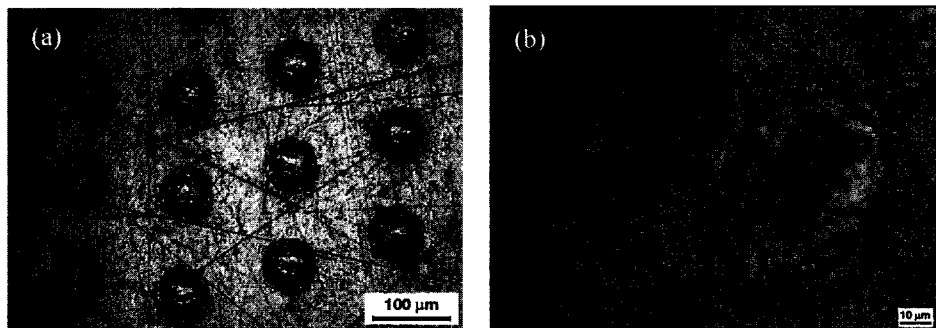


Figure 1.13. Appearance of the surface dimples on the surface with (a) 10% area coverage, (b) 42% area coverage [18].

Rapoport and Moshkovich et. al. [18] also investigated the effect of melted and solidified areas around the reservoirs during the laser drilling. They observed that the samples initially enter into seizure due to the formation of these regions (Figure 1.13 and 1.14). These areas form rings around the reservoirs and causes bulging around them, which would significantly change contact conditions around reservoirs when surface interactions occur. They compared the wear life of samples with bulging to the samples lapped through until the half-way of the bulge and samples lapped until the entire bulge was gone. They reported that the best wear life was achieved with the samples lapped to the half-way point. Another aspect of their research was the effect of depth of the reservoirs. They found that when the amount of solid lubricant provided from the reservoirs increases, the wear life of the overall surface increases.

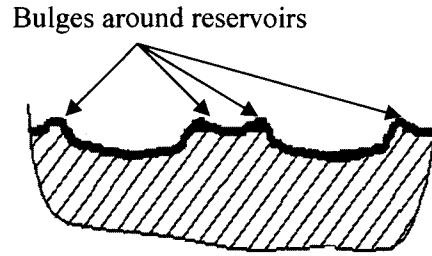


Figure 1.14. Schematic profile of laser drilled reservoirs [modified after 18 to emphasize the appearance the bulges circling reservoirs].

Another recent study that includes coating texturing is the work of Basnyat et.al. [19]. Texturing of TiAlCN coating was achieved by reactive ion etching by using a stainless steel mask. The shape of the reservoirs is rather rectangular with an edge size of $70\ \mu\text{m}$ and the depth of the reservoirs is about $1\ \mu\text{m}$ (Figure 1.15).



Figure 1.15. Rectangular reservoirs created by reactive ion etching [19].

Although the study is more focused on adaptive lubrication with mixtures of $\text{MoS}_x + \text{Ag}$ they also did pin-on-disk friction-wear tests with only MoS_2 solid lubricant. The results of these tests performed with silicon nitride ball with 6 mm diameter under dry air conditions are given in Figure 1.16. Tests were repeated for “only TiAlCN” and “untextured TiAlCN” coatings. The benefit of reservoirs, although they are wide and shallow, was observed as the textured TiAlCN coating having about 1.5 times longer

wear life until the coefficient of friction increased to the values of “only TiAlCN coating”.

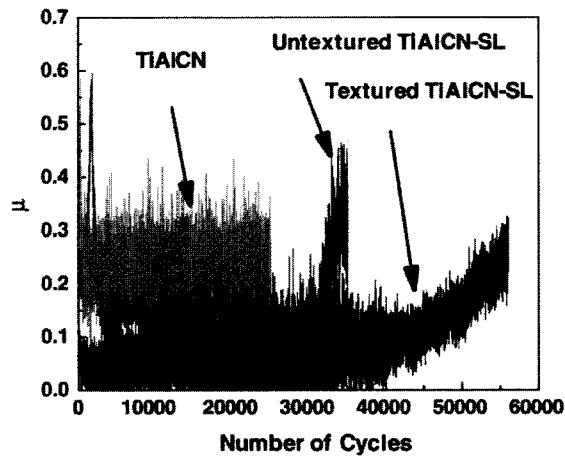


Figure 1.16. Pin-on-disk friction-wear tests performed with MoS_2 as a solid lubricant (SL) under dry air [19].

Krzanowski et. al. [20] fabricated a 3D-structured hard coating by using semiconductor patterning processing. The steps of the photolithography process are shown in Figure 1.17. According to this process, silicon wafers are first spin-coated with a $1.4\ \mu\text{m}$ -thick photoresist film. After baking, the photoresist film was exposed to ultraviolet (UV) light. During this step, a mask was also used to cover the some areas of the photoresist film. The areas that were exposed to the UV light were cross-linked and remained after development step while other areas dissolved. After development of the film, the remaining photoresist islands had slightly negative edges as shown in Figure 1.17, which caused shadowing and reduced coverage of the hard coating around the photoresist islands during the magnetron sputtering. However, this helped lifting-off of the photoresist after the hard coating deposition. Patterned islands with a $2\ \mu\text{m}$ diameter and $7\ \mu\text{m}$ spacing are shown in Figure 1.18.

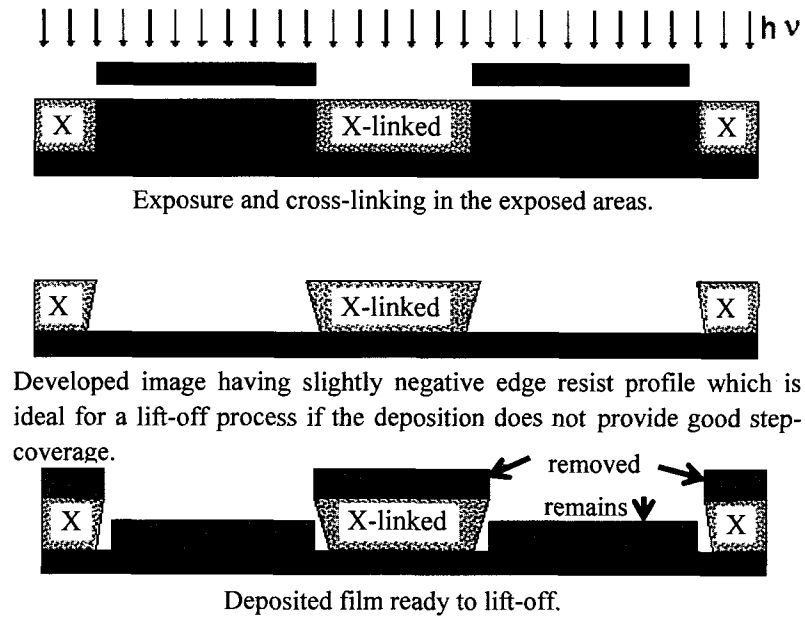


Figure 1.17. Steps of photolithography and coating processes to obtain a hard coating containing reservoirs [13].

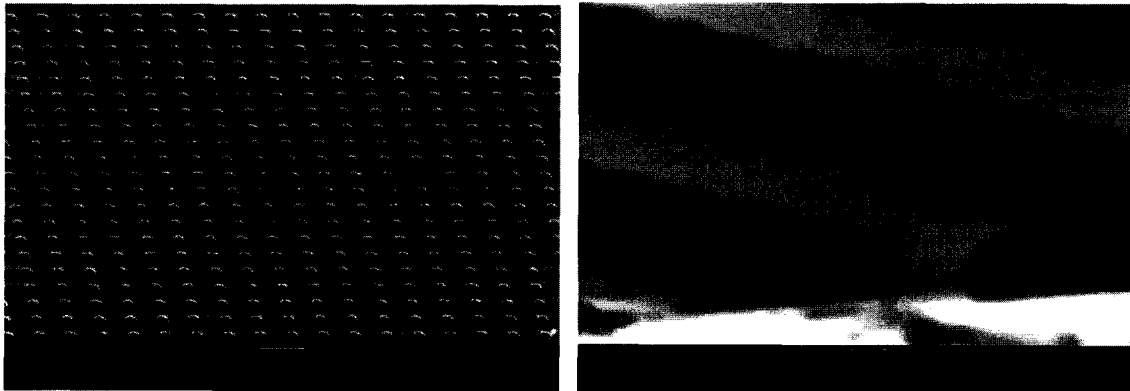


Figure 1.18. SEM picture of pattern prepared on silicon samples by photolithography [20].

Krzanowski et.al. [20] fabricated Cr and TiC hard coatings with reservoirs by using these patterned wafers using this technique and several results are shown in Figure 1.19. The specimens in these images show the deposited Cr coating. Removal of the patterning islands were achieved by ultrasonic agitation in acetone. Appearance of the coating after this step is shown in Figure 1.20 (a). They next applied MoS₂ solid lubricant

film on top of the sample with TiC reservoirs (Figure 1.20 (b)). Figure 1.20 (c) shows a wear track after pin-on-disc test. A closer view of this wear track given in Figure 1.20 (d) shows what was proposed to be MoS₂ transferred on TiC coating outside the reservoirs, originated from filled reservoirs. Their study showed that the photolithography process has a potential to fabricate composite coatings with embedded solid lubricant reservoirs.

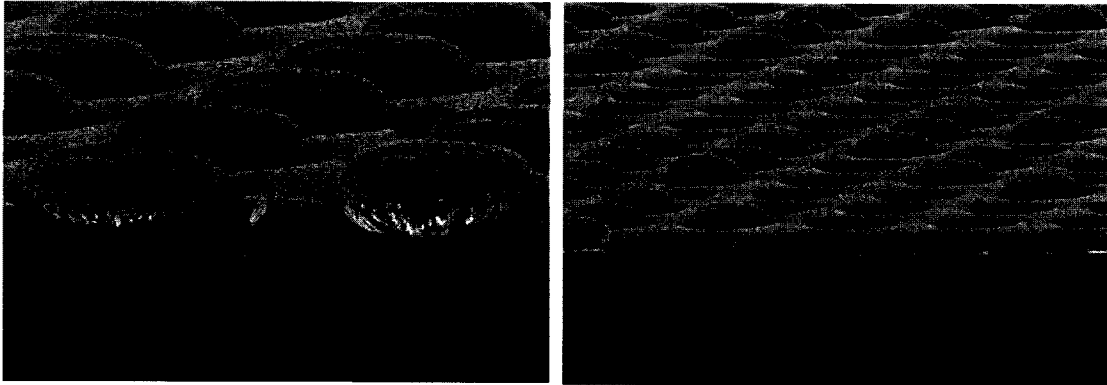


Figure 1.19. SEM images of the patterned silicon samples after Cr-coated by magnetron sputtering process, on the left before cleaning of the mask, on the right after some cleaning process applied [20].

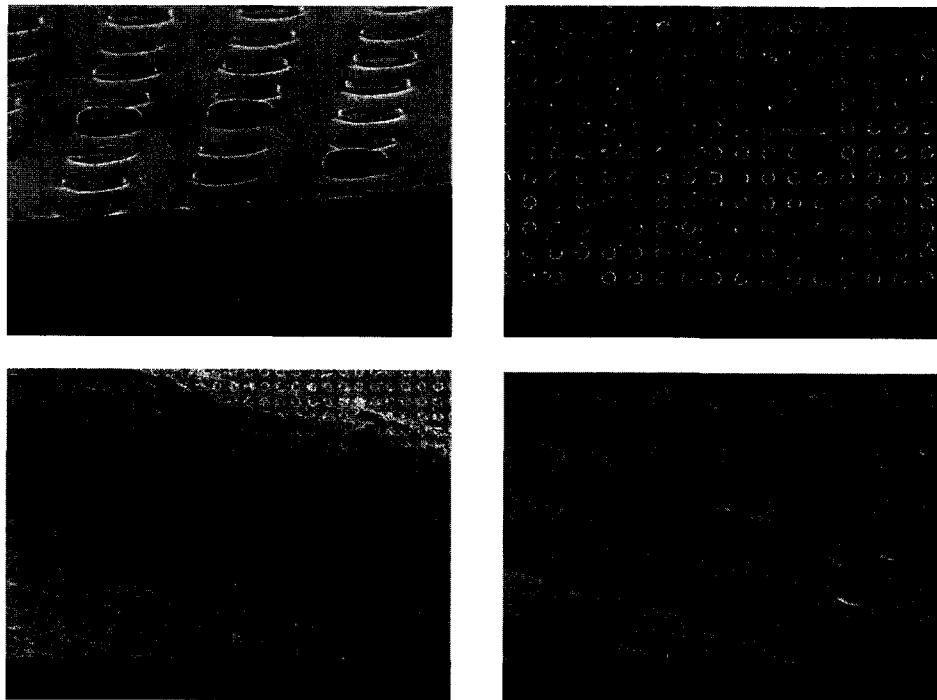


Figure 1.20. Scanning electron micrographs of TiC-MoS₂ composite coating: (a) View after cleaning of mask (a few remaining), before MoS₂ coating. (b) View after MoS₂ coating. (c) Appearance of a wear track after pin-on-disc test. (d) Closer view of the wear track showing MoS₂ filled reservoirs.

In summary, laser drilling is a controllable technique to pattern coatings in terms of location, spacing, and area coverages of the holes; however it is an expensive method in general, despite the fact that initial costs have been decreased with improvements in laser technology. Additionally, the technique itself results in melting and evaporation of some areas of the coating and creates solidification cracks around the holes as shown in the recent work of Voevodin and Zabinski [17] (Figure 1.21), which would be expected to decrease the overall strength of the coating; although the authors report that they confined the laser affected area from the order of 100-150 μm to 30 μm by decreasing the wavelength and this can be reduced with further developments in laser technology. Another aspect of the laser drilling is that the cross-section of the reservoirs is not controllable, because of the melting process. This is illustrated in Figure 1.22, taken from the study of Rapoport et. al. [18]. The melting process also affects the size tolerances. In the study of Rapoport et. al. [18], where the reservoirs were drilled on steel substrates directly, the tolerance is given as $\pm 15 \mu\text{m}$ for 65 μm sized holes.

Reactive ion etching is another controllable technique for the locations, sizes and area coverage. Because there is no melting in this process, the adverse effects of bulging around the holes do not exist. Nevertheless, reactive ion etching is performed under a vacuum environment. There is also a need for mask fabrication. Both of these, especially the ion etching, increase the cost of the production of these coatings with small reservoirs.

Photolithography is another technique that was used to successfully fabricate 3D architectures in hard coatings. Precise size and location tolerances for the reservoirs can

be achieved with this technique. However, its application area is currently limited to silicon substrates, and it is also an expensive technique.

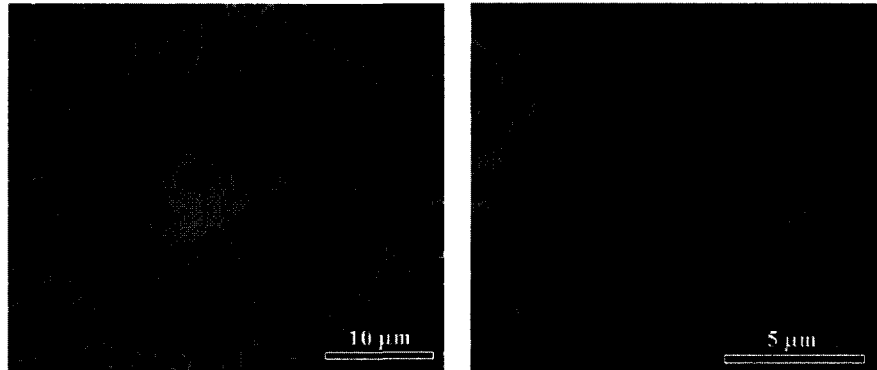


Figure 1.21. Detailed picture of a laser drilled 10 μm sized reservoir [17].

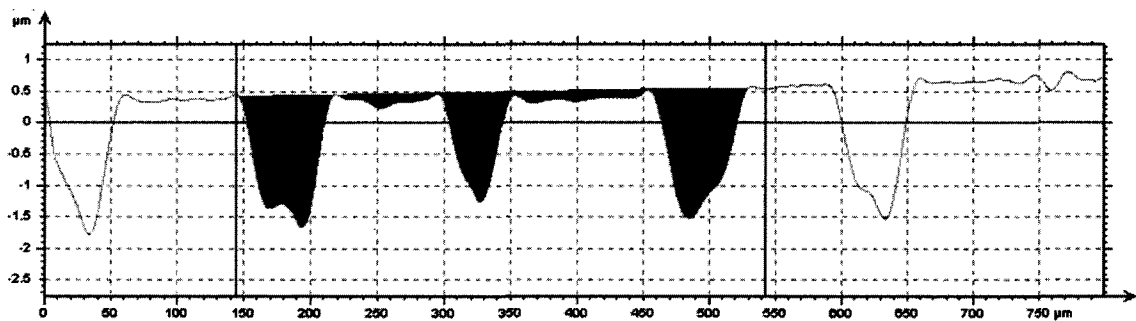


Figure 1.22. Profile of laser processed steel surface with area coverage of 26% [18].

One potential application of composite coatings is the area of machining. Coatings for cutting tool inserts are widely used to reduce friction and extend tool life. However, cutting fluids are still used during machining of metals, and the use of cutting fluids for machining has become economically and environmentally disadvantageous [21-23]. Their share in machining costs is high and the management of their waste has become complex due to the environmental regulations [22,23]. Elimination of the cutting fluids (dry machining) is a solution, but results in the loss of all benefits provided by cutting fluids, namely cooling, lubricating and flushing the chips [21,22]. The machining

environment will become harsher in terms of temperatures and cutting forces without the help of cutting fluids. To facilitate dry machining numerous research studies have been conducted, focusing on improving tool materials, tool coatings and/or finding tool geometries appropriate to conditions of dry machining [21-23]. While TiN and TiAlN are commonly applied hard coatings for machining applications, solid lubricant coatings are attractive for further reduction in friction. Although solid lubricants have existed for a long time, they have generated renewed interest in order to reduce the use of liquid lubrication [10]. Graphite, along with dichalcogenides such as MoS₂, soft metals such as Pb, In, Sn, Ag, Au, organic polymers such as PTFE and nylon are the most commonly used solid lubricants [10].

Indium (In) is a soft metal that has been used in tribological applications for its lubrication capacity [10,24,25]. Fox-Rabinovich et. al. studied the effect of ion implantation before hard coating on the wear resistance of the machining tool inserts [24]. In this study, before hard coating (Ti(Cr,N)), they implanted 16 different elements into the surface of High Speed Steel (HSS) indexable inserts after they were hardened by ion nitriding. For comparison, again before the Ti(Cr,N) hard coating deposition by PVD, other HSS inserts were coated with several anti-friction materials such as a copper based alloy or a lead based alloy to mix with surface layers after hardening. Turning tests were conducted and wear life of the inserts (defined as machined distance until 0.3 mm flank wear) for each implanted element was recorded. This data was compared to the data taken from the insert only coated with Ti(Cr,N) after ion nitriding. Adhesion of the coatings was evaluated by scratch tests. Ion implantation was proved to be able to

provide up to 2-3 fold increase in wear life depending on the element. Indium gave the optimum adhesion-wear life (2.4 fold in dry machining and 2.1 fold in wet machining).

Additionally, In is also important in terms of being frictionally compatible with Fe. Here it is necessary to emphasize and explain *compatibility* concept. '*Frictional compatibility*' is the opposite of metallurgical compatibility of metal pairs, and means when two metals slide against each other, they give low friction and wear [26]. Based on binary phase diagrams, Rabinowicz provided a metallurgical compatibility chart, see Figure 1.23 [24,26,27]. Rabinowicz used term '*metallurgically compatible*' for a metal pair if they mix at least 1 volume % in liquid state and at room temperature if they dissolve in each other completely. '*Partially compatible*' pairs make a solution when they are liquid, and they only can dissolve in each other between 0.1-1 vol. % at room temperature. '*Incompatible*' metal pairs behave as a two different liquid when they are molten, and don't have any practical solubility at room temperature. Partial incompatibility is defined between partial compatibility and incompatibility. Hutchings [26] is also related the term '*tribological compatibility*' with mutual solubility (among other factors) and accepted guidance of binary phase diagrams, especially under severe normal load, adhesive wear conditions. Tribological compatibility is 'reluctance of opposing surfaces to form an interfacial bond' according to Hutchings [26]. One can expect In would also be more resistant to adhesive wear against steels than other materials that are more metallurgically compatible to steels. With these results, In has a potential to be used as a solid lubricant coating on machining tools.

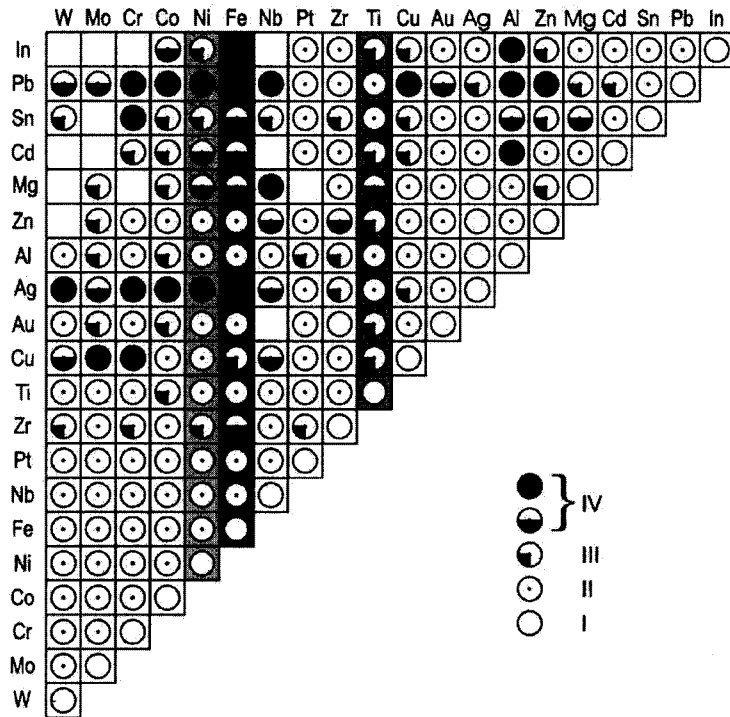


Figure 1.23. Mutual solubility of metals based on the binary phase diagrams, I is good mutual solubility, IV is low mutual solubility [24].

While solid lubricants such as silver, In and MoS₂ can reduce friction, their wear rates can be high, which is why composite coatings are attractive. As discussed earlier, fabrication of composite coatings can proceed using various methodologies, and the characteristics of each needs to be fully investigated.

The aim of this project is to investigate the friction and wear behavior of the hard coatings that incorporate *micro-reservoirs* that store solid lubricants and replenish them to the surface. The research method to fulfill the aforementioned goal includes:

- Fabrication of composite coatings that contain micro-holes applied by means of a “*micro-beading method*” or photolithography;

- Inspection of the coatings by scanning electron microscopy (general appearance, hole aspect ratios, hole sizes, coating thicknesses, chemical analysis of the coatings are screened);
- Testing of friction performance by pin-on-disk experiments of these coatings with or without solid lubricants;
- Analysis of the friction tracks with optical microscopy;
- Modeling of the coating with micro-reservoirs by the finite element method (FEM);
- Testing of machining performance of these coatings in turning operations (turning of high-strength steel, both dry and lubricated);
- Chemical analysis of the turning tool inserts after machining tests by x-ray photoelectron spectroscopy (XPS).

CHAPTER II

EXPERIMENTAL METHODOLOGY

In this chapter, the *coating fabrication method* and the experimental procedures that were used in the scope of this thesis are presented. These includes the microbeading technique, the coating method, i.e. magnetron sputtering, lubrication materials and equipment, the friction-wear testing, optical microscopy, scanning electron microscopy, turning for machining tests and x-ray photoelectron spectroscopy.

II. 1. Microbeading Technique

In the microbeading technique, micron-sized glass or silica spheres (provided by G.Kisker GbR or Duke Scientific Corporation) in ethanol mixtures were sprayed on to substrates (Figure 2.1). Spraying was first carried out using a mist sprayer in the previous work [28]. In this study, an “*air-brush*” has been used to increase the homogeneity of spray. Initially, compressed air was used as the pressurized gas, later argon gas was preferred. A homogeneous (in terms of both beads and liquid parts of the mixture), fast drying, smooth, thin liquid film spread on the specimen surface was achieved in the spray process after many attempts. This was achieved by optimizing the gas and mixture flow rates yielding a smooth mist consisting of small droplets of the mixture carrying approximately the same amount of beads. Any large droplets in the spray created splashes that would either take too long to dry or dry individually (starting from outside of the

droplet and proceeding through the inside), both of which would increase agglomeration of the micro-spheres on the specimen surface. The densities of the bead-ethanol mixtures were kept constant (1 gram microbeads per 200 ml of ethanol), except for the tests where the area coverage of the beads were to be increased. Three sizes of the micro-spheres were used in the tests: 1.5 μm , 5 μm and 10 μm .

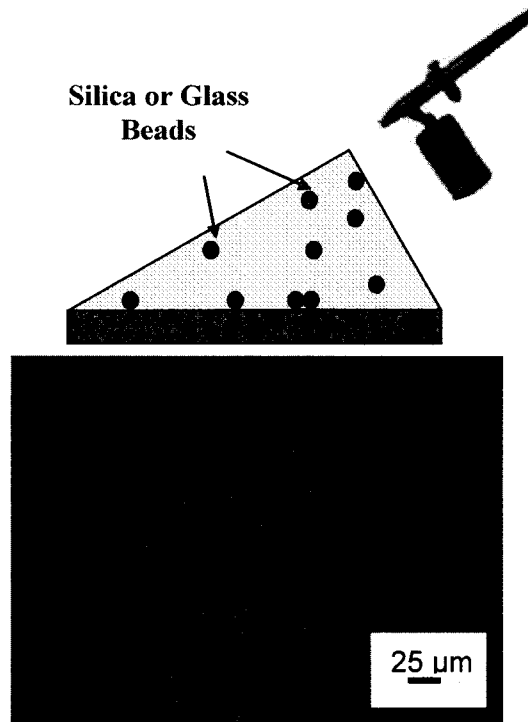


Figure 2.1. Schematic view of the bead spraying technique with an optical picture of 10 μm sized beads on the specimen surface.

After spraying and drying, the specimens were transferred to the vacuum chamber and glued on the specimen holder with a conductive silver paste. The surfaces of the samples were protected carefully in Petri dishes so as not to disturb the beads on the specimen surface. Specimens were coated by a TiN reactive magnetron sputtering method (details of the experimental setup will be given later in this chapter). The thickness of the coating has to be less than half of the bead diameter, otherwise the micro-spheres may be buried in the coating. The deposition process is shown

schematically in Figure 2.2 with examples of scanning electron micrographs of 1.5 μm bead sprayed and coated surfaces.

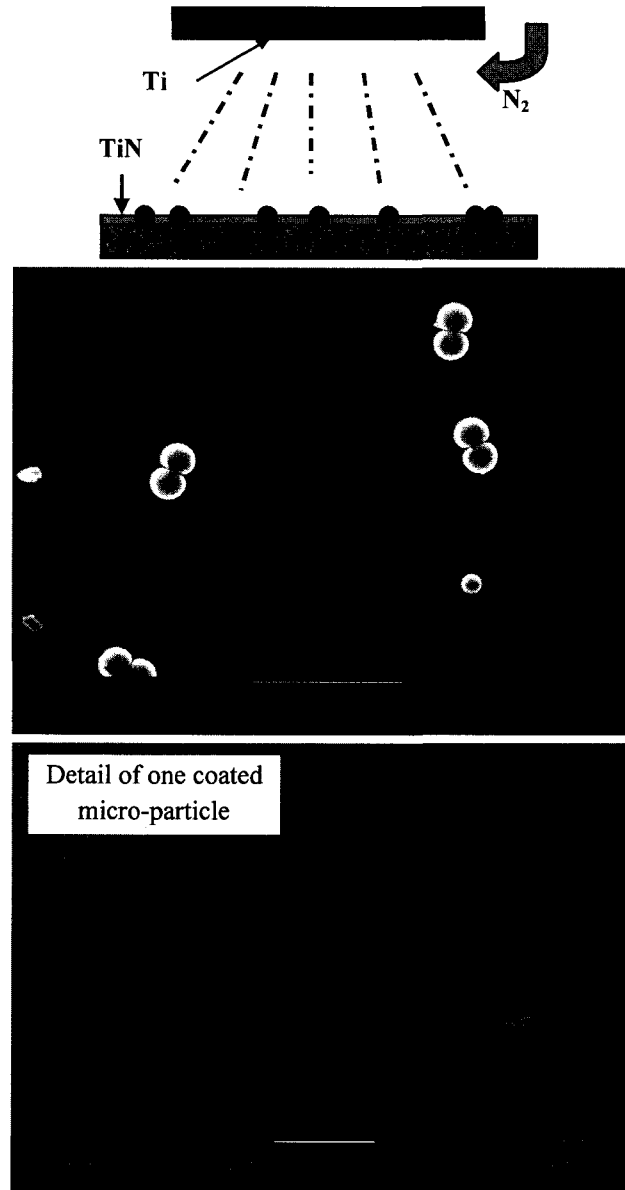


Figure 2.2. Schematic view of the magnetron sputtering process on the micro-particles-sprayed surface. Micro-sphere size used for this sample is 1.5 μm .

After the deposition, samples were placed in a container of ethanol within an ultrasonic cleaning tank for several minutes (Figure 2.3.). This process allows the micro-particles to detach from the coating structure leaving their places behind as “reservoirs”(Figure 2.4 and Figure 2.5).

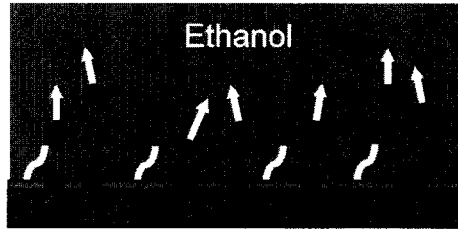


Figure 2.3. Schematic view of the micro-particle cleaning process.

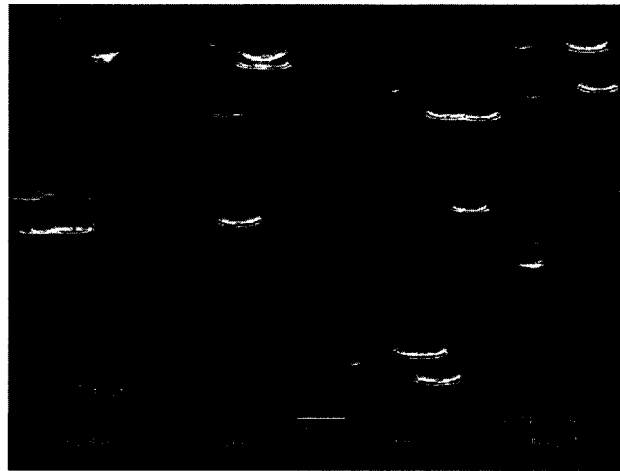


Figure 2.4. SE micrograph of reservoirs with a 5 μm diameter on the coating surface.

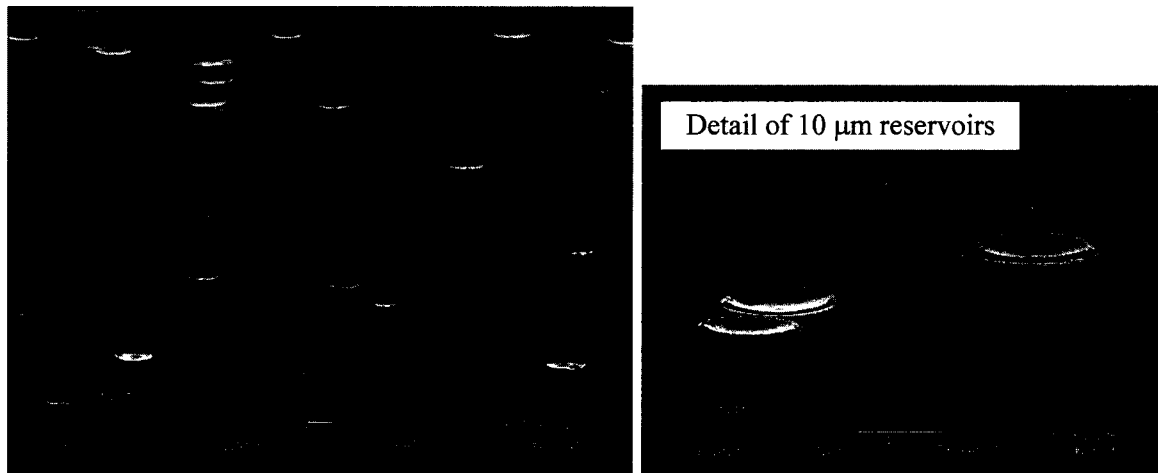


Figure 2.5. Scanning electron micrographs of reservoirs with a 10 μm diameter on coating surface.

Having the reservoirs, various solid lubricants were applied on the surface. First, natural microcrystalline grade graphite powder with a particle size of 2-15 micron,

provided by Alfa Aesar was used as a solid lubricant. In addition, magnetron sputtered carbon or indium were also applied to the surface as solid lubricants.

For graphite lubrication, a 2g-per-100ml-dense-mixture of graphite particles with 200-proof-ethanol was prepared to be sprayed on the specimen surfaces with a mist sprayer. The appearance of the sprayed graphite flakes on the specimen surface is given in Figure 2.6.

When a multicrystalline block of a solid lubricant with lamellar structure such as graphite or MoS_2 is forced onto a flat surface, the platelets detach from the block and they deposit on the surface as a flat layer [29]. The coefficient of friction (CoF) for graphite is about 0.1 when it is forced parallel to the lamellas; but if it is forced perpendicular to the lamellar structure, the CoF of graphite becomes about 0.3 [29].

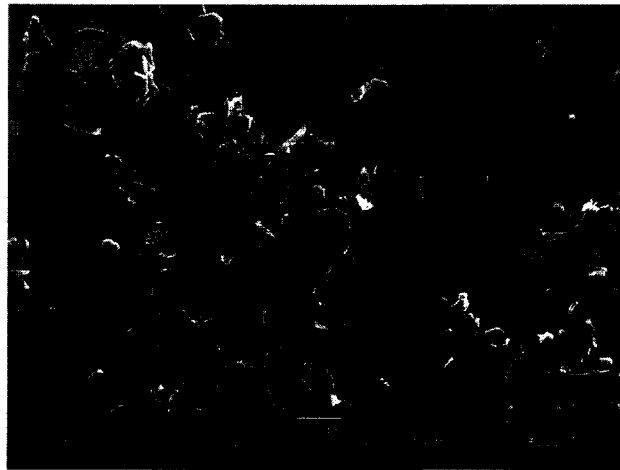


Figure 2.6. Appearance of the sprayed graphite flakes on the specimen surface.

When samples were involved in surface interaction, graphite particles both were swept/forced into the reservoirs. When they were entrapped between the counterface and the surface, they smeared on the surface as a layer which was parallel to the surface (Figure 2.7). This layer of graphite was expected to provide lower coefficient of friction values.

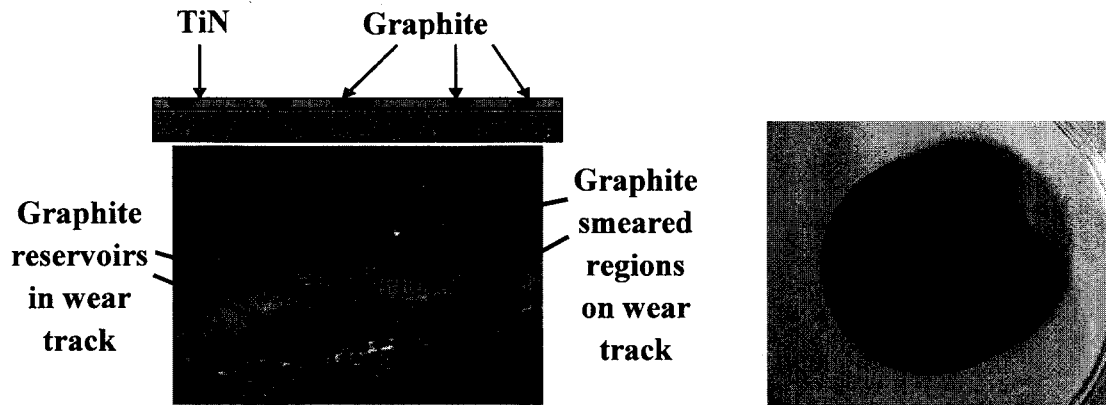


Figure 2.7. Filled reservoirs (with graphite) after sprayed graphite particles forced into the reservoirs (on the left) and graphite sprayed steel sample with wear tracks (on the right).

During the course of attempts to increase the area coverage of the reservoirs on the coating, a modified “*dipping*” process was devised; this method is described below. The reported friction-wear test results involving the micro-beading method use primarily the spray technique. Nevertheless, several turning tool inserts were applied micro-beads by dipping method. Samples labeled as *lower density* were fabricated by spraying micro-beads, whereas samples labeled as *higher density* were fabricated by submerging the insert into a bead-ethanol suspension.

In the dipping method, substrates were submerged into homogeneously mixed bead-ethanol suspension by means of a perforated container which lets the mixture flow in and out (Figure 2.8). Micro-beads settled onto the surface of the substrates due to gravity and samples were drained without disturbing bead settlement. Excess ethanol evaporated quickly and beads became immobilized with their layout fixed. TiN was then deposited on the samples by magnetron sputtering as previously stated.

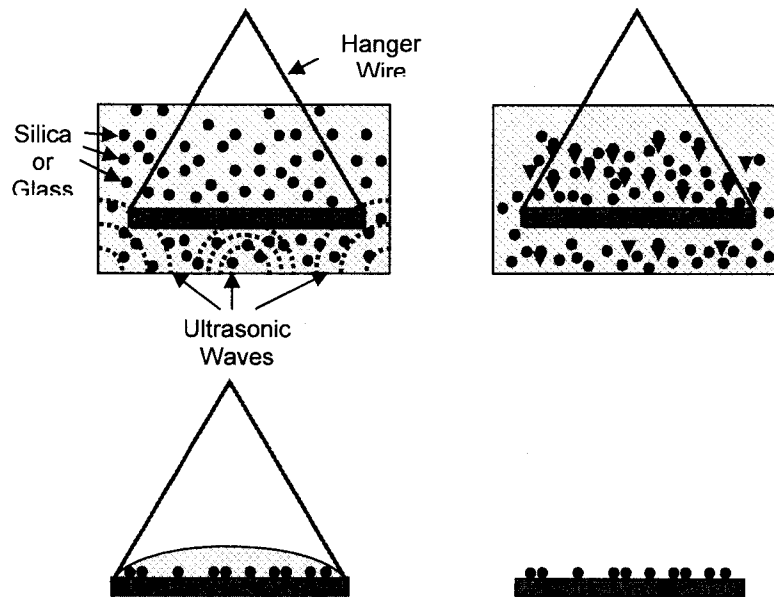


Figure 2.8. Schematic explanation of the “*Dipping Technique*”.

II. 2. Coating Deposition

The coating system used was a custom-designed and custom-made magnetron sputtering chamber incorporating power, vacuum, heating and mass flow-meter and cooling units (Figure 2.9). The base vacuum level was about 5.0×10^{-7} torr, which is in the range of a “*high vacuum*”. Before deposition, a rough vacuum is first reached by a mechanical pump (up to 1.0×10^{-1} torr); then high vacuum levels are achieved by a turbo pump as shown in Figure 2.9. The system has a deposition rate monitor next to the substrate holder (Figure.2.10.). The coatings applied in the scope of this thesis are TiN, amorphous carbon, indium, with the majority of them TiN. A typical setup for these depositions uses two titanium targets to achieve maximum deposition rates, argon as the sputtering gas and nitrogen as the reactive gas. A heating rheostat unit embedded in substrate holder is used for high temperature depositions (Figure 2.10. and Figure 2.11.). Details of the different sample types and the deposition conditions are given in Table 2.1.

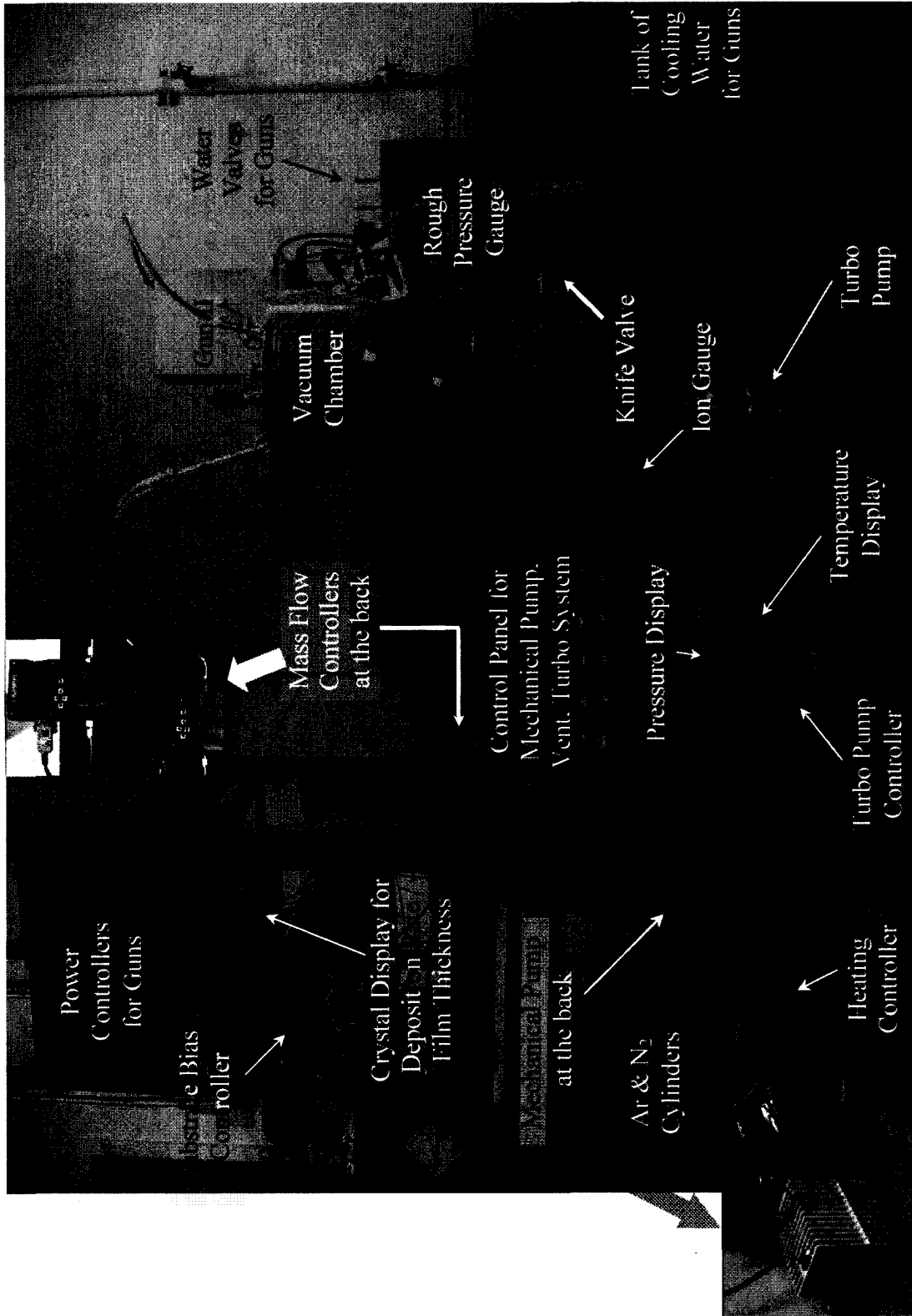


Figure 2.9. Magnetron sputtering system.

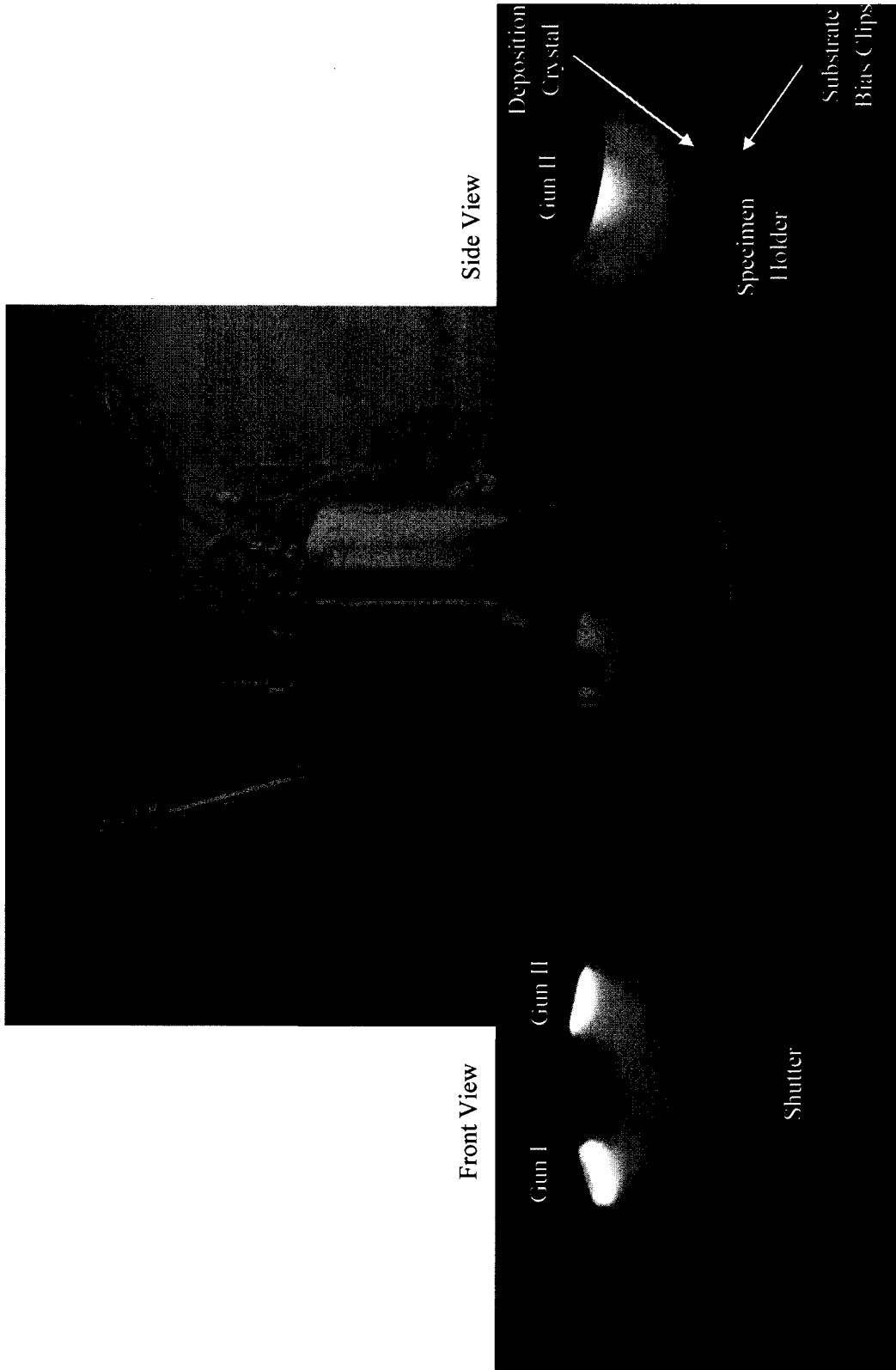


Figure 2.10. Magnetron sputtering chamber with front and side views during deposition.



Figure 2.11. Substrate holder of the magnetron sputtering system with two of the 440C stainless steel and a silicon sample after TiN coating.

Table 2.1. Samples and Deposition Conditions used in the scope of this thesis.

Samples	Size	Targets	Vacuum Level/ Deposition Gases	Temperature, °C	Bond Layer	Deposition
Stainless Steel (440C or 316 type)	φ25 mm or φ35 mm	2 Ti	<i>Pressure before any deposition</i> $< 5 \times 10^{-6}$ torr <i>Deposition Gases:</i> Ar: 20 sccm N ₂ : 2 sccm	300	2 Ti targets with 100W and -50V substrate bias, 30 nm thickness	185 W for 2 Ti targets, -150V substrate bias, 75-120 min deposition time depending on the thickness desired (0.7-1.5 μm)
Silicon, first batch	2cmx2cm squares			200		
Silicon, second batch	2cmx2cm squares			150		
Carbide Turning Inserts	SPG422 type			300		

II. 3. The Friction-Wear Tests

A schematic view of the pin-on-disk friction-wear tester is shown in Figure 2.12., and the picture of the system is shown in Figure 2.13. The counter-face used for testing was a 6.35-mm diameter ball. Depending on the purpose of the test, the ball was chosen from different materials, including stainless steel, alumina (Al₂O₃) or aluminum. There were several rotational speeds and weight options. The majority of the tests were performed at 200 rpm and with 1 N dead load on the ball. Several other tests were performed at 200 rpm speed with 2.2 N dead load or at 67 rpm with 0.5 N dead load.

Higher loads are employed to determine the strength of the coatings or to examine the performance of lubricants under higher loading conditions, but most of the time the load was chosen to get comparable wear amounts within reasonable time periods. The lubricant properties and tribological behavior of the solid lubricant materials can be affected by the humidity level of the environments as previously mentioned in Chapter 1. For instance, MoS₂ is a very good lubricant in a space environment where there is no air and humidity; but it loses these good properties in a short period of time under humid air environments [30,31]. Substantial research has been conducted to solve this problem. The reverse of this problem is true for graphite: while it is a good lubricant in a humid environment, it cannot provide its low friction in dry environments [29-31]. Because the tester is in a closed chamber, the humidity level can be adjusted in a range of 25%-65% relative humidity (RH) levels. In the scope of this thesis, the humidity level was kept low at 25% relative humidity for most of the experiments in order to obtain comparable results. Dry air or nitrogen gas was used to decrease the humidity if the room humidity is higher than 25% RH. Several high relative humidity experiments have been performed to observe the characteristic behavior of the graphite; the humidity increase was provided by a glass container with deionized water agitated with dry air bubbles.

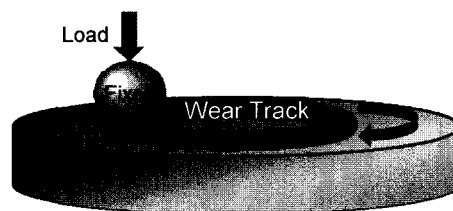


Figure 2.12. Schematic view of the pin-on-disk friction-wear tester.

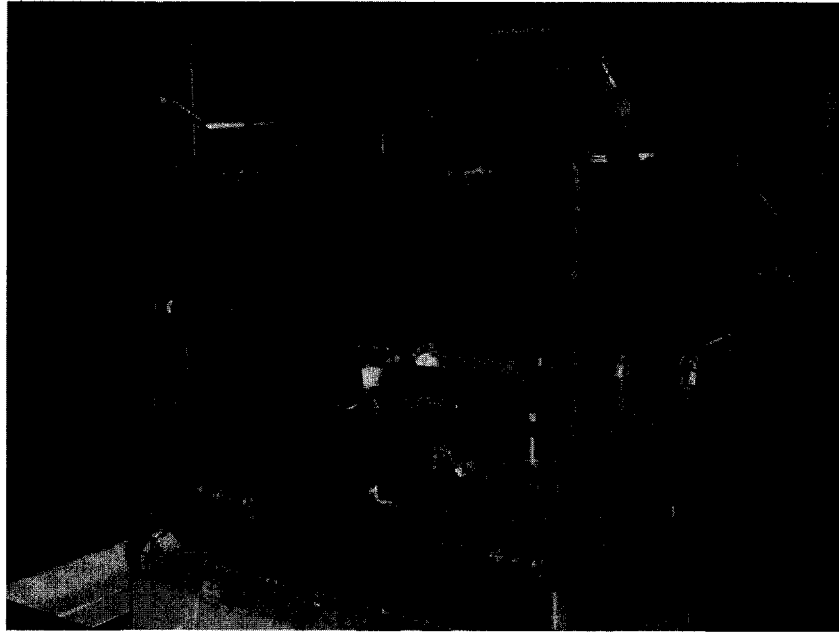


Figure 2.13. Friction-wear testing chamber.

II. 4. Microscopic Inspections

Optical microscopy was used at every stage of this study:

- Observation of bead settlement on specimen surface after spraying beads,
- Control of reservoir formation after coating and sonication,
- Observation and evaluation of wear and the function of reservoirs to compare specimens after friction-wear tests.

Optical microscopes can provide micrographs with magnifications up to 1000x. When higher magnifications or high depth of field images were necessary, scanning electron microscopy (SEM) was used. The thickness measurements of the thin films, flat or tilted cross-section and surface appearance inspections of the films with reservoirs were carried out using an Amray 3300FE SEM. For thickness measurements and cross-section inspections, silicon substrates deposited together with the other specimens were scratched on the back side with a diamond scribe and broken into two pieces; one of the broken

pieces was placed in a vertical inspection microscope holder. Flat surface inspections were performed on the whole specimens glued on a SEM 1-inch diameter stub with conductive silver or carbon paste. In the scope of this study, the accelerating voltage used for the Amray 3300FE SEM was 7,000 V. Magnifications used depended on the feature sizes of the coatings examined, and were typically in the range of 50x-50,000x.

II. 5. Machining Tests

One common and wide application area of tribological coatings is machining tools and inserts. The performance of the coatings with reservoirs developed at our laboratories were also evaluated under turning conditions. A schematic representation of an insert during machining and a SEM picture taken after machining are given in Figure 2.14. These tests were performed at McMaster University Laboratories under the supervision of Dr. German S. Fox-Rabinovich and Prof. Stephen C. Veldhuis. The coatings on the SPG422 type turning inserts were deposited in our laboratory using the equipment described in Section 2 of this Chapter. The rake face of the turning inserts was beaded with either the spraying or submerging beading techniques. The inserts were then coated with their rake face on top by magnetron sputtering similar to the case of stainless steel substrates. Machining tests were conducted on a Nakamura SC 450 turning center either with or without cutting fluids.

The work material cut was AISI 4340 steel with a hardness of 50 HRC. The cutting speed was chosen as 180 mm/min as it could provide traceable wear rates with comparable tool lives. The feed rate was 0.11 mm/rev and axial depth of cut was 0.25 mm. The progress of the wear at the flank of the tool inserts were measured

intermittently. A SE micrograph of a sample with flank wear is shown in Figure 2.14; a typical flank wear vs. testing time curve is shown in Figure 2.15(a) with a schematic representation of the flank wear in Figure 2.15(b).

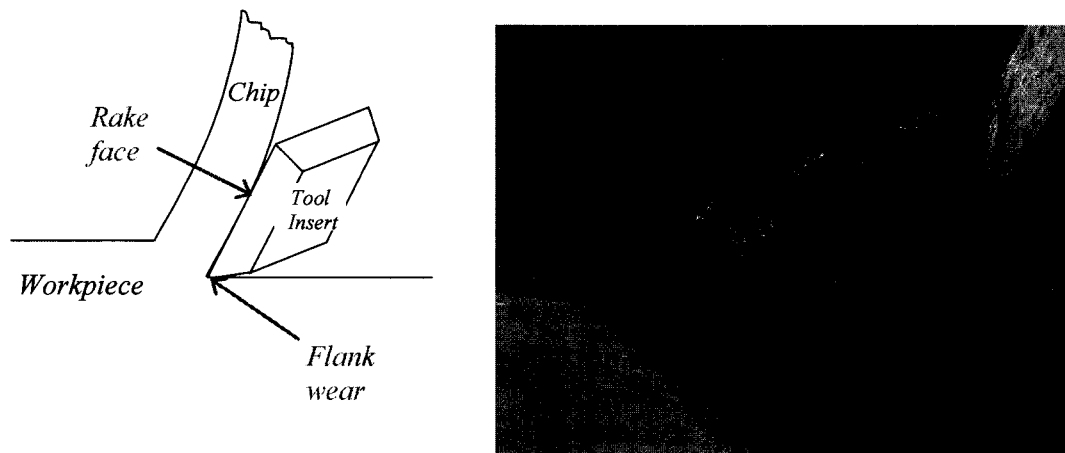


Figure 2.14. Schematic view of the turning insert while machining, on the left; a SE micrograph example of a worn tool insert from this project, on the right.

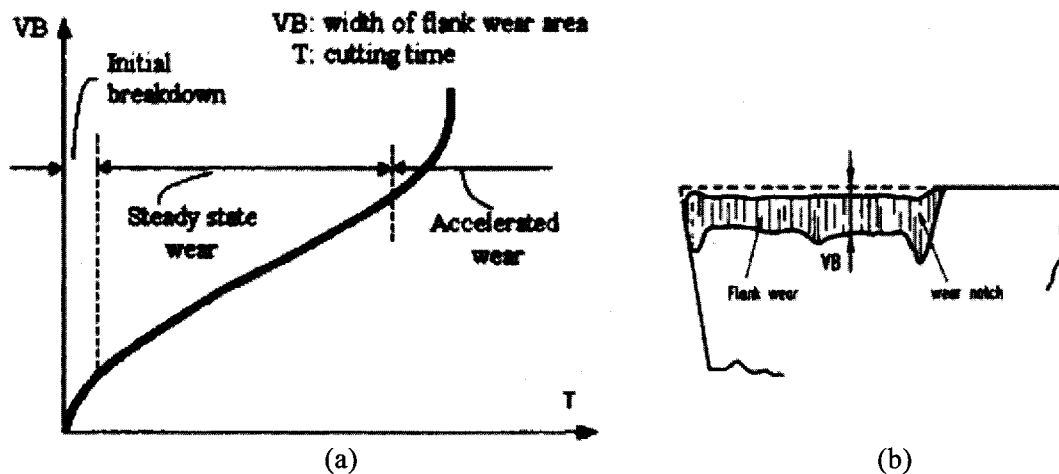


Figure 2.15. (a) Sample flank wear graph showing important stages of the tool wear from Ref.[32], (b) schematic representation of the flank wear on a tool from Ref. [33].

During machining, some samples of the chips were also taken for inspection. Wear marks on the surfaces of tested tool inserts were also evaluated by JEOL JSM-7000F SEM equipped with an EDS (energy dispersive spectroscopy) unit at McMaster University by the same research group.

II. 6. Machining Simulation Tests

The effect of temperature on the surface interaction of some chosen coatings and work material was investigated. A special apparatus designed to simulate the heavy adhesive interaction at the tool-workpiece interface was used for these tests. It is known that adhesive interaction controls wear performance during cutting as explained in Ref. [34].

A coated pin sample of the tool material (cemented carbide with hard coating) was rotated between two polished work material samples (Figure 2.16 [34,35]). The workpiece material (steel 4340) was heated to different temperatures in the range of 150-1200°C. A normal load which causes plastic strain in the contact region was applied to the pins. The shear strength of the adhesive bonds between tool and the work material (τ or τ_m) was recorded. The ratio of this strength to the normal stress applied (P_m) is defined as “*coefficient of friction*” (CoF) in this work (Equation 2.1). This value can not directly be compared to CoF values obtained from traditional pin-on-disk friction-wear testing values. In Ref.[34] it is proposed that when the CoF calculated here is equal or higher than 0.38-0.35, seizure occurs between contacting couple. Accordingly, it is better for a tribo-couple to have a lower CoF value to be far from seizure [34].

$$CoF = \frac{\tau}{P_m} \quad (2.1)$$

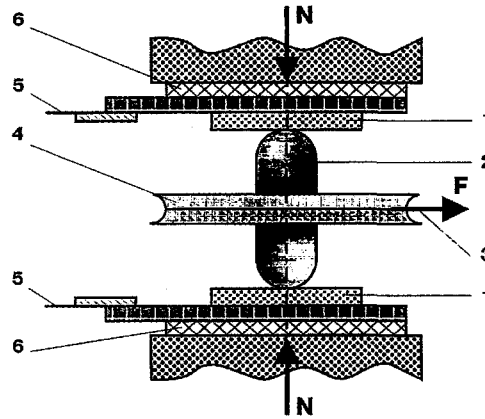


Figure 2.16. Schematic view of the equipment used to simulate adhesive conditions at machining (1: Workpiece material, 2: Sample made of tool material, 3: driving rope, 4: driving disc, 5: electrical contact wires, 6: isolation system (Ref. [34,35])).

II. 7. X-Ray Photoelectron Spectroscopy (XPS)

Film composition analyses on some of the selected samples were performed with XPS on a Kratos Axis HS XPS instrument using a MgK_{α} X-ray source. In order to clean the surfaces from contaminations and to obtain film composition, samples were first ion etched with Ar^{+} ions for 10-15 min. Calculations of atomic percentages were carried out using the relative sensitivity factors supplied with the Kratos instrument software. Typical film composition obtained when reactive TiN deposition was performed is 55% Ti, 43% nitrogen and 2% oxygen. Composition evaluations were periodically conducted on Si wafer substrates coated along with steel and turning tool insert samples.

Some chosen turning insert samples were also analyzed after machining with the XPS system. On these samples, film composition determination and depth profiles were carried out. The x-ray source used was also MgK_{α} operating at 15 kV. Depth profiles were conducted by ion etching at 4 kV and 10 mA for steps of 1-10 minutes. Scans were run at a pass energy of 160 eV and a step size of 1 eV. XPS results from regions on the

rake surface, but away from the cutting affected zone, were obtained for comparison. These regions were etched and depth profiles of the traces of the surface elements were followed.

II. 8. Other Techniques

There are also some techniques which were used occasionally in the scope of this thesis. One of them is X-ray diffraction analysis which was used to determine the structure of the films. This analysis showed that TiN coatings deposited in this study had a B1 rocksalt type structure. The typical hardness of the TiN films deposited at 300°C was determined by nano-indentation using a Berkovich indenter, and was found to average 19 GPa.

CHAPTER III

FABRICATION OF HARD COATINGS WITH EMBEDDED SOLID

LUBRICANTS BY MICROBEADING AND TRIBOLOGICAL EVALUATIONS

The objective of fabricating tribological coatings with embedded solid lubricant reservoirs is to form or to help/support the formation of a sustainable protective and/or low friction interface on the hard coating. A technique, “*Microbeading*”, devised in our laboratory [11,12,28] was used to introduce solid lubricant pockets to the coating structure as described in Chapter 2. This method was further developed to decrease the agglomeration and to increase the area coverage of the microbeads. In addition, the effects of the various sizes of the reservoirs, counter-faces and solid lubricants on the friction and wear resistance of the coatings were investigated.

III.1. The Micro-beading Method and Agglomeration Effects

The Microbeading method was outlined in chapter 1. The first step in this method is to spray a solution containing microparticles onto the surface of the substrate. However, agglomeration of the micro-particles often occurs before the ethanol is evaporated (an example is shown in Figure 3.1). It is not clear whether these particles had already are already agglomerated in the spray droplets in which they are being carried, or if they agglomerate on the surface after spraying. While the use of an air brush with an

adjustable air flow to the system brought about better spraying control, it was still unlikely that the fine mist created would carry only one bead per droplet with this system.

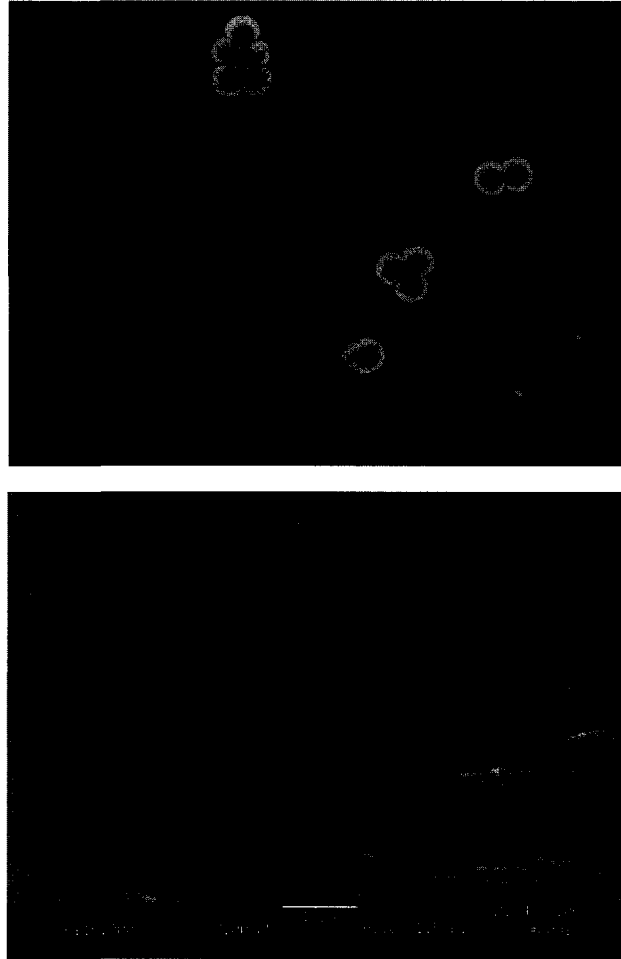


Figure 3.1. SEM pictures showing the agglomeration on a 1.5 μm sized particles sprayed sample (after TiN coating).

Dispersed particles in a liquid media have natural tendency to agglomerate [36]. There are attraction forces between particles traveling in the liquid [36]. The total surface energy decreases with a decrease in surface area, and as a result multiple particles adhere and form a clump. Because the surface to volume ratio increases with the decreasing size of the particles, the severity of the agglomeration problem is likely to increase. Therefore, the most severe agglomeration cases have been observed on the specimens that were

sprayed with 1.5 μm beads; and severity decreased through 5 μm then 10 μm beads (Figure 3.2.).

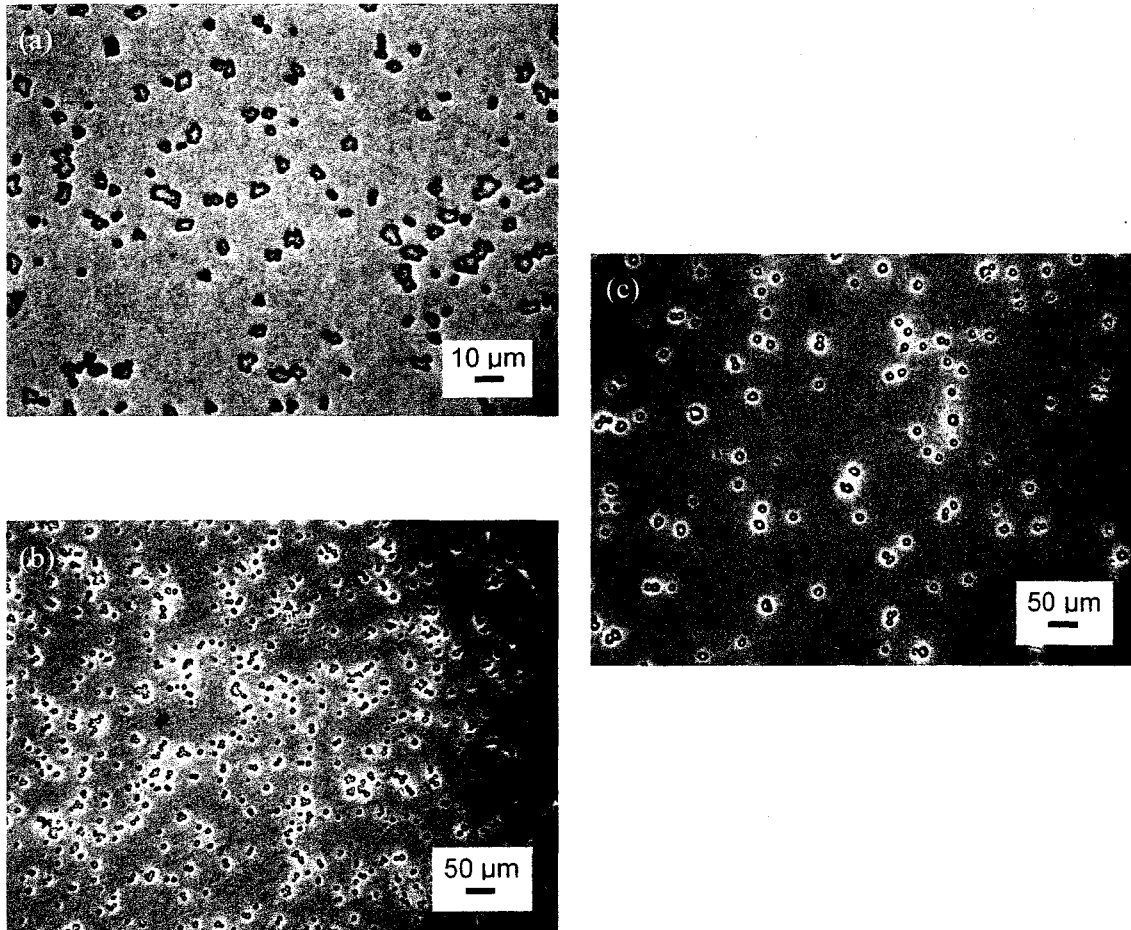


Figure 3.2. Optical micrographs showing agglomeration for a: 1.5 μm beads-, b: 5 μm beads-, c: 10 μm beads-sprayed sample. Pictures were taken after beads were removed from coating.

The water present in the sprayed ethanol-microbeads mixture was found to delay the evaporation substantially, increasing the agglomeration of the micro-beads. Before this was realized, the mixtures were prepared from 50mg/ml dense water suspensions provided by G.Kisker GbR. Therefore, we decided to evaporate the water from the suspension on a hot plate to reduce water content in the spray mixture. Later, dry borosilicate glass particles from Duke Scientific Corporation were used to prepare the

spray mixtures. Previously, the spray gas used was pressurized air provided by a compressor; to avoid moisture contamination to the spray mixture, we changed to pressurized argon. Additionally, because the evaporation rate is important when spraying, all the spraying parameters such as gas pressure, flow rate of the mixture, air gun speed passing over the sample were adjusted to promote formation of a fast evaporating thin liquid film on the sample which would not allow particles to migrate and gather. As a result, some improvements with better homogeneity were obtained; although further improvements are still needed.

Adding surfactants to carrier mixture is a common conventional solution to agglomeration problem. However, any chemical residue may affect the adhesion of coating to substrate surface, which is vital to good coating performance. Therefore no research on application of surfactants was done in the scope of this thesis.

III. 2. Results and Discussion

III.2.1. The Results for Specimens without Reservoirs

Initial testing was conducted to establish a reference using the pin-on-disk (POD) tests on the samples with no coating and the sample with TiN without reservoirs; the tests were conducted with an alumina ball as a counterface. Tests results are given in Figure 3.3 as friction coefficient against number of cycles. The friction coefficients (FC) obtained for stainless steel substrate is in the range of 0.5-0.6. TiN coating in the dry condition (without lubricants) gave a friction coefficient value of about 0.3-0.4. When graphite lubrication was applied, the FC decreased to a value about 0.2. The optical microscopy picture of the wear track after the test with graphite is shown in Figure 3.4.

Most of the graphite was swept away from the wear track, yet occasionally we observed a crater formed in the wear track that functioned as a lubricant reservoir (in terms of storage and replenishment of graphite.) This demonstrates the concept we are pursuing that involves using patterned surfaces that will provide lubrication in a more controlled manner than relying on coating defects or surface roughness to act as lubricant reservoirs.

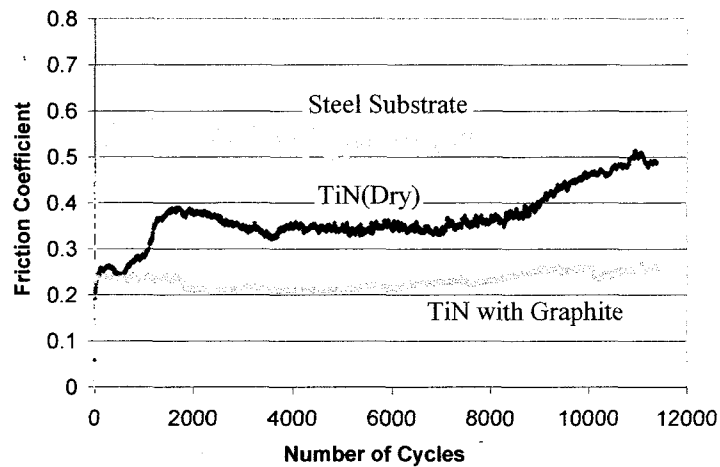


Figure 3.3. Reference pin-on-disk tests performed on the plain stainless steel substrate, TiN coating without any reservoirs or lubricant, and with graphite lubrication.

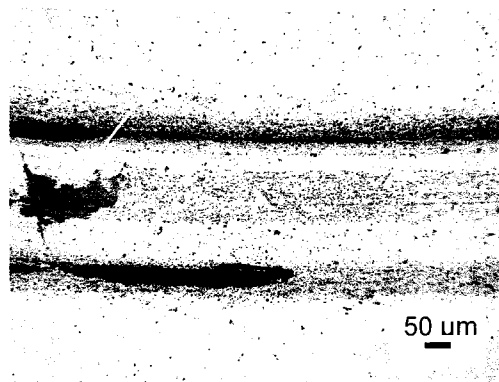


Figure 3.4. Optical micrograph of the wear track after the test on TiN with graphite lubrication. Coating failures can behave as reservoirs that store and replenish graphite.

III.2.2. Results for the Tests with Graphite Lubrication and Various Reservoir Sizes

Pin-on-disk tests were performed on the coatings with 1.5 μm , 5 μm and 10 μm reservoir sizes with and without the use of lubricant. In Figure 3.5, representative friction curves are given for many of the specimen tests.

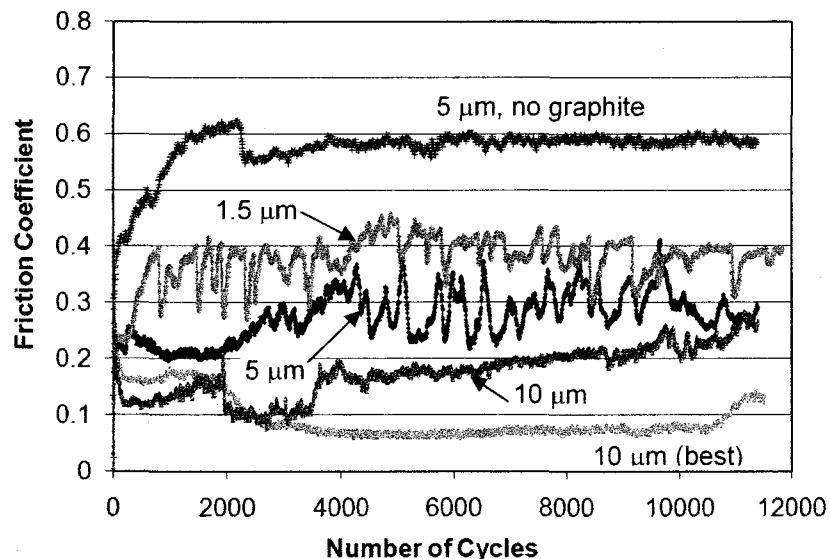


Figure 3.5. Pin-on-disk results for various sizes of the reservoirs: highest curve belongs to dry test (no graphite) others are all with the graphite application.

When coatings with reservoirs were tested without graphite, the friction coefficient curves of all type of reservoirs show similar results to the curve of coating with 5 μm reservoirs. Most likely the coating wears through soon after the interaction starts. This suggests that the existence of the reservoirs decreases the integrity of the coating when there is no solid lubricant.

When graphite lubrication applied, in the case of 1.5 μm reservoirs, the friction coefficient is about 0.4, which is similar to dry TiN. As can be seen in Figure 3.2, in the case of 1.5 μm reservoirs, there is agglomeration that results in the formation of wide reservoirs. For 1.5 μm beads, the coating thickness is also limited to 0.5-0.7 μm , which would result in shallower reservoirs. Because of extensive agglomeration, the reservoirs

are large yet shallow for 1.5 μm beads, which would not seem to be effective in storing and replenishing of the graphite. When the tracks were evaluated after the test, it can be seen that they are not worn through as in the case of dry TiN; there are cracks in the coating but also the reservoirs are still present as shown with arrows in Figure 3.6(a).

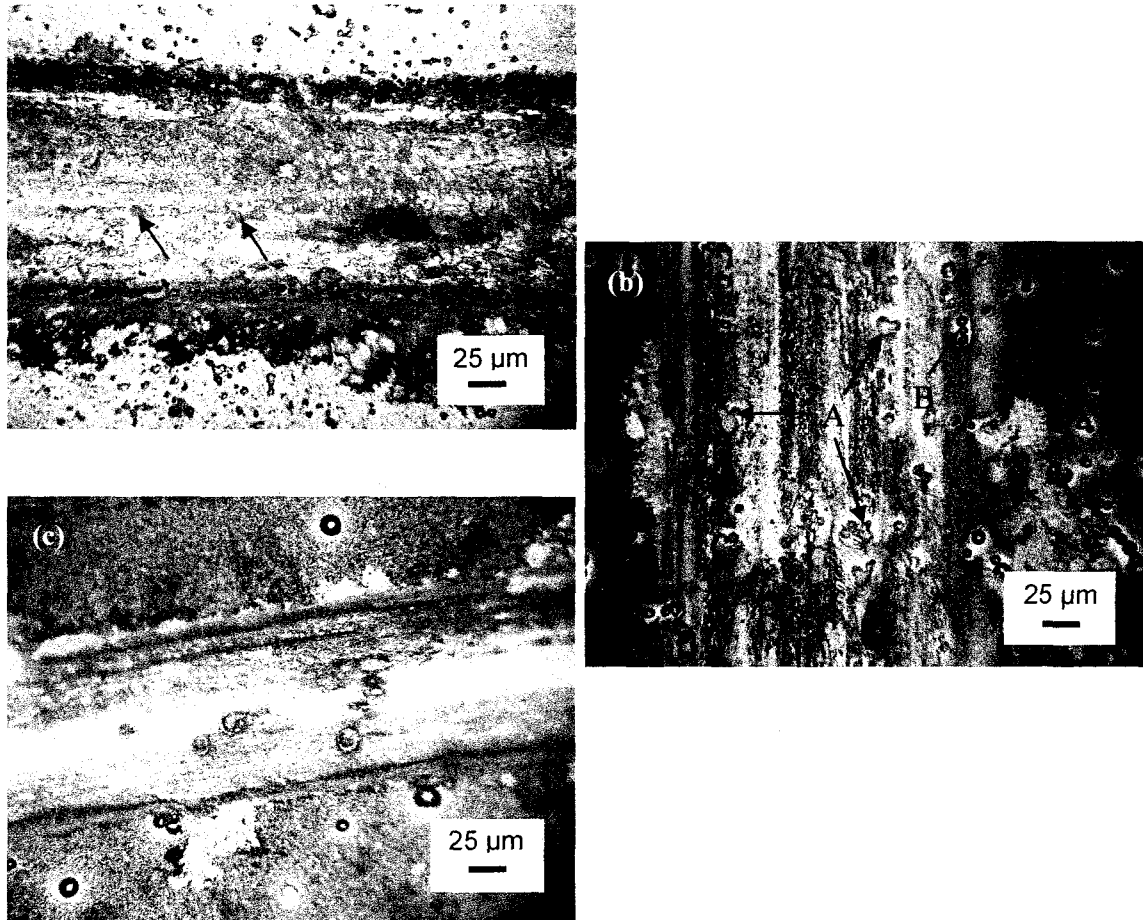


Figure 3.6. Optical image of the wear tracks after POD test on coatings with (a) 1.5 μm , (b) 5 μm , (c) 10 μm reservoirs. In (a) there are still filled holes despite the damages, in (b) filled holes (A) in the track and the empty holes (B) at the edge of the track are marked.

For 5 μm reservoirs, the FC is about 0.3 which is slightly lower than that of 1.5 μm reservoirs. When the wear tracks were examined after the test of the 5 μm samples, there were both worn through areas and areas covered with graphite. As in Figure 3.6,

one can identify filled reservoirs in the track. These images will be discussed further in section III.2.5.

The 10 μm beads (the largest size investigated) gave the lowest FC values, about 0.2. Repeated experiments showed some variation in results; for example the best result for the 10 μm case is shown in Fig. 3.5 and exhibits a FC near or below 0.1 up to about 11,000 cycles. The wear track after the test as can be seen in Figure 3.6 and shows a good spread of graphite on the track.

III.2.2.1. Area Coverage Study using 10 μm Beads In one attempt to increase area coverage of the reservoirs, the density of the bead suspension was doubled to 1 gram per 100 ml ethanol. An area coverage of 2.3% was obtained in comparison to a sample with area coverage of 1.4%, which was sprayed a mixture of 1 gram glass particles per 200 ml ethanol; however, agglomeration also increased. Wear test results for these samples are given in Figure 3.7. In detailed area coverage inspection of randomly taken optical pictures of these samples, *only 44% (68.5 holes) of the total reservoirs (156.5 holes) were single holes for the sample with higher area coverage, while 70% (143 holes) of the total reservoirs (204 holes) were singles for the sample with lower area coverage.* The substantial difference was in mostly number of triplet-holes on two samples subject to comparison.

Dry wear test results are similar to the 10 μm samples when comparing the increased area coverage. However, the sample with higher area coverage and more agglomeration could not maintain the low friction coefficient for a long time and the wear track was worn through at the end of the test. The sample with lower area coverage and less agglomeration kept the low friction coefficient for a longer period of time and it was

not worn through at the end. These results suggest that it is not only the size of the reservoirs, but their dispersion within the coating that is important.

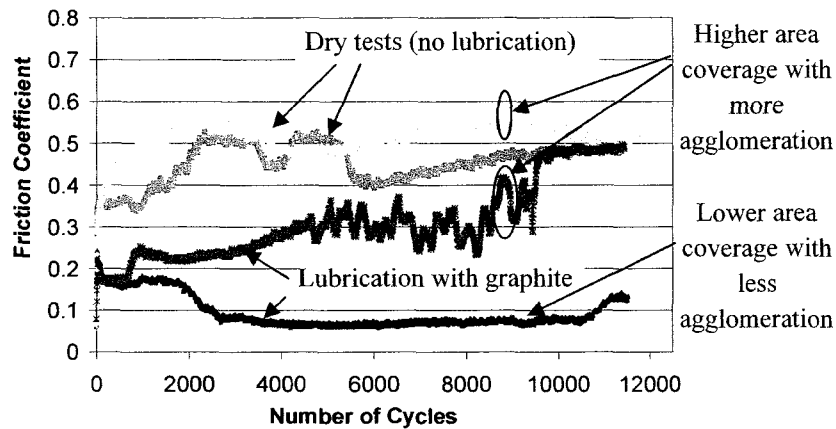


Figure 3.7. POD friction-wear test results for two 10 μm samples having two different area coverage and agglomeration levels (The unmarked dry test belongs to sample that has lower area coverage with less agglomeration).

III.2.3. Results for the Specimens with Sputter-deposited Carbon

The use graphite lubrication on samples with micro-reservoirs allows the graphite flakes to be swept along the wear track and fill the reservoirs. While this happens, the TiN coating wears (and possibly fractures) until the surface is covered by graphite. If the surface is covered by carbon before the coating fails, good frictional behavior can be obtained. Alternatively, a deposited carbon film should provide filling of the reservoirs before the surface interaction starts, limiting the need for in-situ filling of the reservoirs. To test this concept, TiN coatings with 10 μm reservoirs, were tested dry and with a carbon film. The curves are given in the Figure 3.8 for tests performed with an alumina ball. The carbon coating was deposited by magnetron sputtering. With this film, the friction coefficient curve starts around 0.1, then decreases to about 0.05 and stays at a slightly higher value until it starts to increase again at 40,000 cycles. Because this low FC was not observed with the graphite spray, this decrease can be attributed to the carbon

coating itself. Between 40,000 and 50,000 cycles FC increases to about 0.15, and then stays there for 10,000 cycles. It is proposed that during the increase (40,000-50,000 cycles) the carbon coating wears, and between 50,000 and 60,000 cycles the reservoirs become effective, as in the case of graphite spray samples in Figure 3.5. After 60,000 cycles, the coating failure occurs and the coating wears to the steel substrate.

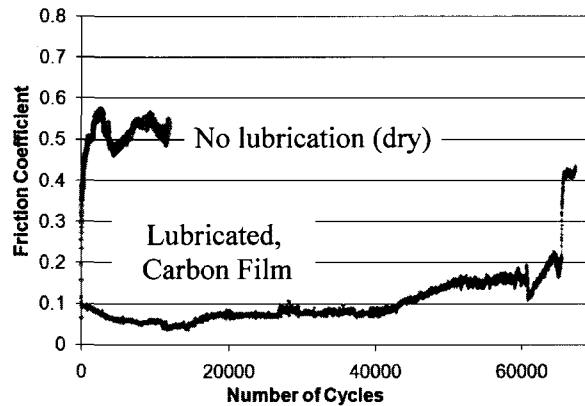


Figure 3.8. Pin-on-disk test results of a sample with 10 μm reservoirs with and without carbon coating.

III.2.4. Results for the Pin-on-Disk Tests with Aluminum Ball

In addition to the tests performed with alumina ball some additional tests were conducted with an aluminum ball on coatings with no reservoirs and 10 μm reservoirs. For these tests, high friction coefficient values were obtained for the tests done with and without reservoirs when graphite lubrication used (Figure 3.9). As a soft material compared to alumina, aluminum is worn from the beginning of test; debris of aluminum ball fills reservoirs together with the graphite. Aluminum is transferred on wear track; thus surface interaction occurs only between aluminum ball-aluminum on the track. Aluminum (or compounds of aluminum) in reservoirs and on the surface degrades lubrication provided by graphite. Therefore, high friction coefficients were obtained. No benefit of reservoirs was revealed (Figure 3.9).

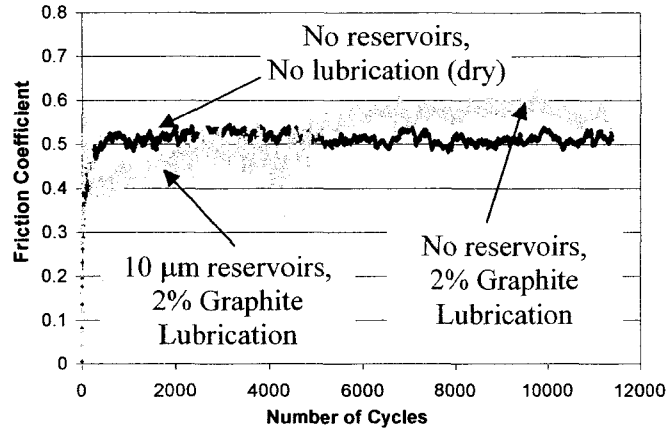


Figure 3.9. Pin-on-disk test results on a sample with no reservoirs (dry or lubricated with 2% graphite) and 10 μm reservoir sample with 2% graphite lubrication.

When carbon deposition was applied, the character of the wear tests changed as shown in Figure 3.10; the application of the carbon by magnetron sputtering is more effective than graphite. Although there were fluctuations, some decrease in FC (to a value about 0.2-0.3) was observed when carbon coated/no reservoir sample was tested with aluminum ball. The substantial decrease was obtained for the pin-on-disk test on the 10 μm reservoir sample after carbon sputtering; FC is about 0.1 for more than 8000 cycles.

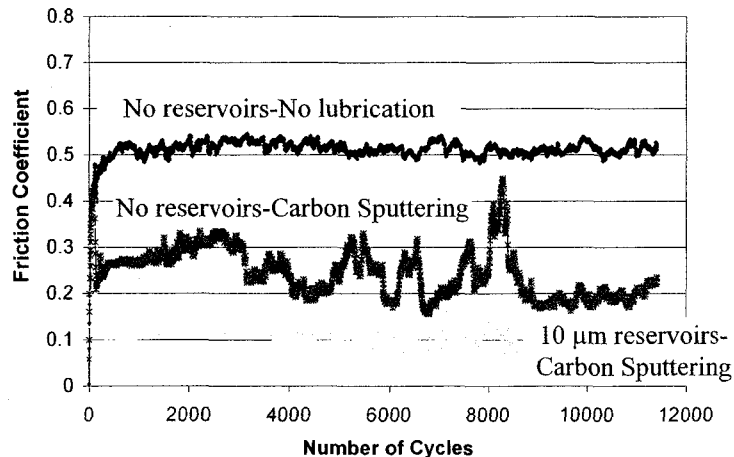


Figure 3.10. Pin-on-disk experiment results on no reservoir in dry and lubricated with carbon sputtering and 10 μm reservoirs coating with lubrication with carbon sputtering.

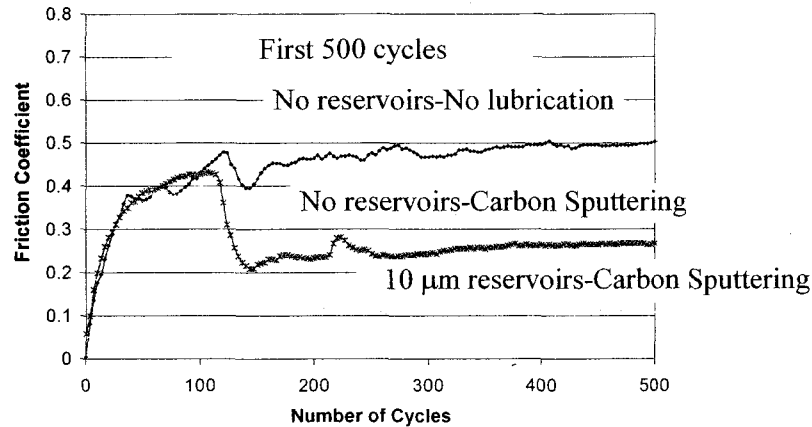


Figure 3.11. Detail of first 500 cycles of POD experiment results on no reservoir in dry and lubricated with carbon sputtering and 10 μm reservoirs coating with lubrication with carbon sputtering (Detail of the graph given in Figure 3.10).

When first 500 cycles were evaluated in detail (Figure 3.11), all three curves start with the same slope, they all increase to a FC of 0.4; after 100 cycles they differentiate. Therefore, in the beginning the behavior is independent of the substrate, and should be more related to the running-in process - initial wear on the aluminum ball. While of the sample with no reservoirs, in the dry condition continues to increase to about 0.5; samples tested with the carbon film show a decrease in the FC after first 100 cycles. A decrease occurs between 100-150 cycles, and the coating with no reservoirs stops decreasing at above 0.2 and then starts to increase again, while the coating with reservoirs drops to 0.1. Transfer films are most likely forming between 100 and 150 cycles. It is proposed that for the no-reservoir-sample the transfer film loses its effectiveness after 150 cycles, while the coating with reservoirs has more effective transfer film because of the replenishment provided.

III.2.5. Examination of the Wear Tracks

Pin-on-disk (POD) wear tracks were inspected after the tests to identify the stage of the wear in the tracks and to check if the solid lubricant had filled the reservoirs. Optical micrographs were taken to document wear tracks for future reference.

Three different characteristic regions were identified after the inspections on the specimens with the tracks after the tests with alumina ball and graphite:

1) A region outside of the interaction between ball and the coating surface; therefore both the coating and the graphite flakes were not affected. Graphite flakes on the surface appear randomly dispersed by spraying.

2) A region clear of graphite flakes, but the coating and the reservoirs seem intact and not filled with graphite.

3) The actual wear track which is typically 150 μm in width.

Inspection of the alumina ball revealed two different regions on the ball: a region in the middle with no visible transfer and the sides of this region covered with loose graphite particles. Therefore it can be deduced that the graphite flakes next to the wear track region were transferred to the ball.

The images of the wear tracks after the POD tests were shown in Figure 3.6. Figure 3.6 (a), showing the coating with 1.5 μm reservoirs, one can both see the filled holes and the cracks perpendicular to the track direction. Also there are some holes in the lower section that are not filled. The friction coefficient of this track at the end of the test was 0.33. Because the effective sizes of the reservoirs are big and the reservoirs are also shallow, it can be concluded that the lubrication observed in the track is not sufficient to protect the overall coating from damage and failure.

In Figure 3.6(b) the wear track after the POD experiment with alumina ball and graphite lubrication can be seen. The reservoirs in the track are filled as marked with “A” and reservoirs at the edge but outside of the track are not filled as marked with “B”.

Another important observation from some of the tracks should also be mentioned here that reservoirs may function better with some surface roughness on the TiN, because these can act as secondary smaller-scale reservoirs. The benefit of having higher surface roughness was emphasized before in studies on friction behavior of sputtered MoS₂ [37-38].

When the coating with 10 μm reservoirs (Figure 3.6(c)) was examined after POD test, it was found that the track was covered with graphite, both filling the reservoirs and smearing on the coating surface. The friction coefficient recorded for this track at the end of the test, which corresponds to this micrograph, was 0.14.

The wear tracks of pin-on-disk tests performed with aluminum ball and sputtered carbon were also inspected by optical microscopy. Some tests were repeated for a short time in order to understand the progress of the interaction. Figure 3.12 shows optical pictures from the tests on the specimen with 10 μm reservoirs: On the left, the wear track of the test conducted for a full period of time (Figure 3.10), on the right, the wear track after 2000 cycles can be followed. The loss of the carbon coating on the track after full period (8500 cycles) shows that almost all carbon around the reservoirs is gone. This can be followed in Figure 3.13 more detailed, but the reservoirs are still filled to provide lubrication and to keep the FC low. Figure 3.13 also shows the detail of the wear track of the 2000 cycles test. Again the reservoirs seem to be filled with carbon and there is a lot of carbon on the surface: some are smeared on the surface, some are in particle shape.

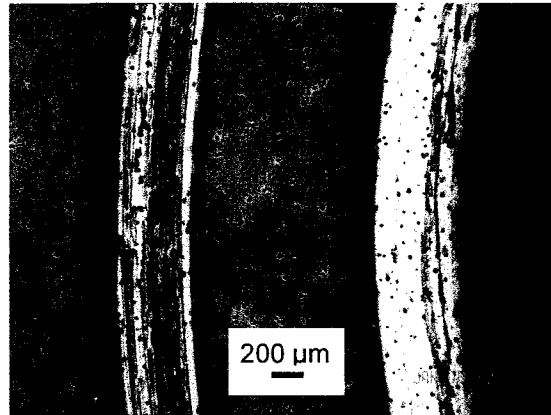


Figure 3.12. Optical views of the wear tracks of the POD experiments with aluminum ball and sputtered carbon coating lubrication after 2000 cycles (on the left), and 8500 cycles (on the right). The carbon coating around the holes was completely worn on the track after 8500 cycles.

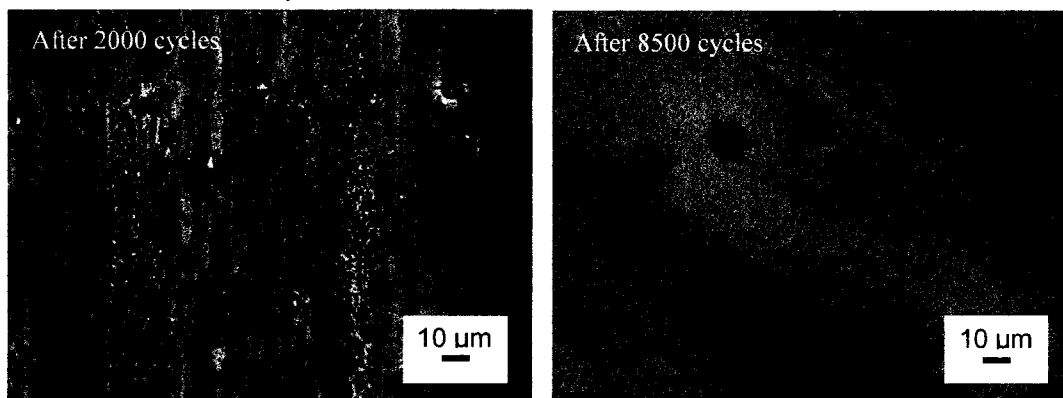


Figure 3.13. Optical views of the wear tracks of the tests performed with aluminum ball on the samples with 10 μm reservoirs and carbon coating (These views are from the same tracks in Figure 3.12, left track is the left one and right track is the right one).

III.3. Discussion

In this part of the study, a new method to form a hard coating incorporating solid lubricant has been further developed following the work of Zimmerman et.al. [11,28]. Previous methods applied to create composite coatings with reservoirs include photolithography [20], laser processing [17] and reactive ion etching [19]. Our newly developed method has some advantages over previous methods. It is likely to be more economical the methods listed above. Also, it avoids the cracks melted areas common to

the laser processing methods. Our new method, which is termed “*microbeading*” creates smooth transitions from the reservoir to the coating structure without any defects or cracks. Basically, the micro-spheres only act as placeholders on the substrate surface before coating. In this study the placement of the micro-spheres was performed by spraying these spheres in a solvent to the surface. Agglomeration of the micro-beads (especially for the smaller sizes) became a problem by increasing the effective reservoir size and by decreasing distance between reservoirs. This problem was reduced by adjustments in spray parameters such as gas pressure and sprayed liquid amount. Currently, the agglomeration is not a significant problem for 5 and 10 μm spheres but it is still a problem for smaller sizes. Smaller sizes create another problem: Because the micro-beads should not be buried into the coating, they limit the coating thickness by their radius. The practical sizes to be applied in this method should be larger than 3 μm . Suspensions with 22.5 μm -sized-beads (also commercially available) were also prepared to apply. However, because they are heavier than the others, it was not possible to retain a homogeneous suspension during spraying.

For the tests performed with graphite as a lubricant, a general behavior was observed: As the size of the reservoirs increases the friction coefficient decreases. In order to show this result quantitatively, average friction coefficients were calculated from each test. The overall average friction coefficient was also calculated for each reservoir size both for unlubricated and lubricated with graphite cases (Figure 3.14). In Figure 3.14, a small decrease was visible for the unlubricated samples. However, for the samples lubricated with graphite, a significant decrease in friction coefficient was observed as the applied bead size decreases. Results in Figure 3.14 are consistent with the optical

inspections of the wear tracks. The best lubrication was observed in wear tracks of the samples prepared with 10 μm beads (Figure 3.6(c)).

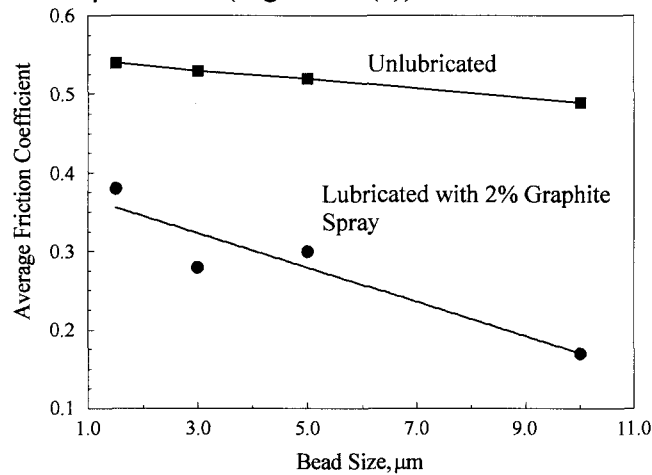


Figure 3.14. Applied bead size vs. average friction coefficient data for unlubricated and lubrication with graphite samples.

When 1.5 μm beads were used, the thickness of the coating applied is less than the others, because the removal of beads could become difficult or the beads could become buried into the coating. Another phenomenon is the higher severity of the agglomeration for this bead size. The resultant reservoirs are wide and shallow. These reservoirs are not effective in capturing and storing of the solid lubricant which is graphite particles within 2-15 μm size range. Other bead sizes used in reservoir fabrication are 5 and 10 μm . Among these 2 sizes, 10 μm ones gave better results; therefore 10 μm samples had the best performance of all samples. After careful considerations of the size and the cross-section of the reservoirs, it is reasonable to conclude that there should be an optimum size and aspect ratio or cross-section for the capture and the storage of solid lubricants. When graphite particles are used as solid lubricant there is an *in situ* lubricant filling into the reservoirs. Before this occurs, the reservoirs can act as locations where failure initiates. Therefore, the reservoirs (unfilled) are not generally beneficial to the mechanical integrity of the coating. Nevertheless once

the reservoirs are filled, it appears they are no longer failure initiators, and the mechanical strength of the coating is sufficient. The region around the reservoirs are mostly covered with lubricant, depending on the size of the reservoirs; if there is good coverage there is no direct contact between the ball and the hard coating (TiN). From the friction-wear test results together with optical evaluations of the wear tracks, a reason the 10 μm samples show the lowest friction could be that the 10 μm reservoirs perform best in capturing the solid lubricant. However it should be noted that this not necessarily a general result, but only for graphite. Each lubricant needs to be individually tested to determine optimal reservoir size. The reason for the good results with the sputter deposited carbon film could be related to lack of a need for *in situ* filling action, since the solid lubricant is already in the reservoirs.

How the reservoirs affect the overall coating integrity is important aspect of these coatings. Under dry conditions, all of the coatings show higher than expected friction; but when the holes are filled with the lubricant this weakness disappears. It is likely that the coatings, when run under dry conditions, wear through in the early stages of the tests due to the decohesion between coating and the substrate. Because high amounts of residual stresses are often a problem for sputter-deposited coatings, one may postulate that the existence of discontinuities should help relax stresses, therefore reduce the likelihood for decohesion. However, the reservoirs (especially the ones which are the result of the agglomeration of the beads), can cause stress concentration around their edges which would cause early failure under load. At this point it is not possible to conclude which of these effects dominate the behavior; but obviously there are several unfavorable effects of the reservoirs competing with the favorable ones.

When the wear tracks examined under optical microscope, almost all of the reservoirs appear to be filled with the solid lubricant. Nevertheless, statistically, the density of the reservoirs can differ from one track to another. Increasing the density of the reservoirs, which will mean to have more lubricant supplied per unit area, would be beneficial in order to further decrease friction and extend wear life of a coating. Some of the variations obtained in repeating similar experiments could be because of the probability of having more or less reservoirs in a single track. If the number of the reservoirs is not sufficient, the track even could fail before observing the benefit of graphite, because the behavior of the coating under these tribological conditions is more similar to dry contact between coating and the counterface.

The performance of the coatings with reservoirs created with micro-beading method depends on the materials involved, especially the solid lubricant. The solid lubricant should have some plasticity to be pushed into the holes; if they are not in the holes already as in the case of sputter-deposited lubricants. When a carbon coating is deposited as a film, its mechanical properties may vary; carbon coatings can be soft or hard. However, in both cases they have low friction coefficients. The most appropriate candidate as a solid lubricant here would be a soft material with a low friction capacity. Unfortunately, the number of known solid lubricants is limited. All have finite wear lives; some of them are vulnerable to oxidation, and some age over time depending on environment and surface interaction conditions [8]. The replenishment of solid lubricants is not as easy the liquid ones. The function of coatings with reservoirs is to provide dynamic replenishment during surface interaction, providing a period with low friction allowing the wear life of the component to be extended.

III. 4. Finite Element Model for Surface Interaction between

Composite Coating and a Pin

The interaction between a rigid sphere and a coating with reservoirs was modeled using a commercial finite element package, namely MSC.Marc Mentat. The sphere has 6.35 mm diameter and it is the counterface (ball) of a pin-on-disk friction-wear tester. Two dimensional (2D) models with a plane strain assumption of interacting sphere-coating system were designed to investigate the effects of reservoir size, i.e. reservoir profile on the stresses occurred during the interaction. Coatings with one of the three sizes of reservoirs (2, 5 or 10 μm) were taken into account for each model. The coating thickness is about 1 μm as in the actual samples.

The pin-on-disk test was simulated by calculating the stresses for different positions of the ball as the ball passed over the holes. This is a quasi-static simulation but neglects factors such as heat generation and plastic deformation. Nonetheless, it can provide useful insight into the nature of the stresses developed in the coatings during the surface interactions.

Models are 300 μm long and 16 μm (15 μm -thick-substrate and 1 μm -thick-coating) high. General views of models are shown in Figure 3.15. All of the models represent graphite-lubricated condition. Each model has multiple reservoirs in coating. Modeling on only one reservoir would neglect the effect of neighboring reservoirs and area coverage. Double and triple reservoirs were also added to 2 and 5 μm -models to represent profiles that are result of agglomeration. All profiles at each model were assumed to be the same, i.e. half cross-section of reservoirs.

Area coverage values of models are listed in Table 3.1. These values are in the range of possible area coverage values for each reservoir size. Area coverage obtained experimentally for 1.5 μm -sized-reservoirs is about 8-10%; and for 5 μm - and 10 μm -sized-reservoirs is about 1-2%. Because reservoirs are randomly distributed, area coverage values vary substantially from one point to the other in the microscale. It is assumed that the higher the area coverage, the higher the structural strains in coating. Therefore the lowest possible area coverage was applied to the model of 2 μm -sized-holes (representing 1.5 μm -sized-holes), in order to obtain least critical case for this size to compare with other sizes. For 5 μm and 10 μm , area coverage values differ slightly, because number of holes possible to incorporate in each coating model depends on the size of the reservoirs and to the length of the model.

Table 3.1. Finite element models and their area densities.

Reservoir size (μm)	Area density represented (%)
2	8
5	2
10	1.5

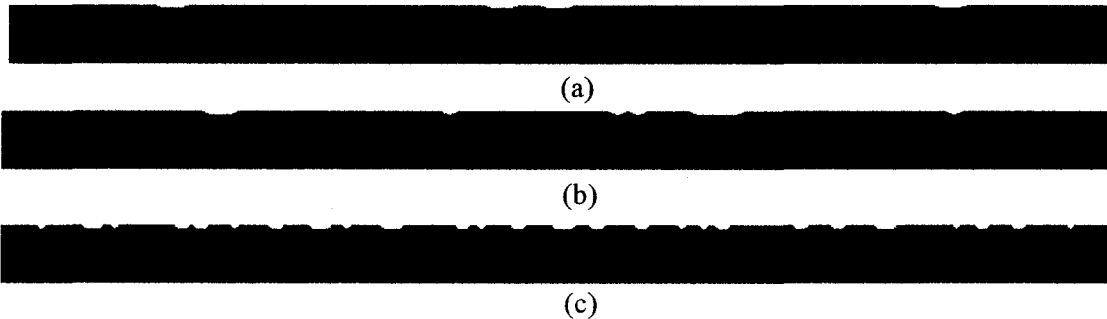


Figure 3.15. General view of model with: (a) 10 μm reservoirs, (b) 5 μm reservoirs, (c) 2 μm reservoirs (Views were taken from MSC.Marc Mentat).

Because deposition of the coating takes place in line-of-sight form in the magnetron sputtering technique, a shadowing effect of the beads on the surface defines the profile of the resultant reservoirs. Therefore the end profile of the reservoirs is a result of bead size and shadowing effects. This effect and the designed sample profile geometry are shown in Figure 3.16.

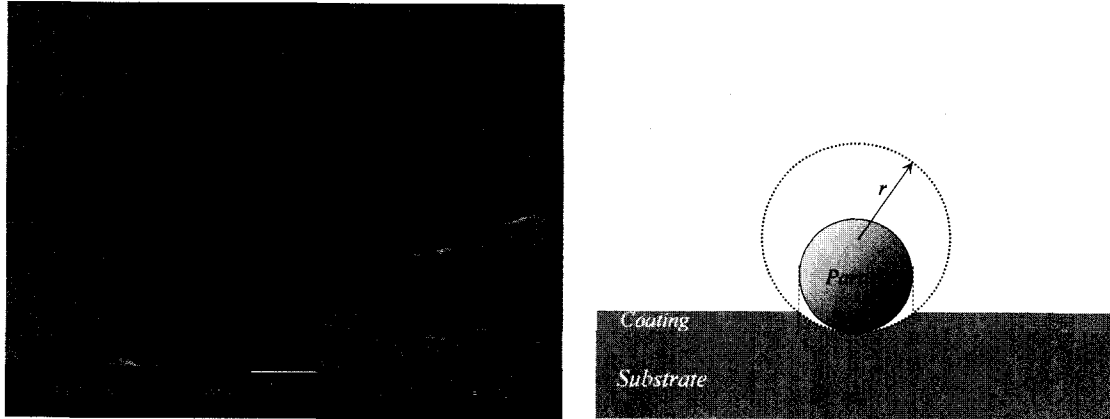
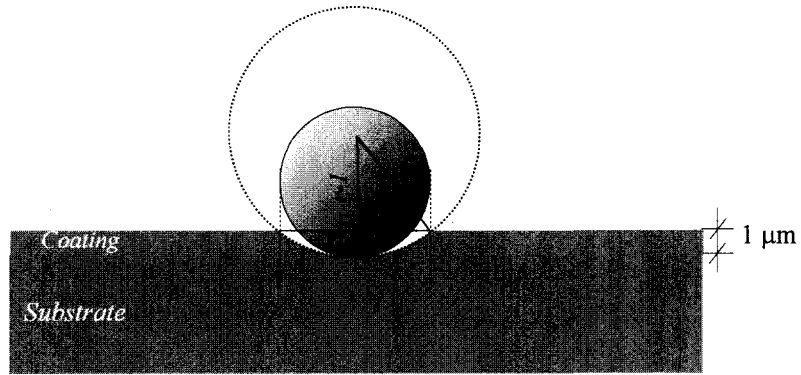


Figure 3.16. Geometry of the reservoirs in our models (on the right) designed according to the actual coating (SE micrograph is on the left).

III.4.1. Geometry of the Model Coatings with Reservoirs

In this section, details on the design process for a coating model with 10 μm reservoirs are reviewed. Shadowing effects change the reservoir geometry so that the opening of the reservoir has the diameter of the applied bead, but the profile actually follows a virtually larger sized bead whose diameter is defined by both applied bead size and coating thickness (1 μm). The model is schematically shown in Figure 3.17 with the calculation of the virtual bead diameter for 10 μm -sized-beads by using Pythagorean Theorem for right triangles.



For particle diameter of $10 \mu\text{m}$:

$$r^2 = 5^2 + (r - 1)^2 \Rightarrow r = 13 \mu\text{m}$$

Figure 3.17. Geometry of the $10 \mu\text{m}$ reservoirs and calculation of the virtual bead diameter.

The necessary angles for creation of this geometry in the MSC.Marc Mentat program are shown in Figure 3.18 with their calculations. The reservoirs are assumed to have an ($y = 2 \mu\text{m}$) opening of substrate at the bottom of the cross-section, which is in agreement to the micrographs of the $10 \mu\text{m}$ reservoirs. A sample of the end model with $10 \mu\text{m}$ reservoir opening is shown in Figure 3.19.

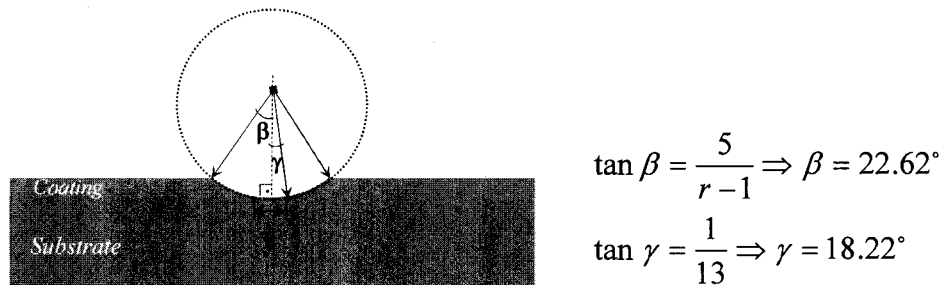


Figure 3.18. Calculations of the necessary angles used for $10 \mu\text{m}$ model.

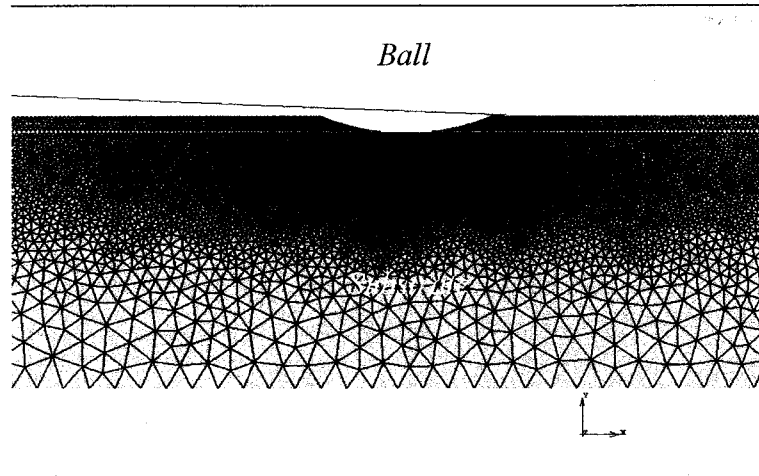


Figure 3.19. A view of the model with 10 μm reservoir diameter.

Models with 5 μm and 2 μm reservoirs were designed with the same approach keeping the coating thickness the same. Geometrical parameters defining all reservoirs are given in Table 3.2. Contours of a 2 μm and a 5 μm hole are shown in Figure 3.20 (a) and (b).

Table 3.2. Geometrical parameters defining holes designed in the model coatings.

Parameter	2 μm	5 μm	10 μm
Radius of the virtual circle	1 μm	3.625 μm	13 μm
β	90°	43.6°	22.6°
γ	14.9°	7.78°	18.2°
Y	0.513 μm	0.98 μm	2 μm

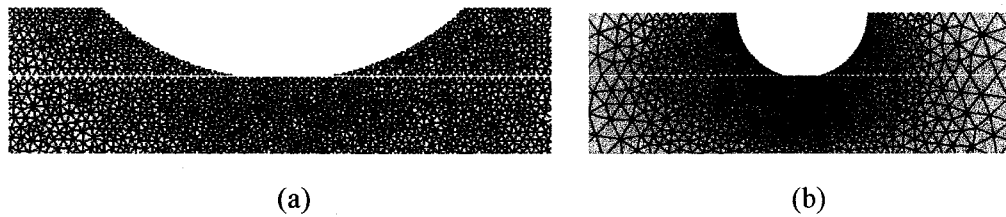


Figure 3.20. Profile of a hole for: (a) 5 μm -sized-hole (b) 2 μm -sized-hole.

III.4.2. Modeling of the Contact between Coating and the Counterface-Ball

For all models used for numerical evaluations, the ball was taken as a *rigid body* which has a deformed and worn shape of counter-face-ball-as shown in Figure 3.21. Bottom profile of the ball was modeled as flat. The length of this section is about 110 μm being comparable to the final width of wear tracks obtained experimentally. The coating was *deformable body* in the models. The actual geometry of the ball is comparably much larger than the modeled section of the coatings. Therefore, only the contacting section of the ball was plotted.

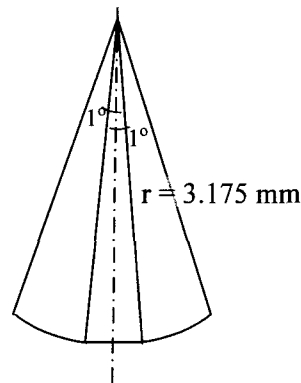


Figure 3.21. Geometry of the counterface-ball-in the models.

III.4.3. Material Properties Selected for Modeling

As the counterface was taken as a rigid body, no material properties were necessary for this component. Both coating and the substrate were modeled as isotropic elastic materials; for substrate material properties of 440C stainless steel was used; for coating properties of TiN was used. Necessary material properties are given in Table 3.3 [39,40]. Applied friction coefficient between the ball and TiN coating was 0.1 corresponding to graphite lubrication [29,41]. Here it is assumed that both surfaces were covered by graphite and friction takes place in graphite.

Table 3.3. Applied material properties in modeling.

Material	E (MPa)	ν
440C Stainless Steel	200,000	0.285
TiN coating	300,000	0.22

III.4.4. Boundary Conditions, Surface Interaction, and Evaluations

The left and right sides of models are symmetric in the x- and z-directions because the material continues in those directions by restricting displacements on side lines.

The modeled action starts with the application of a load of 1 N for a short time. The load is distributed on the bottom nodes. This load is kept constant during surface interaction and represents a dead load applied on pin-on-disc tester. The action of the ball is controlled by controlling its position during sliding. The boundary conditions applied are shown in Figure 3.22.

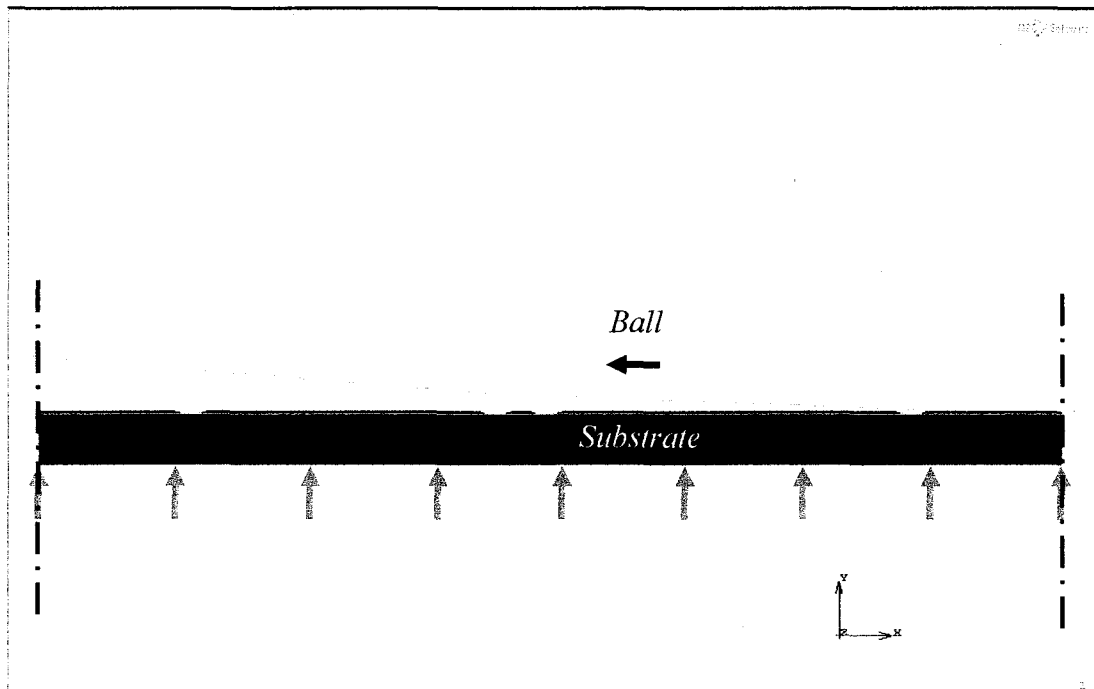


Figure 3.22. Symmetry axes and distributed load applied are shown on the model with 10 μm holes.

After solutions were performed by Marc Mentat, stresses at the bottom of holes on opposite side of ball action were collected for the entire motion (Figure 3.23). There is direct correlation between surface and hole bottom stresses. In fact, the highest stress components are expected on surface, because ball-reservoir interaction takes place on there. However, because the geometry of the ball and reservoirs were simplified, virtual instantaneous peaks are possible. Besides, it is reasonable to expect that after many repeated cycles of ball-coating interaction, there is a high probability of local catastrophic failure of coating to start from the shown locations. Because of the same geometric simplifications, quantitative levels of stresses are not meaningful; they have only comparative meaning. Comparisons of collected stresses of models were performed and results are given in the following section.

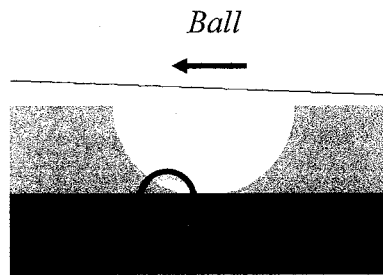


Figure 3.23. Location of stresses followed on a hole (with 2 μm opening size).

III.4.5. Results and Discussion

Compared holes are chosen to be analogues in terms of being single and being at similar locations in the models. Horizontal locations of these reservoirs are around mid-section of each model. Stress components taken into account are σ_{11} , σ_{12} and σ_{22} . σ_{11} is σ_{xx} , σ_{11} is σ_{yy} and σ_{xy} is shear stress. Positive axes directions for these stresses are shown in Figure 3.22. All stresses can be tensile or compressive depending on the position of the ball. Stresses at each reservoir vary in a wide range because of the action of the ball.

In Figure 3.24, shear stress curves belonging to one reservoir at each model are given. Here, we show only the parts of the curves where ball-hole interaction takes place. Higher shear stress levels are observed at hole bottoms, as hole size increase. The curves have U-shape with higher shear stresses at the beginning and the end of surface action. Applied stresses are balanced when the middle of the ball is interacting with hole surface; therefore stress curves has a minimum.

For comparison, the average stress and standard deviation was calculated for these curves, and the results are shown in Figure 3.25. Standard deviations were given as a representation of scatter around averages. The lowest average shear stress was calculated for 10 μm hole with a lower variation in values around average.

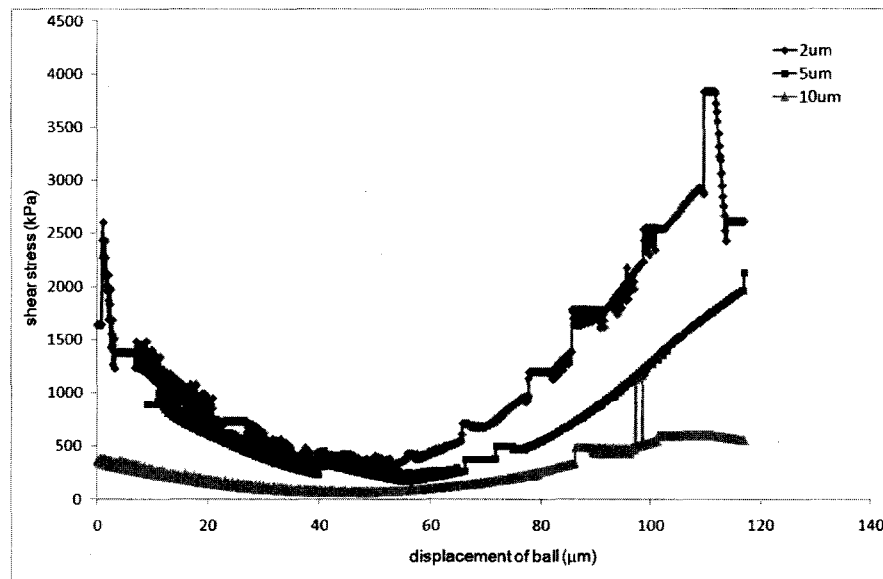


Figure 3.24. Shear stresses (σ_{12}) at bottom of holes while ball interacts with this hole.

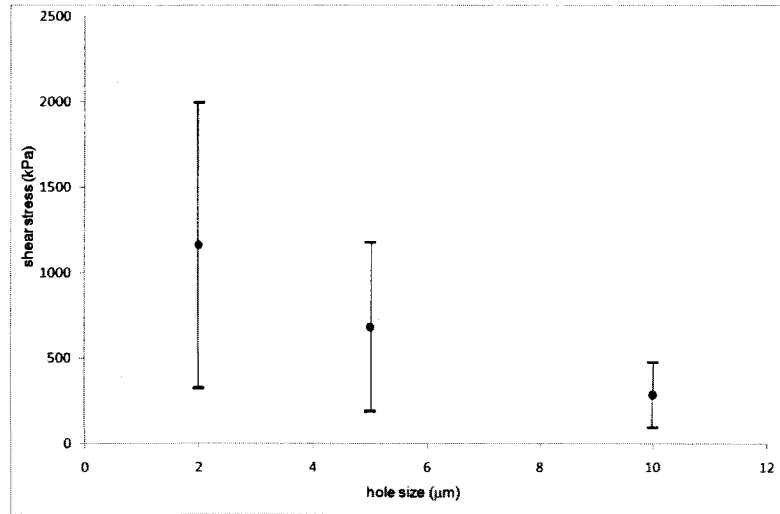


Figure 3.25. Average shear stress values (σ_{12}) with upper and lower limits during ball-hole interaction.

σ_{11} and σ_{22} show a similar characteristics with shear stress and their average stress vs. hole size curves are presented in Figure 3.26 and Figure 3.27. The lowest average and standard deviation values are collected for 10 μm holes for both σ_{11} and σ_{22} stresses as in shear stress.

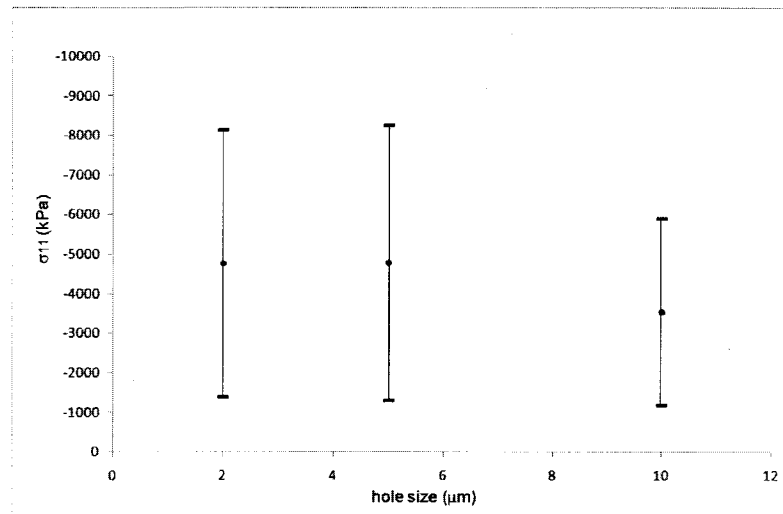


Figure 3.26. Average σ_{11} stress values with upper and lower limits during ball-hole interaction (values are negative, i.e. stresses are compressive).

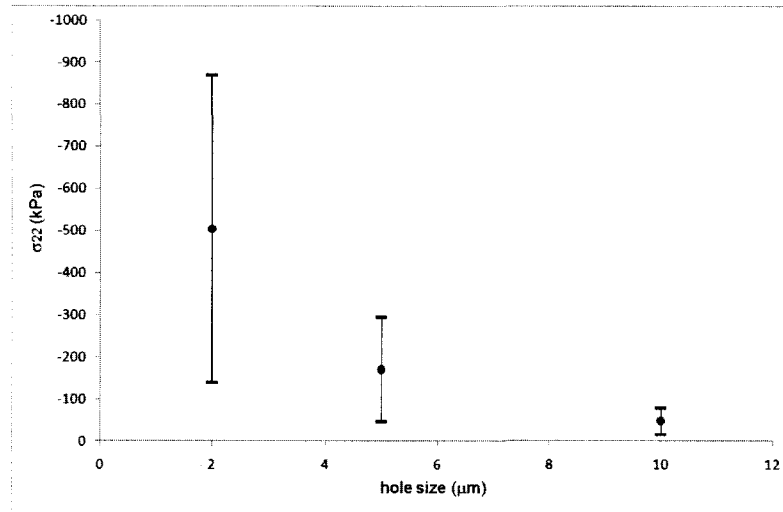


Figure 3.27. Average σ_{22} stress values with upper and lower limits during ball-hole interaction (values are negative, i.e. stresses are compressive).

Wear is a phenomenon that is related to the work done by stress during the course of surface interaction. Although stresses shown here are for hole bottoms, there is direct correlation between surface and hole bottom stresses. Work done over one hole by each stress component was calculated by integrating this stress over displacement of ball; for example, this integration of shear stresses corresponds to the area under the curves given in Figure 3.24. Commercial software-Grapher 8- was used in order to carry out these integrations. Results are shown in Figure 3.28 for shear stresses, in Figure 3.29 for σ_{11} stresses and in Figure 3.30 for σ_{22} stresses. Because of the simplifications done on geometry of the ball and reservoirs, work values are only comparative, not quantitatively meaningful. Work done by each stress component is the lowest for 10 μm holes.

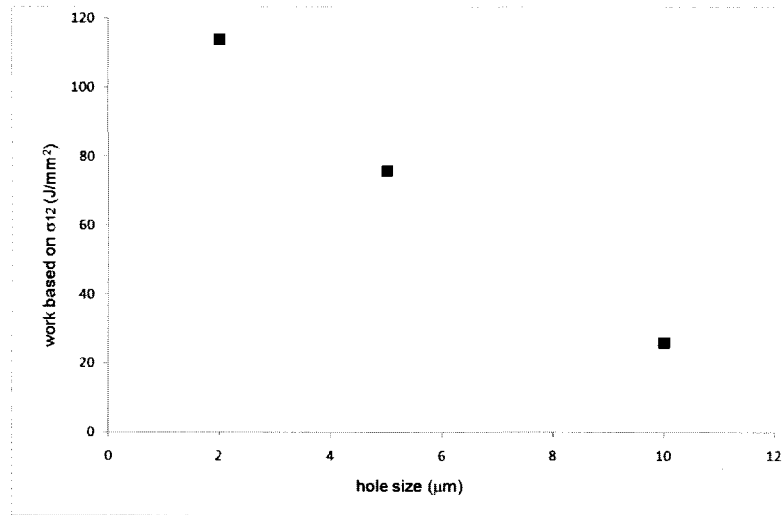


Figure 3.28. Calculated work vs. hole size curve based on shear stresses.

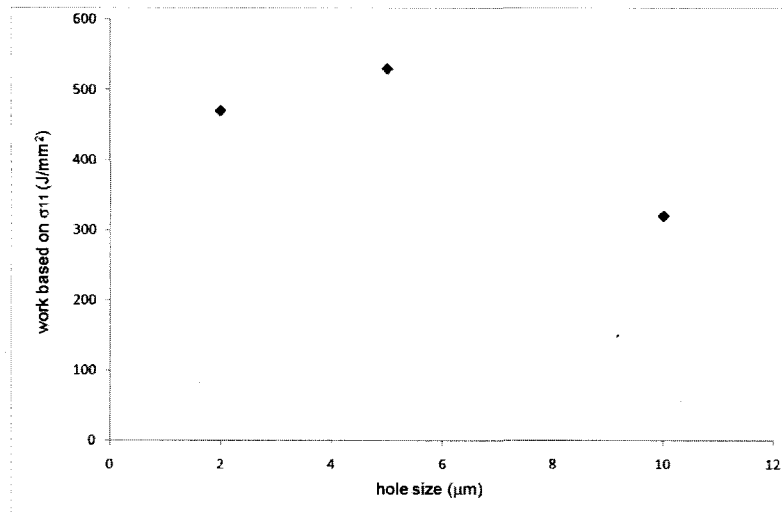


Figure 3.29. Calculated work vs. hole size curve based on σ_{11} stresses.

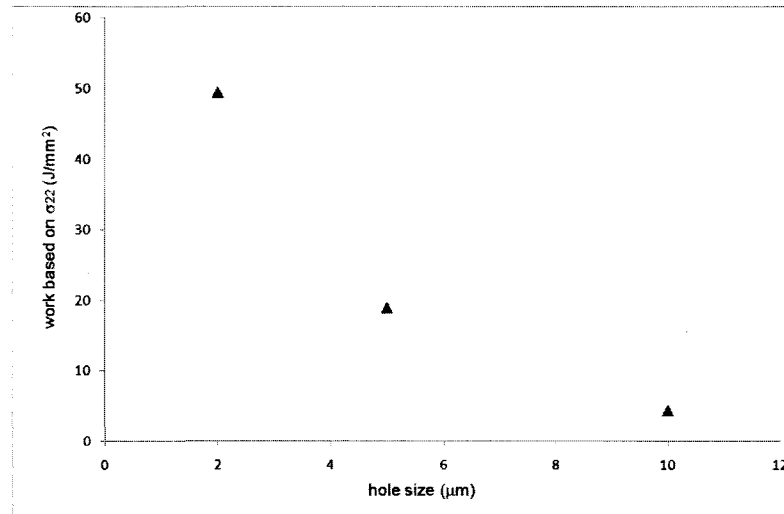


Figure 3.30. Calculated work vs. hole size curve based on σ_{22} stresses.

Previously, 10 μm holes were discussed to be better in capturing and feeding graphite when surface interaction occurs; because coatings with 10 μm -sized-holes gave the lowest friction coefficient values. Because wear taking place during friction tests causes an increase in friction coefficients in tested coatings, keeping lower friction coefficients for longer periods is an indication of less wear. Finite element analysis (FEA) results showed that coating having 10 μm -sized-holes with achieved densities also have lowest stresses at a critical location and lowest calculated work done by these stresses. Therefore coatings having 10 μm -sized-holes are strained less among others, which supports having less wear.

III.5. Conclusions

In this part of the research, composite coatings with embedded solid lubricant micro-reservoirs were fabricated. These reservoirs are intended to store and replenish solid lubricants when surface interaction takes place. It was shown that these micro-

reservoirs function as they are intended. But appropriate size, distribution and area coverage should be provided.

Ceramic or glass micro-beads were used as placeholders. They were successfully removed via ultrasonic agitation. However agglomeration is a problem by increasing both reservoir size and average distance between reservoirs. Arrangements in spray technique helped to decrease agglomeration and improved more homogeneous distribution. Esp. with 10 μm sized beads there were almost no agglomeration.

Unless solid lubricant is implemented, micro-holes are detrimental to coating structure since fast failure occurs. When graphite lubrication was applied, friction coefficients were in the range of FC for graphite alone (0.1) and FC for TiN alone (0.3-0.4). Lowest friction coefficients were obtained with 10 μm -sized-reservoirs among tested range (1.5-10 μm).

When carbon film was deposited on TiN with micro-holes by sputtering, a long wear life for coating was obtained. This is mostly attributed to C coating. However it is thought that lubricant served by micro-holes postponed catastrophic failure. Pin-on-disc tests against Al ball on TiN with 10 μm reservoirs and C topcoat showed lower FC and longer wear life than a similar coating without reservoirs.

Optical microscopic examinations of wear tracks revealed that the micro-holes act as reservoirs for graphite. However micro-holes function together with surface roughness. Smaller grooves in rough surfaces may act as reservoirs as reported previously for MoS_2 .

Because reservoirs cause failure in the absence of lubricant, it is important to trap or fill lubricant to reservoirs before damage occurs.

A limited (not exhaustive) plane strain finite element modeling of surface interaction of a pin with TiN with 2, 5 and 10 μm sized grooves under lubricated condition was performed. Coating with 10 μm sized reservoirs showed lowest stresses and lowest calculated work done at a critical location during surface interaction, which may result in less wear.

CHAPTER IV

TRIBOLOGICAL STUDIES OF PATTERNED COATINGS

The investigation of the coatings fabricated using the micro-beading method (presented in Chapter 3) demonstrated the importance of the effects of reservoir size and area coverage on the friction and wear behavior of the coatings. However, controlling the surface density and area distribution of the reservoirs was difficult. Therefore, a study was carried out using patterned silicon wafers in order to have a better control of the shape, size and the area of the reservoirs. As described in the Introduction (Chapter 1), the patterning required the use of silicon wafers as substrates.

IV.1. Experimental

Silicon samples with controlled patterns were fabricated by the photolithography process at Rochester Institute of Technology. Patterns for the silicon samples were planned in order to identify the effect of the reservoir size and the area coverage, as shown in Table 4.1. The samples coded as 4-7 in Table 4.1 are previously fabricated samples on which we conducted our preliminary tests.

Table 4.1. Properties of the patterned samples.

Sample Coding	Reservoir Size (μm)	Reservoir Spacing (μm)	% Area Coverage
4-7	2	7	26
4-25	2	25	26
4-7	7	25	10
4-25	7	25	10

IV.1.1. Preliminary Samples

Samples prepared by photolithography process explained in Chapter 1 were cut from the silicon-wafer by a diamond saw from their back side in desired shapes about 30 x 30 mm² squares. Because the pattern (placeholders) on the samples is sensitive to any mechanical interaction, we did not apply any cleaning operation before the deposition process. The samples were mounted on the magnetron sputtering deposition holder with silver paste, and the holder was placed into the sputtering chamber. The specimens were coated TiN by reactive magnetron sputtering at 200°C. This temperature was optimized as a temperature close to the deposition temperature of the beaded samples (300°C), but allows the mask still keeps its integrity. During the coating process, an initial 30 nm thick Ti bond layer was deposited to improve adhesion, followed by a TiN film approximately 0.7 μm thick. After the deposition, in order to clean the mask and to form reservoirs in the hard coating, specimens were immersed into an acetone bath agitated by an ultrasonic cleaner. Scanning electron microscope (SEM) images of uncoated silicon specimens with pattern are shown in Figure 1.18 [20]. SEM images of the Cr coated samples (from earlier studies) are shown in Figure 1.19 [20].

Following the preliminary friction-wear testing of these silicon samples, it was decided additional samples with different reservoir sizes and spacing would be useful.

These additional samples were requested from the group at Rochester Institute of Technology. However, the process used to make the original samples was no longer in use. Details of this new process and adjustments necessary to the sample preparation process are described in the following section.

IV.1.2. Tests on Additional Patterned Specimens

These tests were conducted on a new set of silicon samples. Surface of these samples were patterned by photolithography. An improved technique for the mask (in terms of lift-off ability and feature resolutions that can be created) was applied at the Rochester Institute of Technology. For the new silicon wafers, each individual photoresist island has 2 layers: one is *the lift-off layer* that has a smaller diameter and the other is *the main photoresist layer*. The purpose of the lift-off layer is to alter coating coverage around the perimeters of the photoresist islands during the hard coating deposition process. Because magnetron sputtering is a line-of-sight deposition method; the step intentionally created under the top photoresist layer is not covered by the coating (Figure 4.1). This lack of coverage around islands helps us to remove photoresist islands after the coating deposition. The remaining spaces are the reservoirs for solid lubrication.



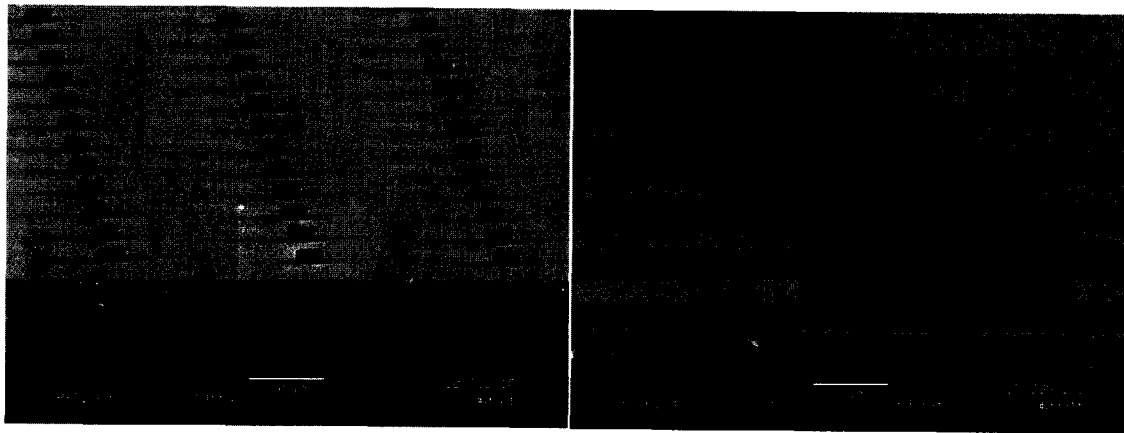
Figure 4.1 Schematic view of surface layers applied to form reservoirs [42].

When fabricating the photo-resist islands on the wafers, a layer of LOR (Lift-Off-Resist) was first laid on the surface by spin-coating, and then a second photoresist layer (OiR 620) resist was put down. Pre- and post-baking steps were then applied. When

developing, the underlayer develops faster and this resulted in an undercut (or step) that should help the removal of the photo-resist after hard coating deposition (Figure 4.1) [43].

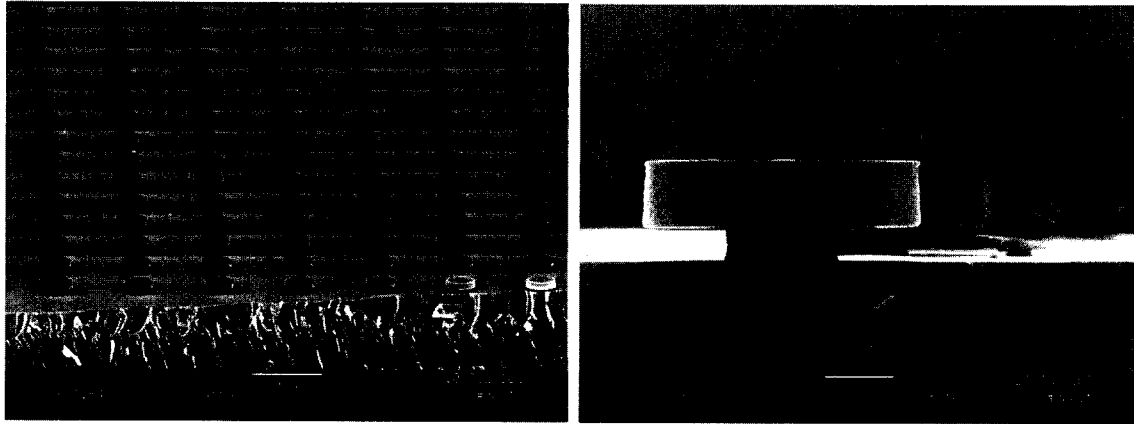
Samples for friction-wear testing were cut from the 150 mm-diameter-Si wafer by a diamond saw. Specimens were cut to a square shape about 30 x 30 mm². Because the initial coatings suffered from peeling and flaking problems, a cleaning bath containing ethanol was added to the preparation process before the deposition. The remaining preparation and deposition processes were the same as the preliminary test samples except that the deposition temperature was chosen to be 150°C, since it was not clear the new photoresist would withstand 200°C exposure.

These newly fabricated patterned silicon samples were inspected by SEM. Because the photo-resist islands become intensely charged by the electron beam, it was not possible to get an image without coating with platinum or gold. Therefore, samples cut from the silicon wafers were first coated. SEM images of each type of silicon patterned sample after short time coating are given in Figure 4.2(a), (b) and (c).

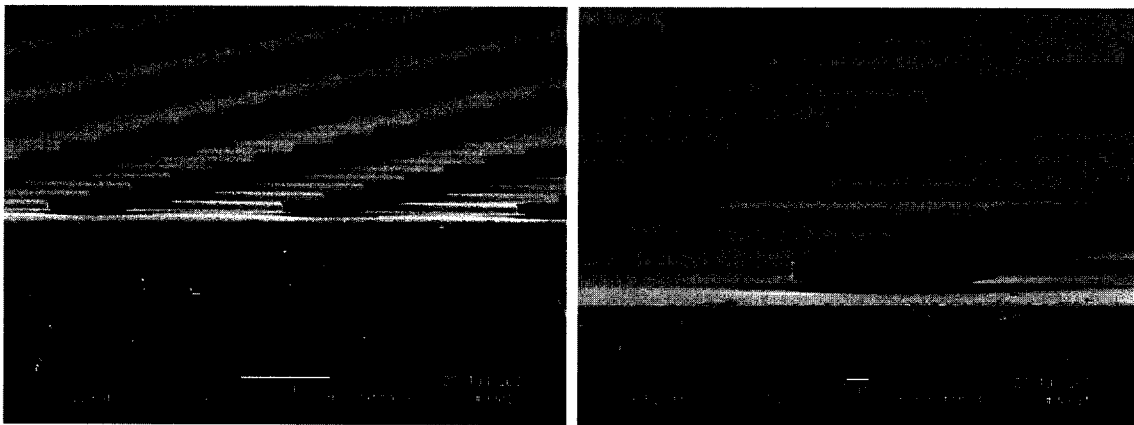


(a)

Figure 4.2(a) SEM images of the 4-25 type silicon samples.



(b)



(c)

Figure 4.2. Images of 4-11 type silicon samples in (b) and images of 9-11 type of silicon samples in (c).

After the deposition process, specimens were first polished using 6 μm diamond on a cloth until the hard coating covering the photoresist islands opens. Several smears applied by hand on the cloth were usually sufficient to just opening the caps- there was no need to rotate the polishing disk covered by the cloth. Individual specimens may differ in terms of polishing times depending on how hard it is to remove the caps. The samples were then immersed into several baths to remove photo-resists (Table 4.2). The removal process was provided from MicroChem Corp. [44]. Cross-section images of coated samples are shown in Figure 4.3, Figure.4.4 and Figure 4.5.

Table 4.2. Cleaning procedure [44].

<i>Bath</i>	<i>Content</i>	<i>Agitation/Duration</i>
1 st Bath	Remover PG (N-Methyl Pyrrolidinone)	Ultrasonic Cleaner/1 min.
2 nd Bath	Remover PG (N-Methyl Pyrrolidinone)	Ultrasonic Cleaner/5-10 min.
3 rd Bath	Isopropyl Alcohol	-
4 th Bath	DI water	-

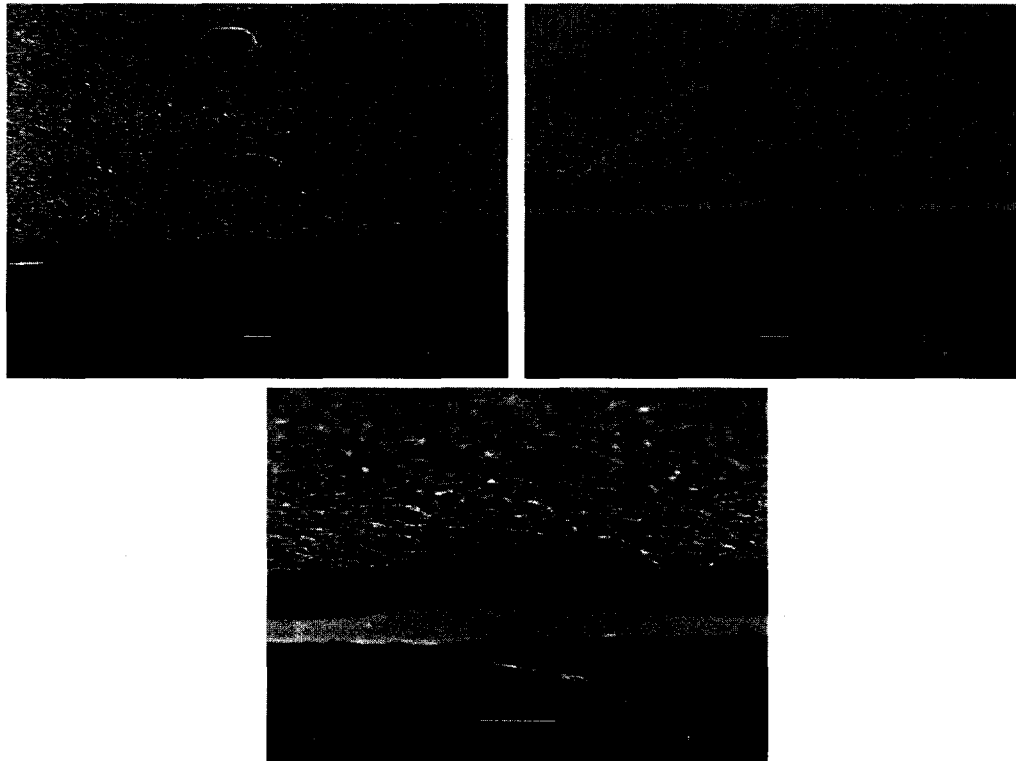


Figure 4.3. Scanning electron microscope images of the 4-25 sample after coating: upper corner is before cleaning pattern mask, others after cleaning the mask.

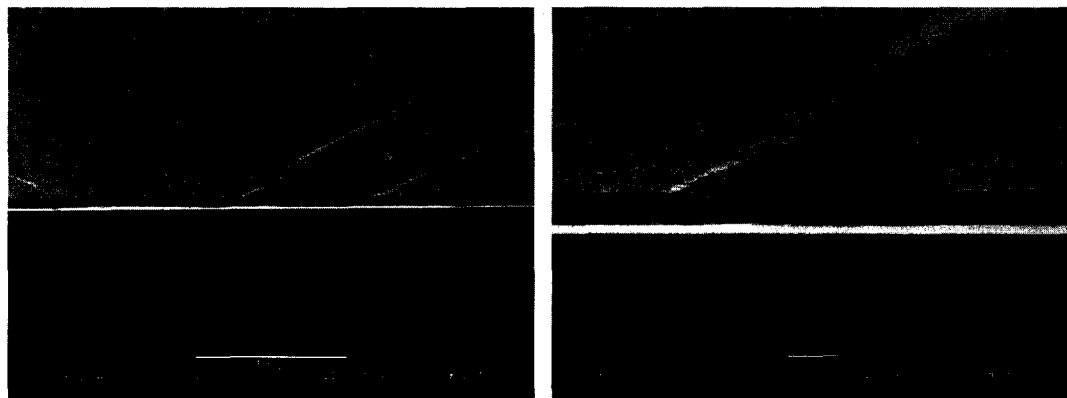


Figure 4.4. Scanning electron microscope images of the 4-11 sample after coating and cleaning of the mask.

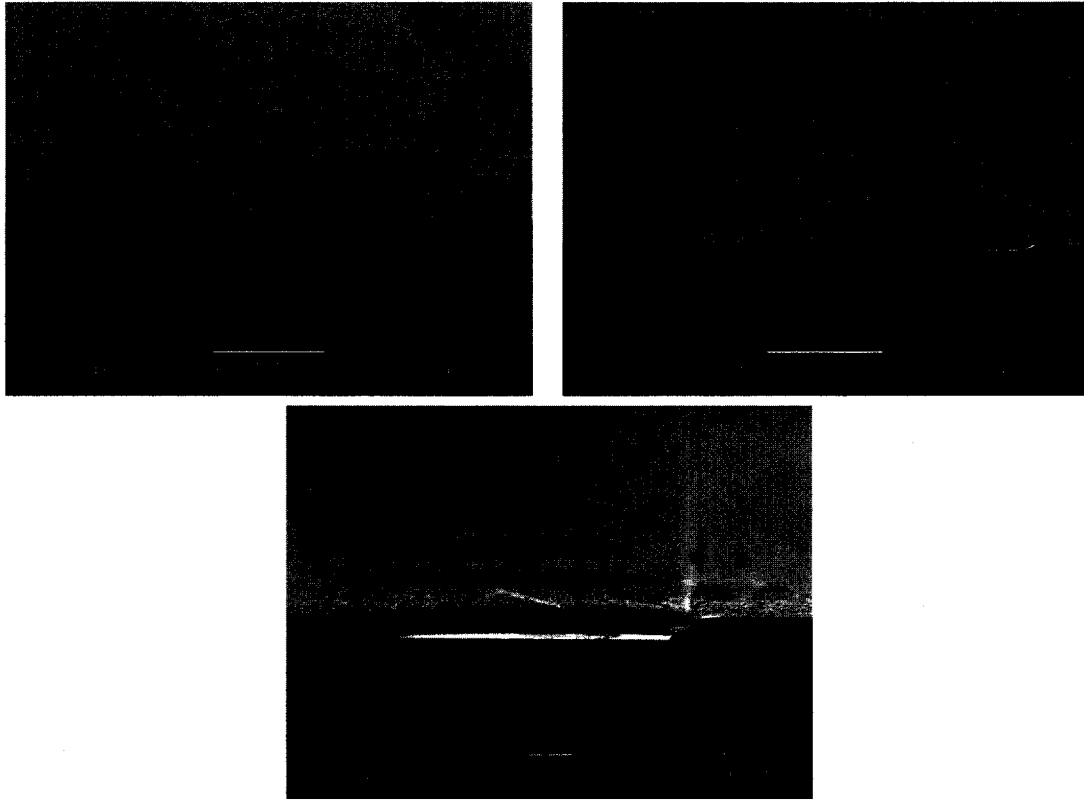


Figure 4.5. Scanning electron microscope images of the 9-25 samples after coating and after cleaning of the polymer mask.

After removal of the mask material and formation of the reservoirs, silicon specimens coated with TiN were sprayed with graphite (in ethanol mixture) by means of a mist sprayer. Pin-on-disk friction-wear tests were performed on the specimens with alumina or 440C steel balls with 6.35 mm diameter. Tests were conducted with 1 N dead weight and rotational speed used was 200 rpm. Circular tracks created during the experiments were 1-2 cm in diameter. Friction coefficient versus number of rotations graphs were plotted after each test.

IV.2. Results and Discussion

IV.2.1. Preliminary Tests on Previously Fabricated Patterned Si Samples

Friction coefficient data recorded during the pin-on-disk friction-wear tests of sample 4-7 are shown in Figure 4.6. These tests were conducted against an alumina ball. The FC graphs of tests performed with 1 N of normal load are shown in Figure 4.6 (a). For the dry test (no lubricant was applied) FC first increases to a value close to 0.4; then decreases gradually until about 2000 cycles; after 2000 cycles FC starts to increase again until terminal failure of the film occurs at 7000 cycles. Here, failure is identified by decrease in FC to characteristic of silicon wafer. Test result of silicon was given also in graph (Figure 4.6 (a)). The initial increase in the FC is expected to be because of the wear of the coating. The initial decrease in FC is probably because of the first openings of some small area of the silicon surfaces start to become dominant. As the TiN film wears through, the alumina ball interacts with the Si surface more which actually reduces the FC. Thus, the ball indents into surface, edges of the ball interacts with the fresh TiN coating, and this results in an increase in the FC once more until the permanent failure of the coating occurs, which decreases of FC again. The pin-on-disk test was also applied to the silicon substrate to obtain reference FC values for when failure of the TiN coating occurs. Failure can be identified with the FC suddenly or gradually reaching 0.2-0.25 corresponding to the FC of silicon-alumina ball interaction. For the dry conditions, it is accompanied by a lot of debris, which causes saw-tooth appearance of the FC graph. When the load was increased to 2.2 N; the interaction of two dry surfaces becomes so severe that permanent failure occurs before 2000 cycles.

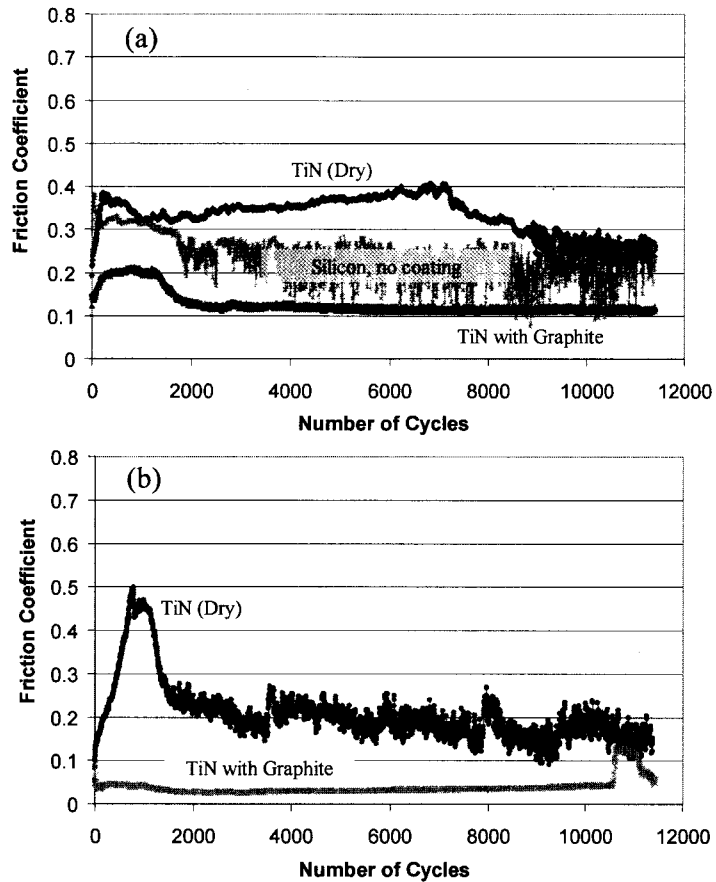


Figure 4.6. FC graphs for pin-on-disk test of TiN coatings and silicon substrate with: (a) 1 N normal load and (b) 2.2 normal load.

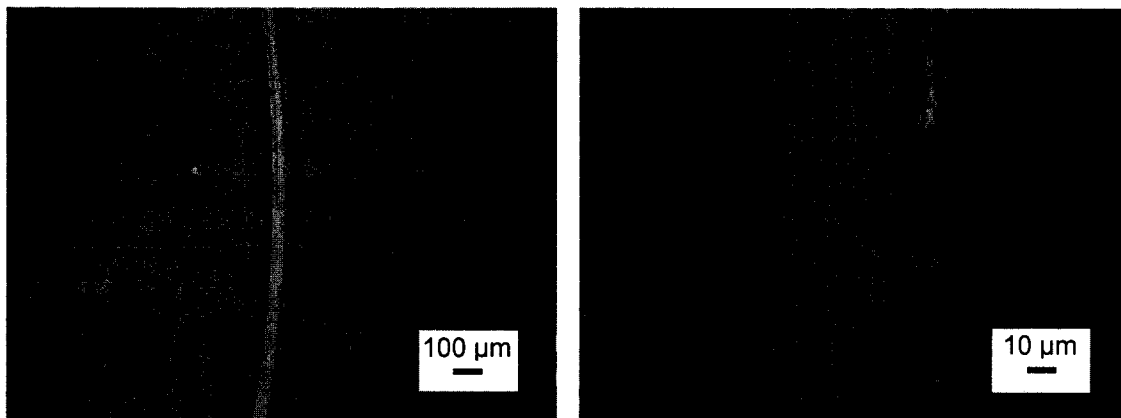


Figure 4.7. Optical micrograph of the coating after full term of pin-on-disk test with 1 N normal load. Graphite smeared areas are the edges of the wear track.

In the presence of graphite, during the initial interaction of dry surfaces becomes less and less severe with the graphite smearing and partly covering the surface.

Simultaneously, reservoir filling occurs, which will provide further graphite supply for later in the test. For the normal load of 1 N, indeed, at the end of the test, after 11,000 cycles, there is no trace of coating failure as can be seen in optical micrographs in Figure 4.7. The smearing regions on these pictures are the evidence of the graphite deformation with its layers parallel to the surface [28]. The sustained FC during the course of the test (after initial interaction) is slightly higher than 0.1. In the case of 2.2 N-normal-load (Figure 4.6 (b)), a friction coefficient of less than 0.05 was observed for more than 10,000 cycles until the failure occurs.

IV.2.2. Results for Additional Patterned Si Samples (Second Batch)

IV.2.2.1. Pin-on-disk Tests against Alumina Ball (First Group) Results of the first group pin-on-disk tests performed with alumina ball are shown in Figure 4.8, Figure 4.9 and Figure 4.10. These tests were conducted *with higher rotational speed (200 rpm) and 1 N load*. There were two specimens for each coating type. Each coefficient of friction (FC) curve is presented with a different color. Curves belonging to one specimen have close colors. Dry friction tests were conducted once for each sample. Lubricated tests were repeated when results of two specimens did not match and when curves presented fluctuations.

Friction behavior for dry conditions are similar for all patterns: All friction coefficient (FC) curves make a peak about 0.6 at the beginning of the tests; then FC decreases to 0.4-0.5 following another peak about 0.5 between 200-300 cycles; most of the graphs slowly decrease although some of them have another peak right after initial ones. Only one of the 4-25 tests continues to increase at the end of the test, probably to have a late third peak.

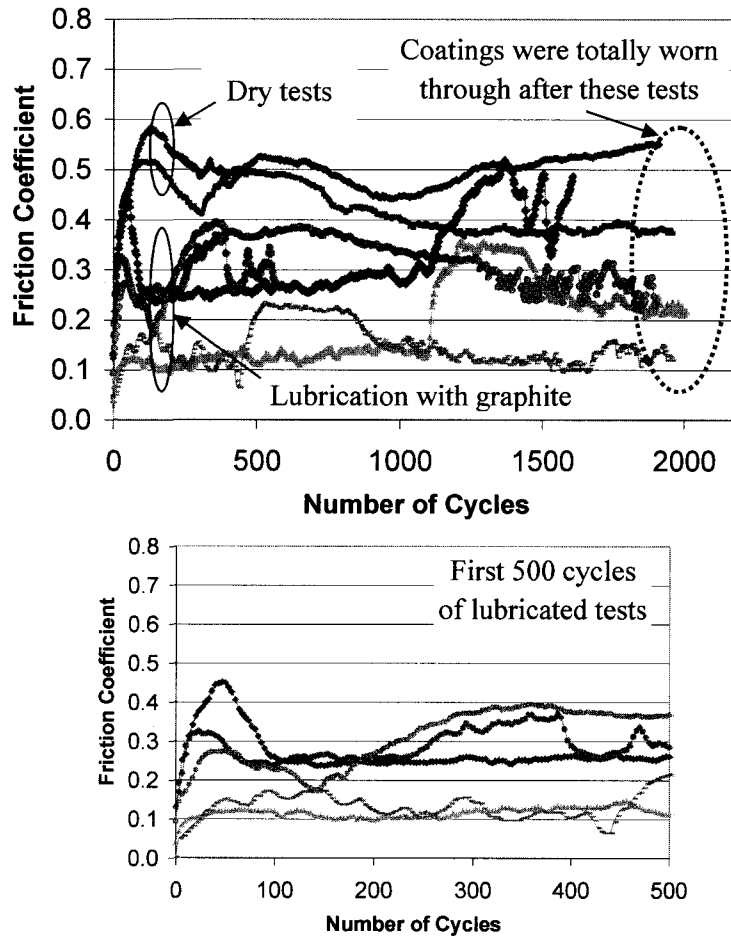


Figure 4.8. Friction-wear tests on two 4-25 on silicon patterned samples. Results of one sample are shown with green color: dry test is marked with dark green, one lubricant test is bright green and other lubricant test is light green. For the second sample, dry test is marked with brown; three lubricant tests are marked with orange and yellow. Lower graph shows the detail of first 500 cycles of only the tests performed with lubrication.

In the dry tests, coefficient of friction first increases to a value of 0.55-0.6; then after a drop increases again to 0.5-0.55. Permanent failure of the coatings occurs after 600 – 1200 cycles with a decrease of friction coefficient. The decrease in the FC curves is because of the continuous wear of the TiN coating with increasing exposure of the base substrate material which has a FC about 0.35-0.4.

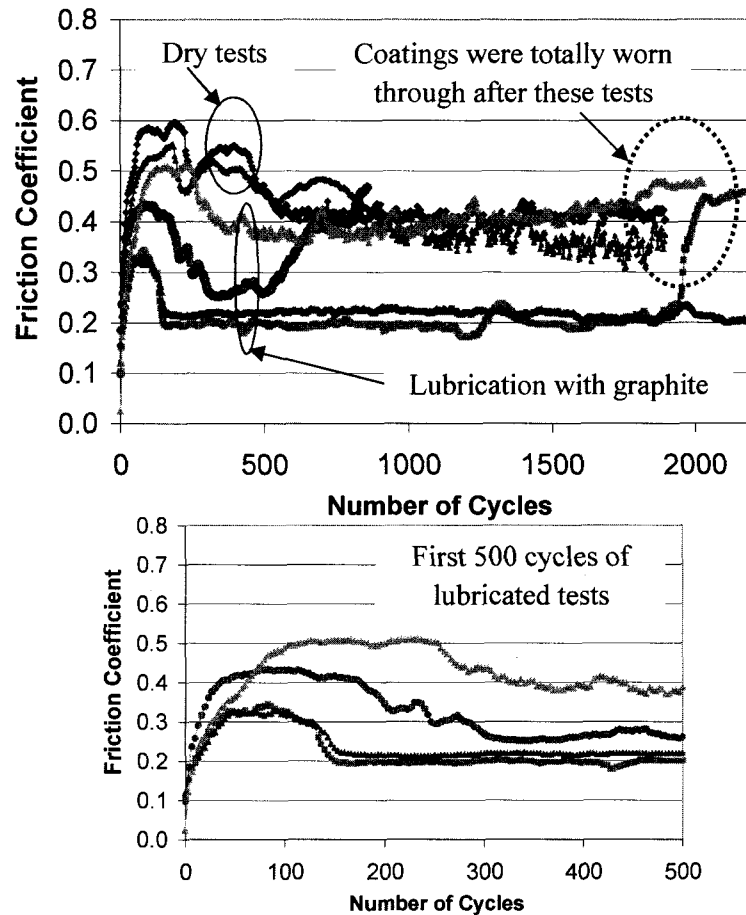


Figure 4.9. Friction-wear tests on 4-11 on silicon patterned samples. Results of one sample are shown with blue color: dry test is marked with dark blue, lubricant test is light blue. For the second sample, dry test is marked with red color; three lubricant tests are marked with dark or light pink. Lower graph shows the detail of first 500 cycles of only the tests performed with lubrication.

When the graphite lubrication was applied, a shift to lower values in all friction coefficient curves was observed for all specimens as shown in Figure 4.8, 4.9 and 4.10. There are still initial peaks for most of the experiments, decreasing after first 100-150 cycles for 4-25 samples and first 75 cycles for 9-25 samples.

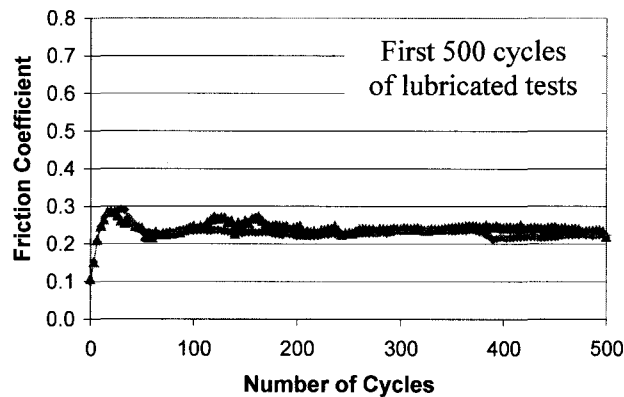
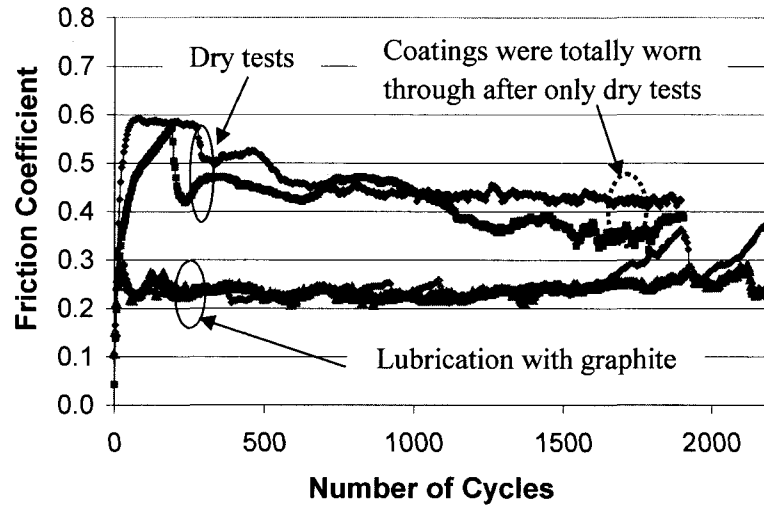


Figure 4.10. Friction-wear tests on 9-25 on silicon patterned samples. Results of one sample are shown with blue color: dry test is marked with dark blue, lubricant test is greenish blue. For the second sample, dry test is marked with brown; lubricant test is marked with red. Lower graph shows the detail of first 500 cycles of only the tests performed with lubrication.

For two of the 4-11 samples the initial peak drops down after 150 cycles. The other two tests show postponed drops with gradual decreases (one is after 300 cycles; the other is after 350 cycles-profile of this test is more like dry tests-). The FC decreases to a value between 0.1-0.25 for 4-25 specimens and slightly lower than 0.25 for 9-25 specimens. The FC values achieved at the end of the drop decreases as the initial peak drops faster. As we follow the graphs, the tests with faster dropping behavior at the beginning also keeps the lower values they achieved for longer cycle times. Two of this

type of tests keeps lower FC value at 0.2 for at least up to 2000 cycles. For the other two tests: one of them worn through faster than others and the other provided lower FC (0.25-0.3) values for only about 200 cycles and the coating couldn't provide a good lubrication as FC started to increase again after 500 cycles, then the test was stopped in order to prevent failure. The two FC curves of 9-25 specimens match almost exactly. The lowest friction coefficients for these specimens are between 0.20-0.25. Both specimens also provided lower friction coefficients up to almost 2000 cycles.

All initial peaks are lower than the peaks of the dry tests, except the test with highest peak, which belongs to one of the 4-11 samples. The coating was worn through quickly for this test. 9-25 samples showed lowest initial peaks. Initial peaks are indication of the dry TiN-alumina interaction; some wear may occur with this interaction as in the case of dry tests. Nevertheless, during this time, the graphite smearing on the surface accompanies to this initial wear. Therefore, the initial peaks do not increase as high as dry test peaks (as long as no detrimental failure of the coating occurs, which is accompanied by an increase to dry test values of the FC). Besides, these peaks generally are confined to a lower number of cycles, which shows that the lubricant effect of graphite becomes dominant after a while and the FC decreases. At this point, interaction of the TiN with alumina ball is partly or totally inhibited and most of the contact occurs between smeared graphite on the sample surface and transferred graphite layer on the alumina ball. During the course of the tests, earlier increases in FC graphs (as in one of the specimens of the 4-25 and 4-11 types) show that the graphite smeared on the surface and fed to the surface by the reservoirs was not enough to protect surface or initial

coverage of the surface with graphite at the beginning of surface interaction was not fast enough to prevent a detrimental failure initiation to start.

More scatter in FC curves (fluctuations at each individual curve) under lubricated conditions was observed in 4-25 samples and this tendency decreases some for 4-11 samples. The most consistent FC curves were provided by 9-25 samples. Average percent standard deviation values for each sample type are presented in Figure 4.11. First, percent standard deviations were calculated for each curve; these were averaged to obtain a comparison values for each type. Because of the scatter observed, pin-on-disc tests were repeated with lower speed and dead weight.

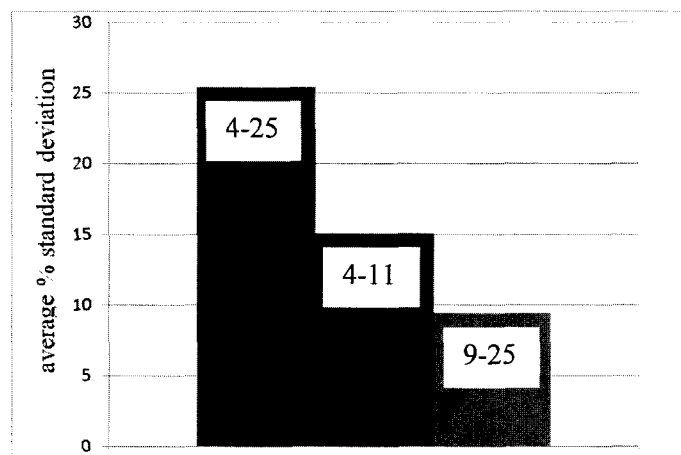


Figure 4.11. Average percent standard deviation values for each specimen type.

IV.2.2.1.1. Evaluation of the First Group Friction-Wear Tracks by Optical

Microscopy Optical micrographs taken after the tests performed with higher speed and weight are given in Figure 4.12, Figure 4.13 and 4.14. Only the tracks that are not worn through can provide information about the reservoirs; therefore only those pictures are provided. All sizes of reservoirs have shown a good capacity to catch and store lubricant (holes are filled). Since the tests shown were stopped during the increasing values of FC to about 0.35-0.4 as these pictures show the case close to, but prior to terminal wear. First 4-25 sample has some graphite smear on the track, but this amount obviously is not enough to provide a stable low FC; thus FC fluctuates up and down before the test ended. The second 4-25 sample does not have much graphite on the surface except the holes and the edges of the track. Therefore, early increases in FC can be attributed to this evidence. Pictures also shows that 4-11 specimen has the ability to inhibit coating-ball interaction with the help of more reservoirs per unit area, which could be the reason 4-11 samples has longer wear lives, compared to 4-25 samples. No 4-25 sample among 5 lubricant test could reach 2000 cycles without wearing through. Also, 2 of the tests for 4-11 samples provided stable FC curve up to 2000 cycles. There is no long time stable behavior in the FC curves belonging to 4-25 samples. The first 4-11 sample shown in the micrograph has a slower drop of FC and a quicker second increase. A slower drop to FC values of graphite increases the chance of hard coating-ball interaction. More damage in coating should be expected. This could be the reason for the higher FC during graphite action and the earlier increase in FC. Smearred graphite on the wear track appears to be more reservoir-based. The second test belonging to 4-11 samples was stopped after 4500 cycles. Although there is substantial damage in wear track, there is still graphite spread

on the track. Areas ploughed by the counter-face become secondary reservoirs for both graphite and excessive wear debris in the track. This function of the damaged areas may postpone further damage of the coating by providing some lubricant and also by storing wear debris that may behave as third body particles in the contact region. These third body particles can cause catastrophic failure of the coating both by suppressing lubricant action and by abrasive wear they may produce if they are hard particles.

Pictures of the lubricated wear tracks so far (tests with higher values of speed and weight applied) on 9-25 specimens are given in Figure 4.14. These tests have gone long times (5800 and 2300 cycles) until they have higher FC about 0.35-0.4. In the mid-track region, the first test still has some graphite in and around the holes. As mentioned previously for one of the 4-11 wear track, because there is some damage in the track around the reservoirs, one can guess that some wear debris was also accumulated in the reservoirs. At the edges of the track, there is more graphite-covered-area. The second test has a narrower track because of the shorter test time. Both tracks have two regions which would match different contact areas under the ball as we can guess: The region with cracks and not much lubricant except the holes is the region right under the ball, which is with more applied stress. The second region has more graphite around the holes and the surface; this region coincides with the one side of the ball. The holes with graphite smearing in both samples show better spread per one hole. In Figure 4.15, the interaction between ball and the one single hole is shown schematically. It is also obvious that even if the smear occurs from one hole, the area covered by graphite would be higher for bigger holes. This is important because the contact area is very narrow and the number of the holes coinciding with the contact area is limited.

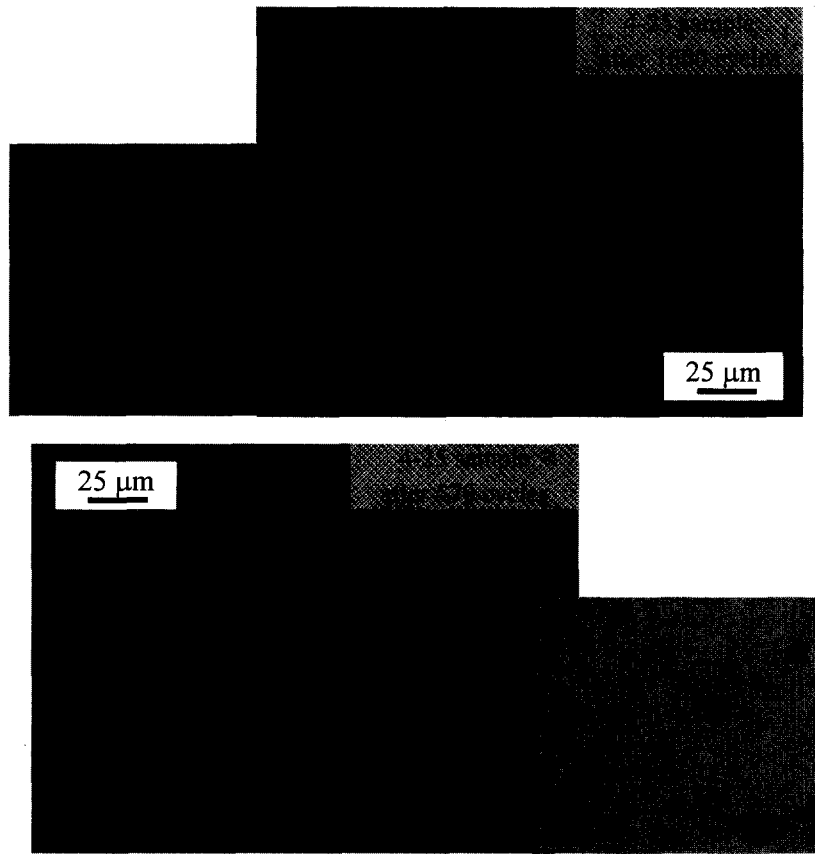


Figure 4.12. Optical micrographs of wear tracks of two 4-25 samples showing details of the reservoirs (the tests performed with higher speed and weight).



Figure 4.13. Optical micrographs of wear track on two of the 4-11 samples belong to the tests performed with higher speed and dead weight.

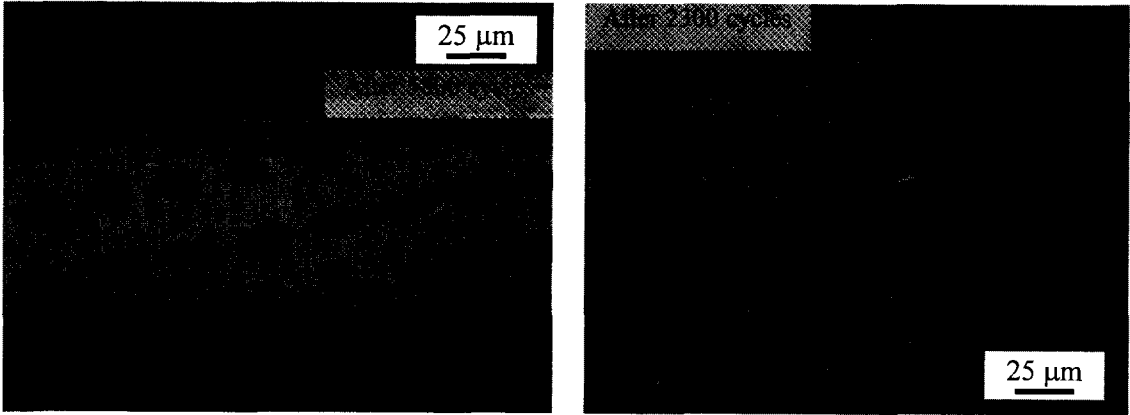


Figure 4.14. Optical micrographs of wear track on the 9-25 samples belong to the tests performed with higher speed and dead weight.

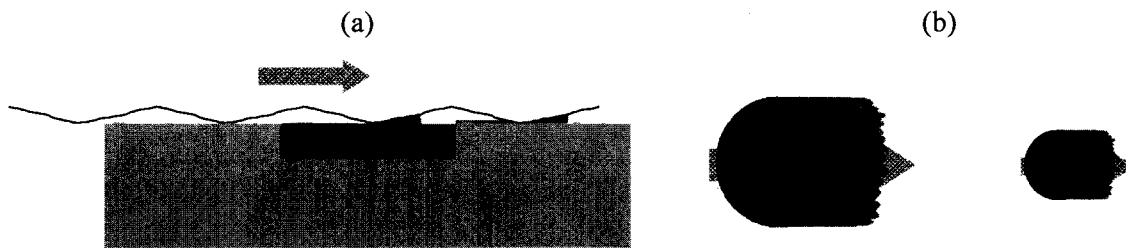


Figure 4.15. Schematic view of a single reservoir-counterface interaction: Scheme on the left, (a), shows how the counterface (ball) would transport graphite from the reservoirs and how the graphite smears on TiN surface. Scheme on the right, (b), shows that smearing area would be larger for each bigger-sized-reservoir.

IV.2.2.2. Pin-on-disk Test Results against Alumina Ball for the Second Group (Lower Speed and Weight) and Optical Microscopic Evaluations of the Wear Tracks

Pin-on-disk tests against alumina ball were repeated at lower speed and lower weight under *lubricated conditions*. It is aimed to decrease the severity of the dry TiN-alumina ball interaction decreases with decreasing load. And more time was provided for graphite smearing and hole-filling actions. Figure 4.16 shows results of initial short time tests. These tests were performed twice for 4-25 and 4-11 samples and once for 9-25 sample for longer time periods (2000 cycles) (Figure 4.17 and Figure 4.18).

The initial peak observed in FC curves of other lubricated tests did not show up. It is related with having less harsh conditions in terms of surface interactions. And there is more time for lubricant to contribute to this interaction. Under these conditions all specimens showed similar behaviors initially (first 500 cycles). Friction coefficient values provided are about 0.1-0.2 at the beginning.

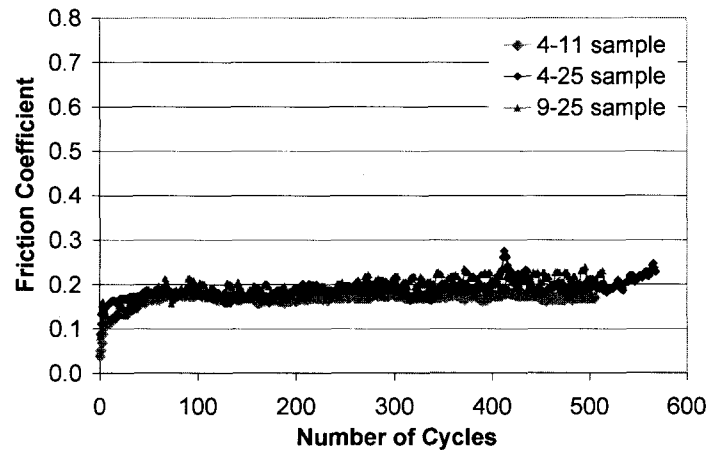


Figure 4.16. Pin-on-disk lubricated friction test results obtained under lower load and speed conditions.

The first separation from the group was shown by 4-25 sample with fluctuations up and down, in one of the tests at as low as 200 cycles. After about 500 cycles, 4-25 and 4-11 samples showed a passage to follow substantially higher values of FC. This can indicate that the graphite amount in the contact region was not enough to keep low values. Nevertheless there are sudden drops in the curve, which could be taken as some trials to turn back to the lower values. At these moments, probably the system was provided some graphite from a source that could be the edges of the track or edges of the ball surface in contact with the coating. Interestingly, the longer test with 9-25 sample exhibited low values of FC about 0.12-0.15 or more than 2000 cycles with a smoother curve. Among these three samples, 9-25 one has shown the most fulfilling function in terms of storing and feeding the graphite.

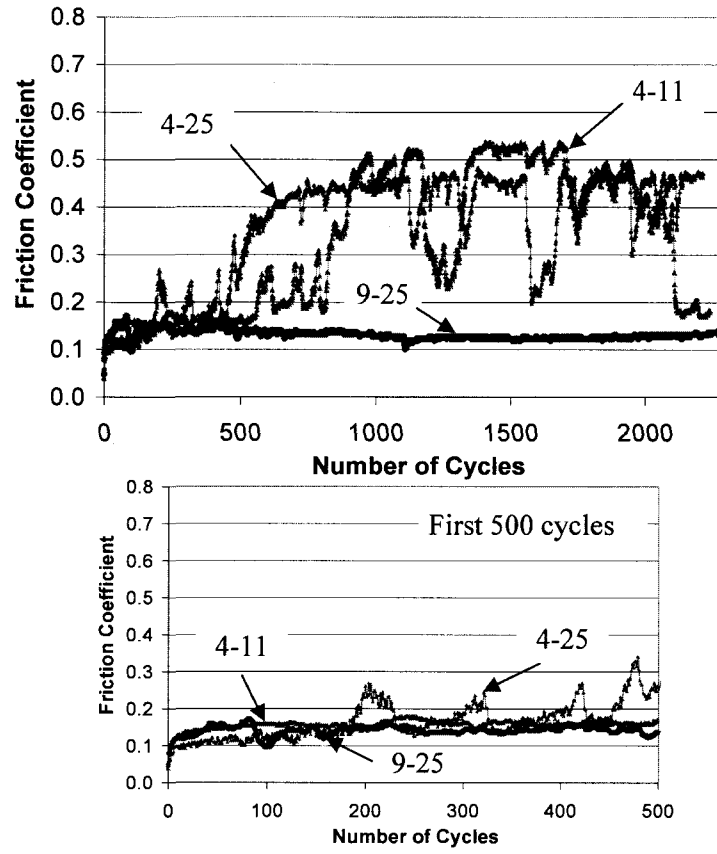


Figure 4.17. Pin-on-disk lubricated friction test results obtained under lower load and speed conditions.

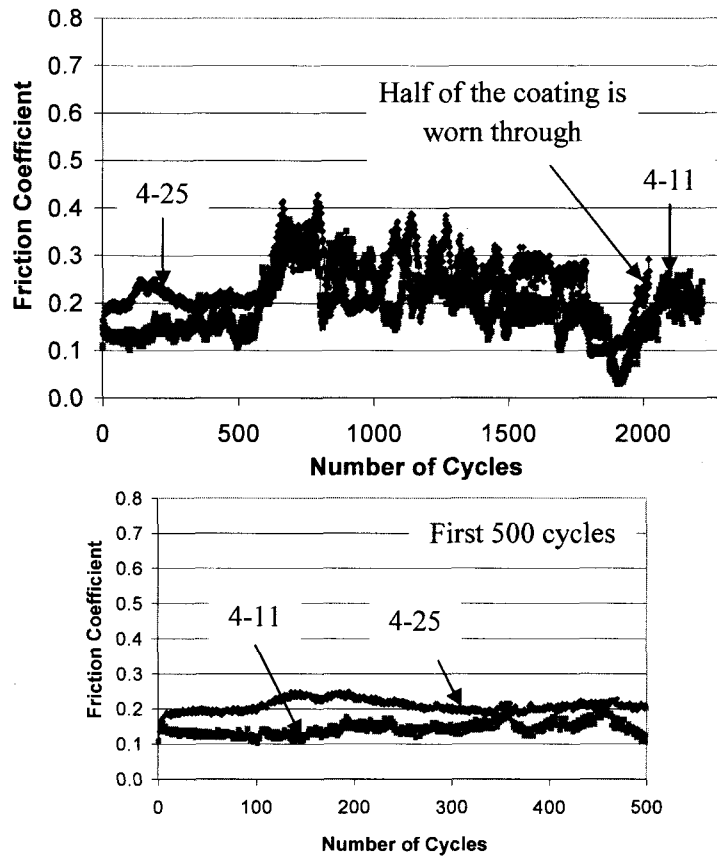


Figure 4.18. Pin-on-disk lubricated friction test results obtained under lower load and speed conditions. These tests are repeats of the tests shown in Figure 4.15.

Coatings for all type of the samples were intact after 500 cycle tests. For the tests performed for longer periods of time, example microscopic appearances of the tracks are given in Figure 4.19, 4.20 and 4.21. FC curves of these tests were given in Figure 4.17. The amount of lubricant spread over the wear track is less in 4-25 samples according to microscopic examination. The most consistent reservoir based lubrication was succeeded by 9-25 sample; although there were some worn areas in the track. Half of the wear circle belongs to the one of two 4-25 sample (sample shown in Figure 4.18) tested for 2000 cycles was worn through.

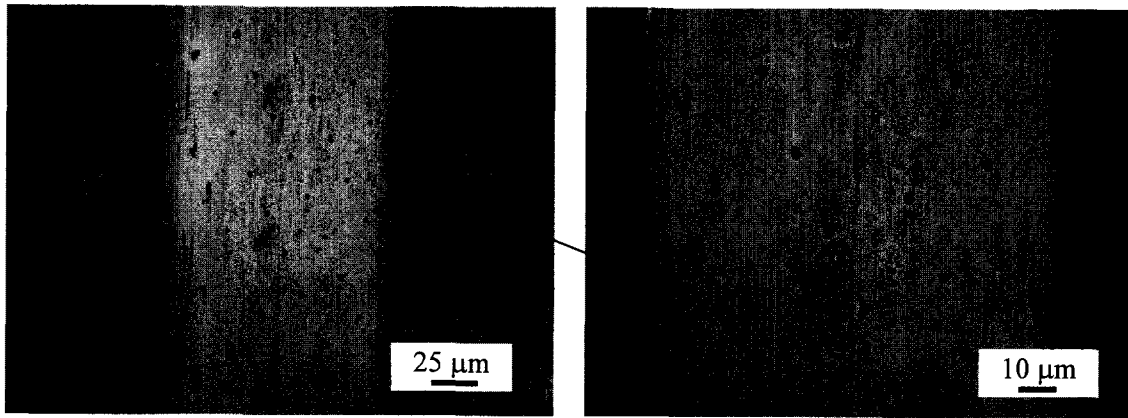


Figure 4.19. Optical micrographs of wear tracks of 4-25 samples belong to the tests performed with lower speed and dead weight (2000 cycles).

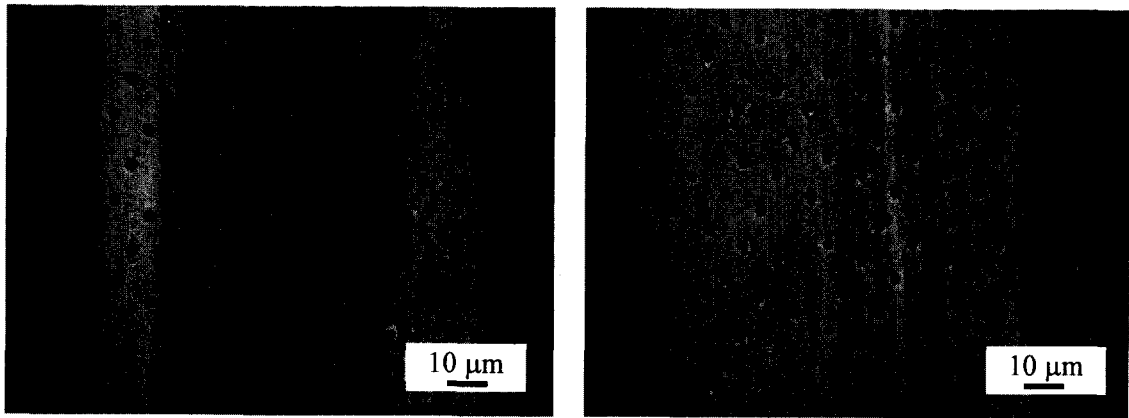


Figure 4.20. Optical appearance of the wear track of 4-11 sample after the test with lower speed and dead weight (2000 cycles).

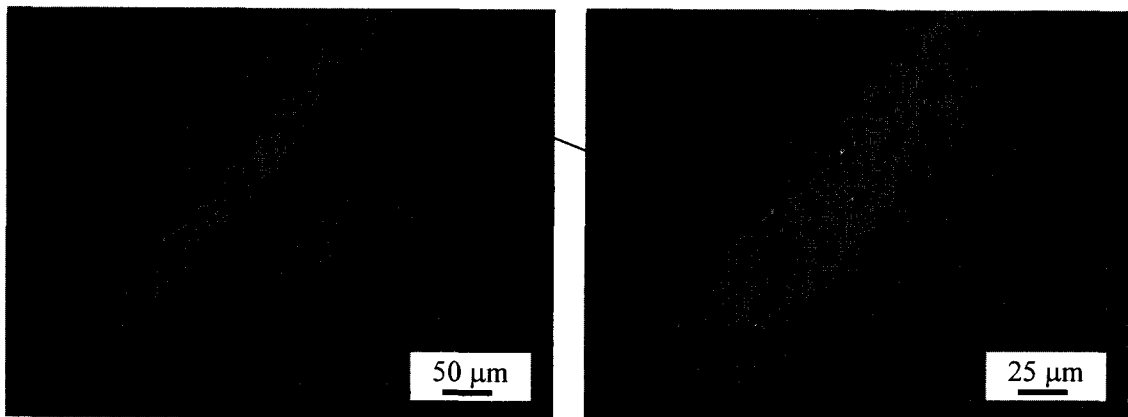


Figure 4.21. Optical appearance of the wear track of 9-25 sample after the test with lower speed and dead weight (2000 cycles).

When we take 4-11 and 4-25 curves into account, as 4-11 sample having higher density of the reservoirs, we can't see a beneficial effect of having more reservoirs on the surface at the beginning process; because graphite coverage of the surface is almost as slow as the wear of the coating process. The reason for that is having very few reservoirs in a narrow track in when alumina ball is used as counterface. The alumina ball showed minimal wear during the surface interaction. Nevertheless, as the track gets slightly wider further in the test, some benefit of having more holes filled with graphite could be mentioned; because the less dense samples in terms of having reservoirs (4-25 type) have shown earlier fluctuations in FC than denser samples (4-11 type). These fluctuations indicate unstable interaction at the contact region. For the tests with higher load and speed, no 4-25 sample reached to 2000 cycles without wearing through, while 2 out of 5 lubricant tracks on 4-11 samples provided lower values of FC at least up to 2000 cycles.

When 4-11 type samples are compared to 9-25 type samples (4-11 type and 9-25 type samples both have the same area coverage), in the tests with higher speed and load, having bigger reservoirs in the TiN coating has provided faster graphite smearing of the surface and it has also prolonged the low FC period. This could be also because of the reason previously explained (Figure 4.15). For the lower load and speed tests, most probably because there were no initial increase and possible wear accompanying to that did not exist, all samples provided similar friction coefficient values. But again, 9-25 sample provided lower value of friction for longer time.

IV.2.2.3. Pin-on-disk tests against Steel ball The results of the pin-on-disk friction tests are given in Figure 4.22; tests were performed with graphite lubrication and 440C stainless steel balls and at higher speed and load levels. Higher load and speed were preferred in order to obtain data comparable to first group of specimens tested with alumina ball under the same load and speed conditions. Both 4-25 and 4-11 type specimens, esp. 4-25 samples did not show consistent friction coefficients on those tests. Steel ball might change this behavior.

According to Figure 4.22, the behavior of the 4-25 sample is distinctively different from other two; i.e. 4-25 sample was worn through quickly after the tests started and the positive effect of graphite was not observed. For the case of 440C martensitic steel ball, some wear of the ball accompanies to the coating. Because of this wear, the tracks are wider, which alters the contact conditions in favor of reservoir function; because there are more reservoirs in the area. Obviously, increase in the number of reservoirs was detrimental for 4-25 sample. Both 9-25 and 4-11 specimens showed some kind of peak at a higher value of FC, and then friction decreases down to a value less than 0.2. Until more than 1,100 cycles there was no other change for 4-11 test, but some increase for both 9-25 samples. Decreases in FCs are evidently because of the lubricating action of the graphite on the contact surfaces (Figure 4.23). In fact, one of the 9-25 sample was tested more than 11,000 cycles, although the friction became unstable with fluctuations further in the test; the wear track was in a good condition with high amount of lubricant on the surface coming out of reservoirs after the test (Figure 4.24).

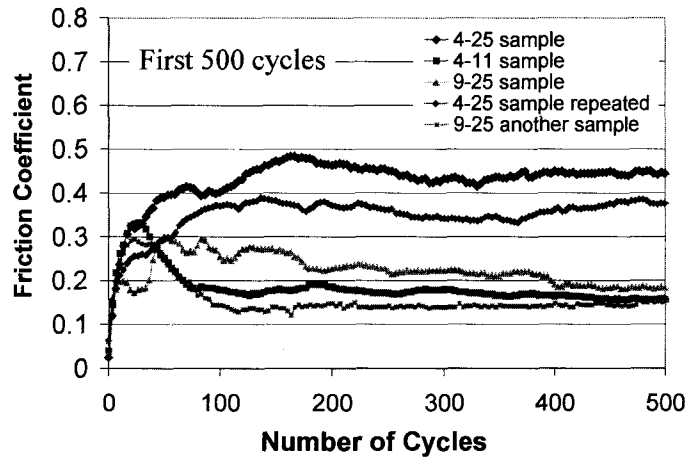
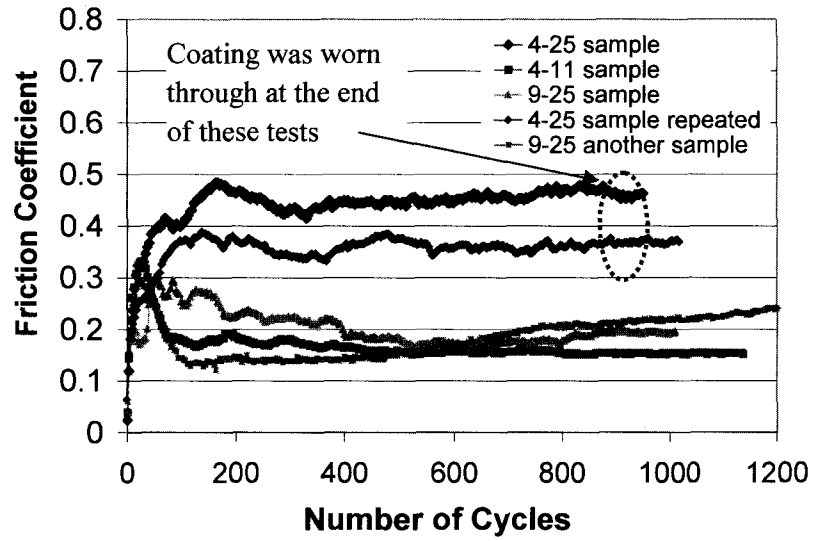


Figure 4.22. FC data recorded for the tests against 440C steel ball: Full range of the tests were shown on the left, only first 500 cycles were shown below.

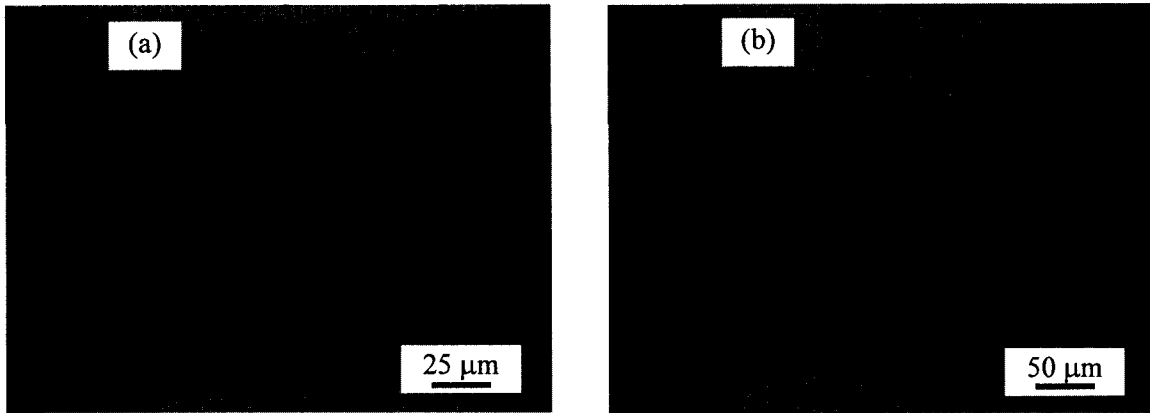


Figure 4.23. Optical micrographs of the tracks after friction tests of (a) 4-11 specimen after wear test, (b) 9-25 specimen after wear test.

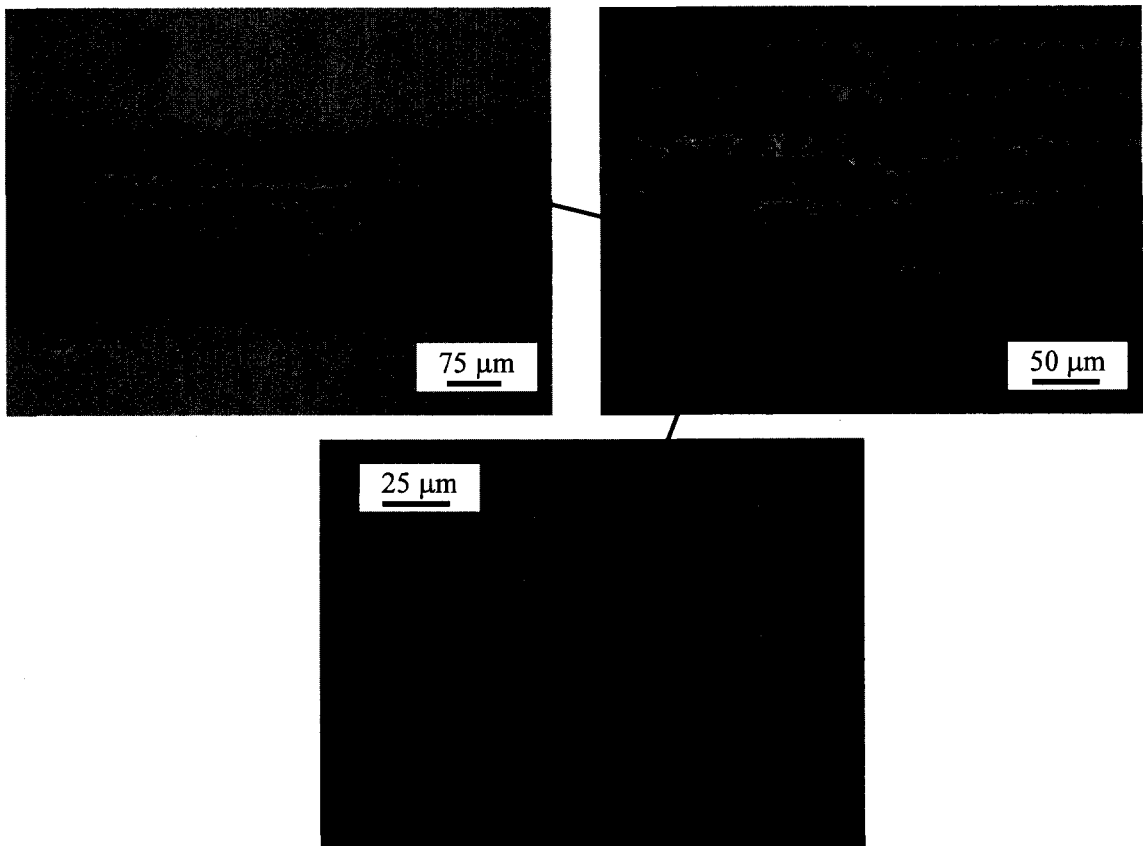


Figure 4.24. Optical micrographs of the tracks taken after friction test kept going until about 12,000 cycles for one of the 9-25 specimens.

IV.3. Discussion

Incorporation of the reservoirs in the hard coating with the technologically advanced photolithography process was successful. Although this new two-layer- photoresist-mask was specially developed to help lifting off the mask after the coating process; high points around the holes were present after removal of the mask resulting in high FC. This was overcome by polishing the samples after the hard coating deposition.

In dry conditions, the reservoirs decreased the structural integrity of the coating and caused fast failures. When graphite was applied as a solid lubricant, a general decrease in friction coefficients was observed. Nevertheless, the tribological performance of the coating was affected by the size and the area coverage of the reservoirs. In case of alumina counterface, smaller sized specimens with lower area coverage have shown the most scattered results under lubricated condition. For alumina ball tests, because the wear amount of the ball is small the matching wear track on the specimen is also narrow. In this narrow area, the probability to have reservoirs may be scattered, too, which would cause different friction behaviors depending on number of the reservoirs in the track. It is not surprising to see any of the 4-25 samples couldn't reach 2000 cycles under high load and speed conditions.

The most consistent results were observed for 9-25 samples. This is attributed to two phenomena: increased solid lubricant provided by higher area coverage of the reservoirs and increased lubricant amount per hole in the interaction with the counterface (Figure 4.15). These are confirmed by the microscopic inspection of the wear tracks after tests.

IV.4. Conclusion

Pin-on-disk tests conducted with graphite on coatings with controlled patterns achieved by photolithography showed holes with 9 μm size (with 25 μm spacing) has the ability to provide faster decreases to lower friction coefficients and stable lower friction coefficients for longer periods of time. Faster decrease to low FCs compared to 4-11 samples having the same area coverage indicates that 9 μm sized reservoirs performed better when surface interaction takes place. The reason could be the ability of bigger holes to serve more lubricant per hole. This could be explained by

- ease of capturing graphite particles having 2-15 μm sizes
- simply storing more lubricant per hole
- serving to protuberances of a counterface easier reaching to lubricant.

Increase in area coverage of the reservoirs provided longer wear lives when samples with same size but different area coverage of reservoirs were compared (when 4-11 and 4-25 samples were compared). In the tests performed with alumina ball and higher speed and load on samples with lower area coverage (4-25 samples) couldn't reach 2000 cycles. This result is more obvious for the test performed with steel ball, where wider tracks occur. Tracks on 4-25 sample was worn through quickly.

CHAPTER V

MACHINING PERFORMANCE OF TiN COATINGS

INCORPORATING INDIUM AS A SOLID LUBRICANT

The machining performance of TiN coatings incorporating indium as a solid lubricant was investigated as a practical application of the patterned coatings. In the present work, the coatings were deposited on cutting tool inserts by means of the “*Microbeading*” method described in Chapter 3. Machining tests on these coated tools were performed on a turning center with and without coolant and flank wear was measured intermittently. Flank wear data of various coatings were collected. Further investigations were performed to explain the differences in wear life data of selected coatings, namely, machining simulation tests, chemical evaluation by X-ray photoelectron spectroscopy (XPS) and morphologic inspection of collected chips with scanning electron microscopy (SEM) [45].

V.1. Experimental

In this part of the study, indium was used both as a thin film overlaying the TiN, as well as a separate indium phase within the TiN coatings. SPG 422 type cemented carbide inserts were used as substrates to allow us to conduct machining tests. Coatings

were applied on only the rake (top) faces of insert samples. The reason is that rake surface includes tool tip where cutting takes place and also metal chip flows on rake surface. Another reason is to decrease coating cycles. In PVD method, only surfaces facing to target is coated effectively (Figure 5.1). To coat other surfaces, (namely the side or flank faces) coating cycles should be repeated or rotated on multiple axes during deposition. During machining operation, high forces and temperatures are applied on a very small area (tool tip). Improving tribological conditions only on rake surface was expected to contribute overall wear life of insert tools substantially.

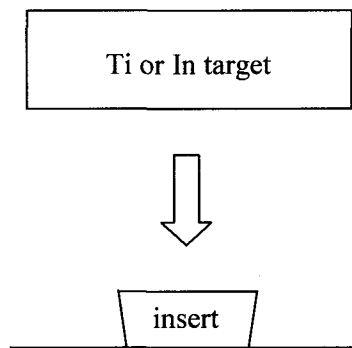


Figure 5.1. Position of rake and flank surfaces when TiN and In deposited.

Application of the micro-beads on the surface and the coating parameters are given in Chapters 2 and 3. Two different methods were used for “*Microbeading*”. One was the spray method and the second is the dipping (or submerging) method. Details of the techniques are also given in Chapter 2. Samples and their fabrication techniques are presented in Table 5.1. Area coverage values obtained on steel samples by the spray method were repeated here on insert samples. Higher values were achieved by the submerging method. Attempting even higher surface coverages would cause an increase in agglomeration when using these methods.

Table 5.1. Cutting insert samples tested at turning operation.

TiN coated inserts				
Sample Name	Relative Density	Diameter of the Microbeads (μm)	Application Method	Area Coverage
TiN	-	-	-	-
TiN-In	-	-	-	-
TiN-In5L	<i>lower</i>	5	<i>Spraying</i>	1%
TiN-In5H	<i>higher</i>	5	<i>Submerging</i>	3.8%
TiN-In10L	<i>lower</i>	10	<i>Spraying</i>	1%
TiN-In10H	<i>higher</i>	10	<i>Submerging</i>	2.3%

Optical micrographs of specimen surfaces taken after TiN deposition are shown in Figure 5.2. Inserts were then transferred to the vacuum chamber once more for solid lubricant-indium-deposition. A 1.5-2 μm thick indium film was deposited at room temperature onto substrates.

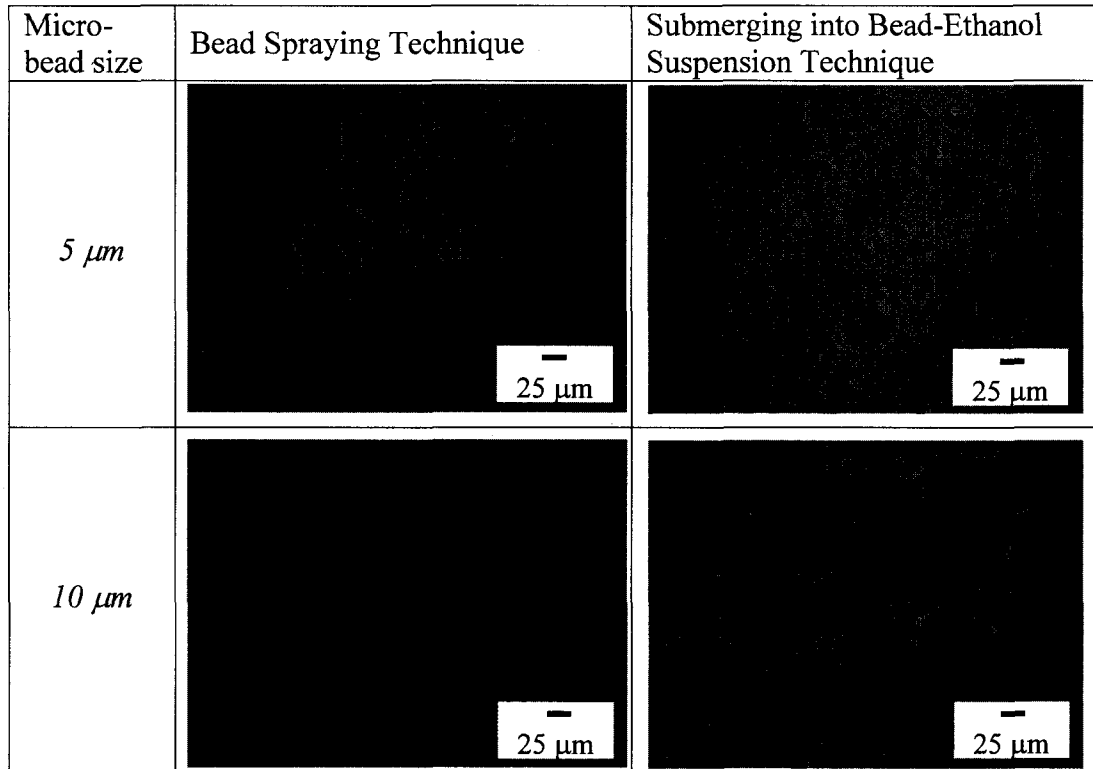


Figure 5.2. Pictures of rake face of the insert specimens after cleaning the micro-beads from the surface; micro-beads left the empty reservoirs behind.

V.2. Results and Discussion

V.2.1. Pin-on-disk friction tests

Before conducting machining studies, pin-on-disk tests were run and results for coatings that were applied on the rake face of the tool inserts are shown in Figure 5.3. To perform these tests, the inserts were glued on steel stubs horizontally with rake faces on top. An alumina ball was used as the counterface. The friction coefficient curves all start with a rapid increase to 0.6 followed by a sharp decrease to 0.5. Subsequently, the coatings with reservoirs show a further decrease to less than 0.5 and keep this value until 500 cycles. The TiN coating with 5 μm microreservoirs filled with indium kept this lower friction coefficient for more than 1000 cycles. Optical micrographs of the wear tracks are given in Figure 5.4. In the case of coating with reservoirs, in the pictures we can see that reservoirs can be used to store the indium; as many small particles spread on the wear track and some indium are in the reservoirs. These results demonstrate the potential for microreservoir-structured coatings to help reduce friction and extend wear life. Similar improvements in tribological properties were found in studies with TiN/graphite coatings [12].

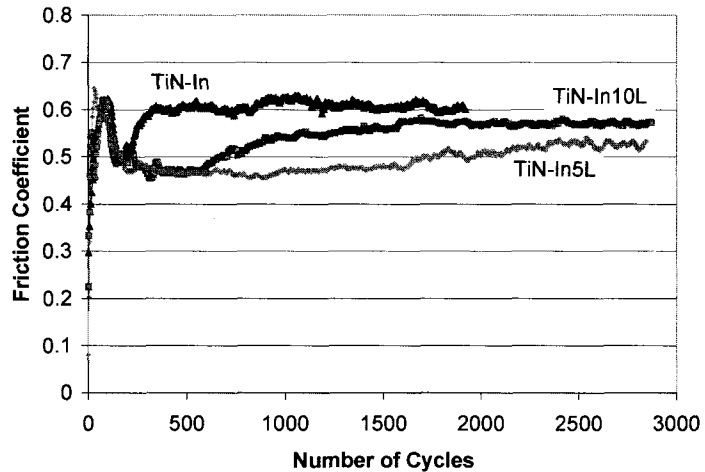


Figure 5.3. Friction coefficient graphs during pin-on-disk tests for the TiN coating without reservoirs; TiN coating with 5 μm reservoirs and TiN coating with 10 μm reservoirs.

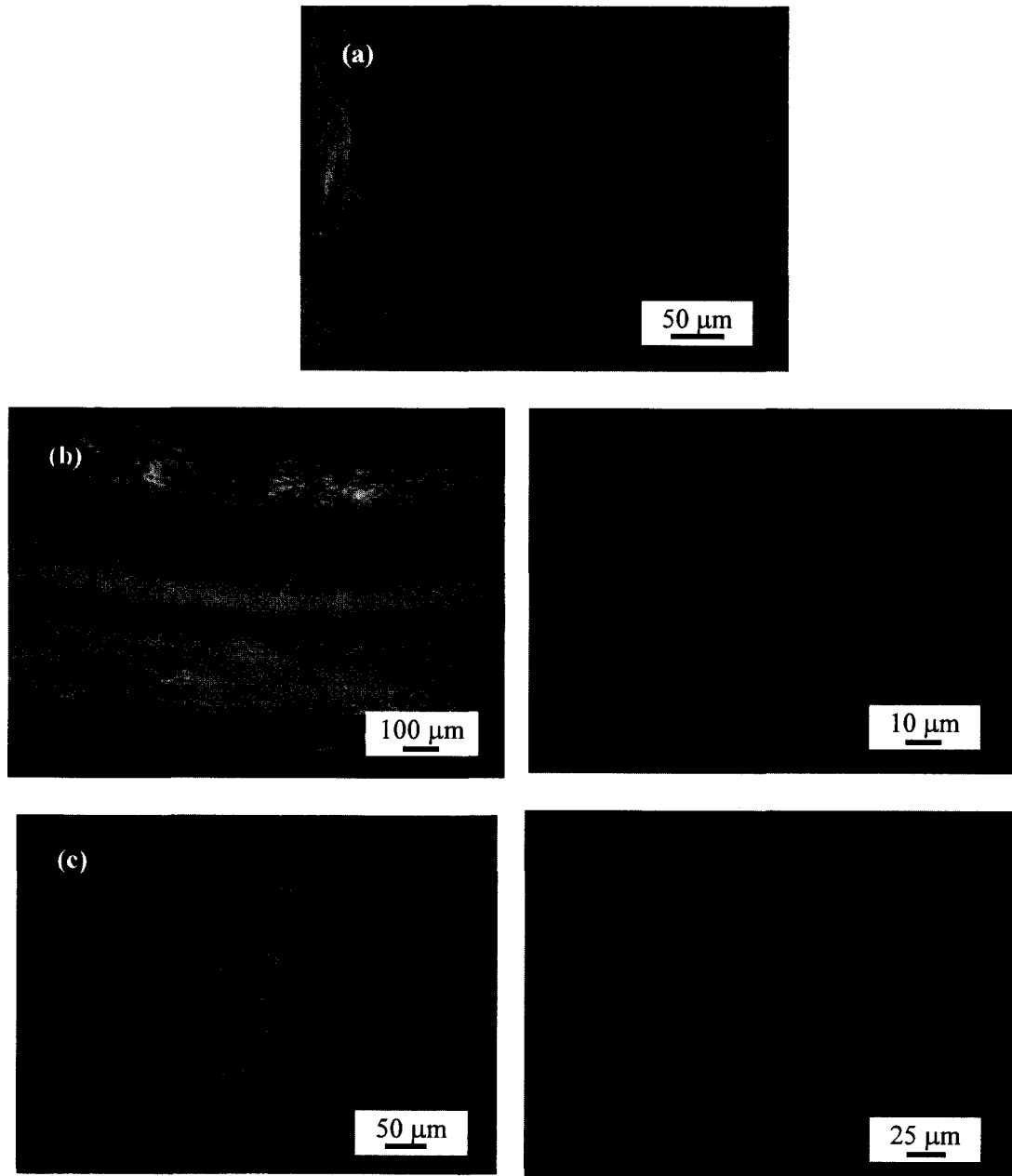


Figure 5.4. Optical micrographs of the wear tracks on indium coated inserts (a) with no reservoirs, (b) with 5 μm reservoirs and (c) with 10 μm reservoirs.

V.2.2. Turning Tests

The flank wear data, measured intermittently during the turning tests, on the tool inserts coated by TiN with or without the indium are shown in Figure 5.5. These tests were conducted in the presence of cutting fluids. The plain TiN coating had the shortest

wear life among the coatings tested; the longest wear life was observed for the TiN-In (no reservoirs) and as well as TiN-In-5H. Wear lives of these coatings are more than 4 times longer than TiN alone. Except TiN-In10H, other coatings with embedded indium had 4 times longer wear lives than TiN.

In general, these results demonstrate the beneficial effects of the In topcoat, with or without the microreservoirs. Because the flank face was not specifically patterned with microreservoirs, it is not surprising that the flank wear is not dependent on their presence. However, even though the sputter deposition process is primarily line-of-sight, i.e. the coating deposits mainly on surfaces facing to material source (rake surface), some In will deposit on the flank faces, with the effect of reducing flank wear compared to the sample coated with TiN only (See Figure 5.1).

The performance of following coatings were also investigated under dry machining conditions: the insert sample with *TiN*, which gave the shortest wear life in wet machining, the sample with the *TiN coating(no reservoirs)* and the insert specimen with *TiN-In5L*. The flank wear results of these experiments are presented in Figure 5.6.

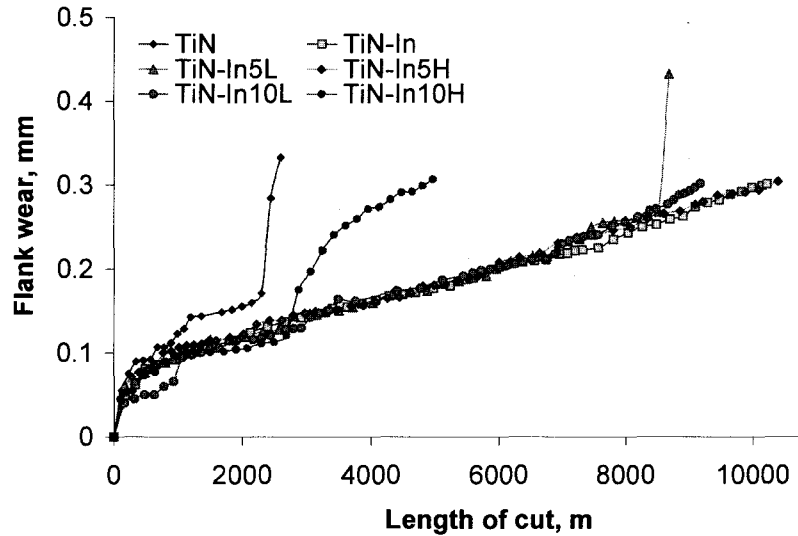


Figure 5.5. The progress of the wear during machining tests performed in the presence of cutting fluids on various coatings: TiN coating without any embedded lubricants (TiN), indium film on TiN coating without any reservoirs (TiN-In) and TiN coatings with lower or higher density of the 5 or 10 μm -sized-reservoirs and embedded lubricants in them (TiN-In5L, TiN-In5H or TiN-In10L and TiN-In10H).

The TiN-In5L sample has shown about 15% longer wear life compared to the plain TiN coating. Using criteria of 0.1 mm of flank wear, the TiN-In5H sample reached this point after about 5000 m length of cut. However, both the TiN and TiN-In samples reached this threshold after less than 2000 m length of cut. In addition, the insert with the plain TiN coating showed extensive chipping due to excessive cratering after the experiment, while the insert of TiN-In5H was in a far better condition. Micrographs taken after 1600 meters length of cut, of the cutting nose for the insert of TiN-In5L and the insert with TiN are shown in Figure 5.7. The pictured regions were cleaned by ion etching to reveal the extent of the wear. TiN insert showed more cratering and also regional flaking through the path of the chip flow.

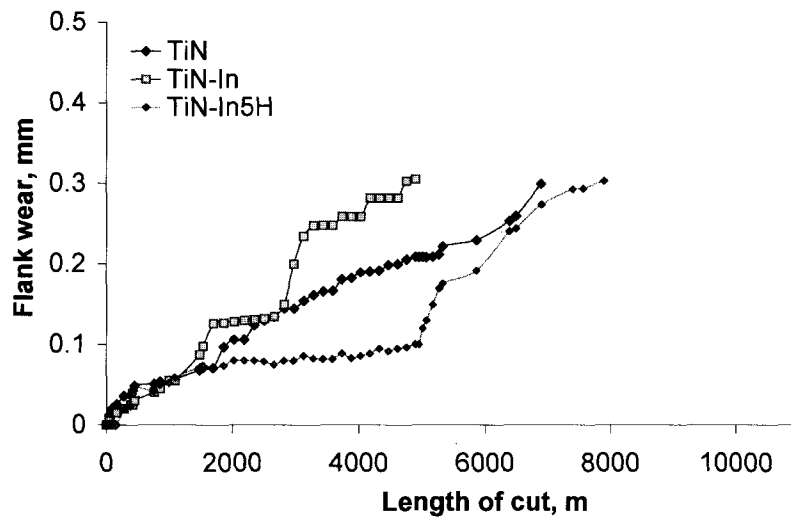


Figure 5.6. Flank wear results of dry machining experiments performed on three samples: tool insert with just TiN coating (TiN), tool insert with indium on TiN without any reservoirs (TiN-In) and tool insert with indium on TiN with high density of 5 μm reservoirs (TiN-In5H).

Because of the intimate contact between chip and the tool faces, one can analyze the interaction between these two by evaluating the morphology of the chips formed during the cutting operation. The morphology of the collected chips from the early stages of the wet machining experiment is shown in Figure 5.8. The SEM pictures of the chips from the wet turning operations reveal that there is a smoother interaction between the chip and tool with the coating of TiN-In5L compared to that of the only TiN coated tool. Generally, a smoother surface indicates a less wear and damage to the cutting edge of the tool.

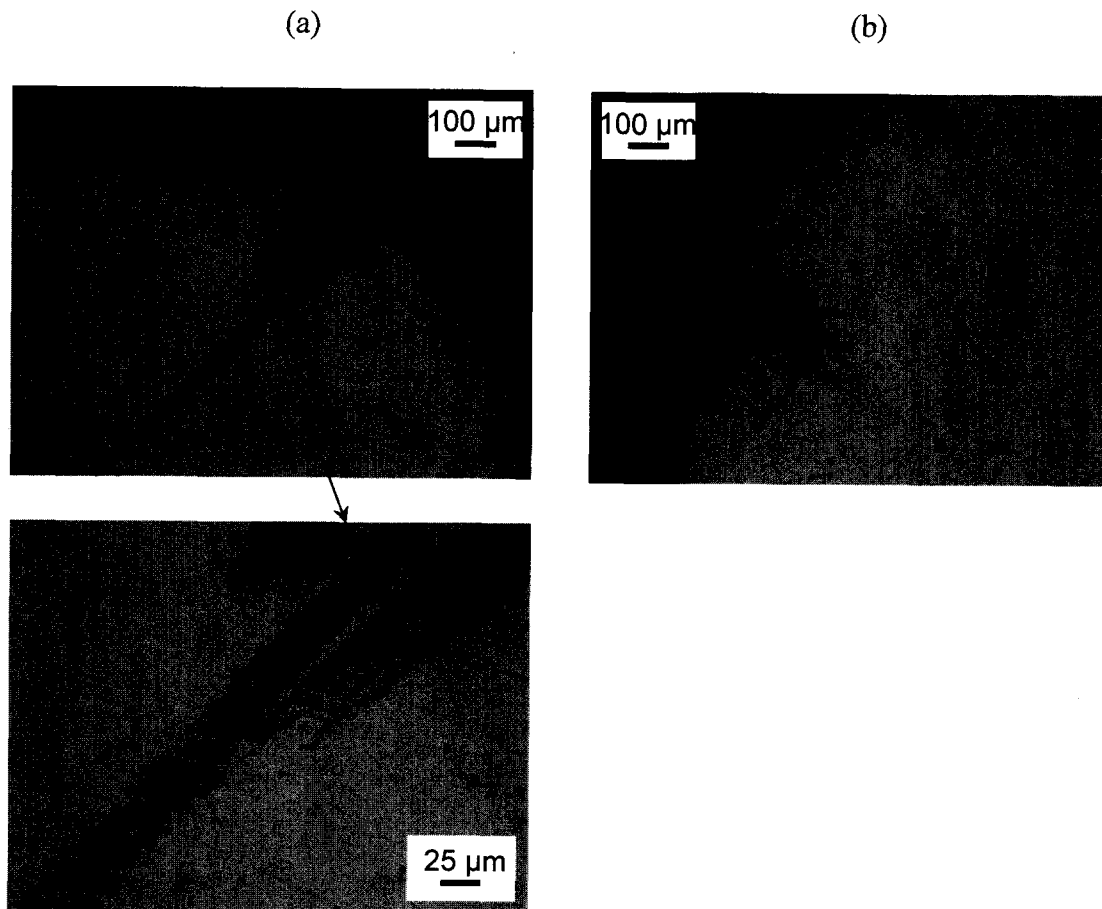


Figure 5.7. Rake surface appearance of the turning inserts after machining experiments: (a) Only TiN coated insert, (b) Insert with indium on TiN with 5 μm reservoirs.

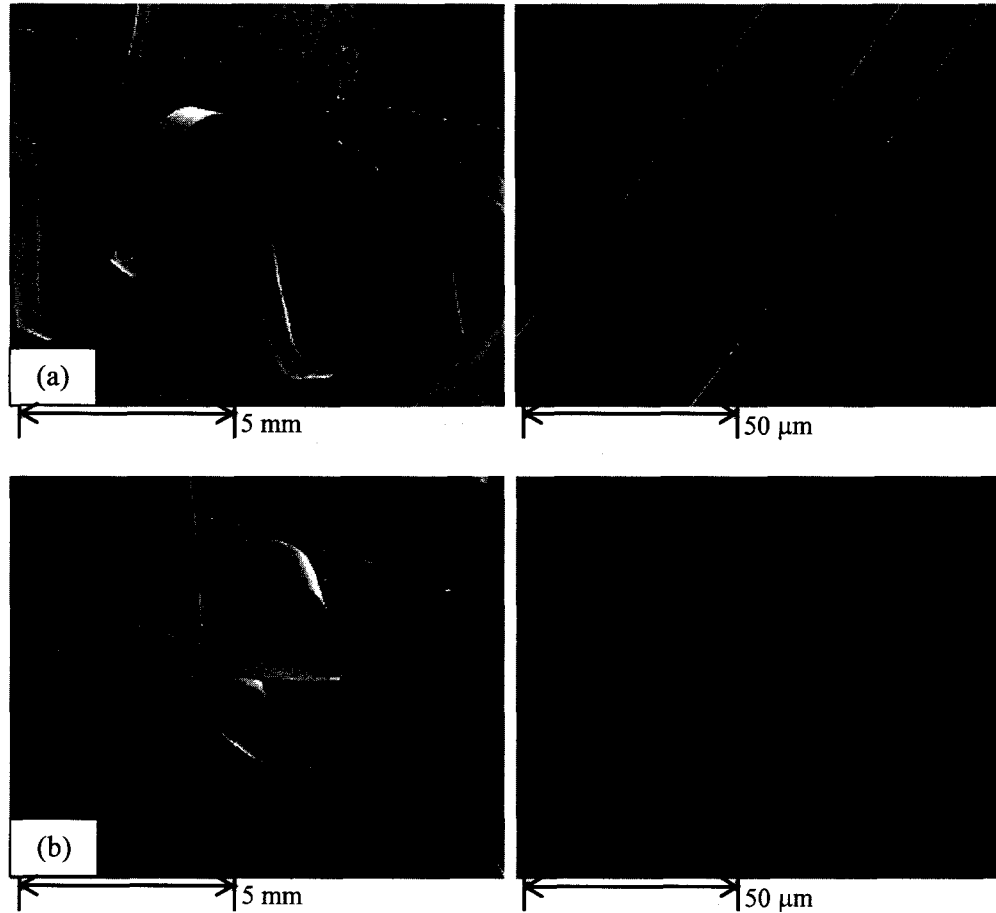


Figure 5.8. SEM micrographs of the collected chips for (a) the tool with plain TiN coating and (b) for the tool with indium layer on TiN with 5 μm reservoirs.

V.2.3. Tribological Simulation of the Machining Operation

The purpose of these experiments (the details of these experiments are explained in Chapter 2) was to simulate adhesive interaction between chip and the coated tool during machining operation. This test gives τ_{nm}/P_m values, defined as *coefficient of friction* for the interaction of workpiece-coating. Two sets of pins were coated for this experiment, one with TiN only, and the second with TiN/5μm holes/In. The spray method was used to create the microreservoirs in the latter sample, but the hole density could not be determined because the hemispherical shape of the surface provided limited

optical microscope imaging capabilities. The results are plotted in Figure 5.9 as τ_{nm}/P_{rn} versus each test temperature. For the temperatures lower than 600°C, the coefficient of friction for plain TiN coating are higher than the values for the TiN-In5; after 600°C, the coefficient of friction is lower for the TiN coating. These results can explain the performance of the plain TiN vs. TiN-In5 under dry and wet machining conditions. In wet cutting, temperatures are lower than dry cutting, and In can reduce friction and extend wear life. However, for the dry cutting, higher temperatures are present, where the plain TiN coating becomes advantageous in terms of friction coefficients. It is proposed that this effect is due to oxidation of the In, resulting in the loss of its low-friction capabilities.

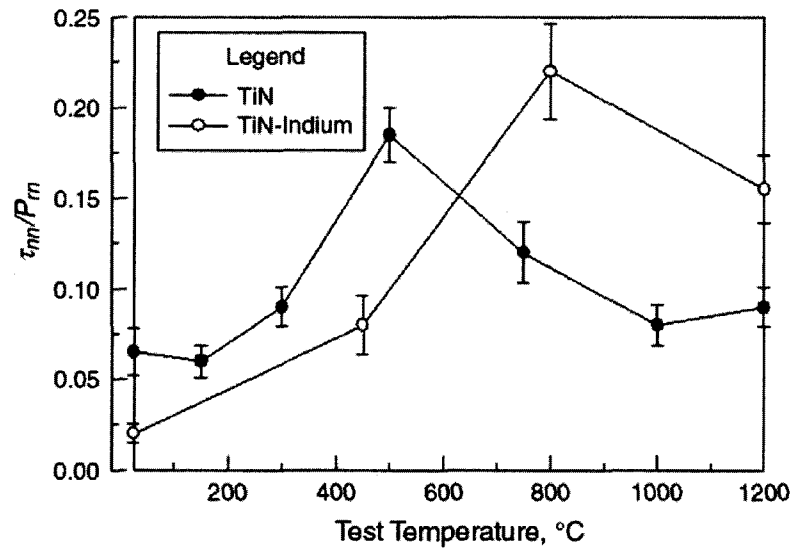


Figure 5.9. Friction coefficient values obtained from the tests conducted at various temperatures for Pin sample coated with indium film on top of TiN with 5 μm reservoirs, and for Plain TiN coated pin sample [45].

V.2.4. XPS Analyses on Tool Inserts

An insert sample with indium on TiN with 5 μm reservoirs that had been tested under dry turning conditions for 1600 m was also analyzed by XPS (X-ray Photoelectron Spectroscopy) after the tests. The point of 1600 m is in the first quarter of dry cutting

tests and there is substantial amount of wear corresponding to this point of tests. Analyses were performed on the rake surface of the tool inserts approximately 0.6 mm from the edge. In Figure 5.10, sample outputs of the analyses are presented: (a) after 4 min. etching and (b) after 14 min. of ion etching on the rake surface. Both graphs show that there is iron transfer from workpiece to the tool surface. After 4 min. etching, indium can be traced, after 14 min. it is not traceable anymore, instead, there is substantial amount of titanium and nitrogen originated from TiN coating. Both the amount of carbon and oxygen atoms decreased after 14 min. etching; carbon amount was decreased more.

The depth profile of each element traced near the cutting tool tip is given in Figure 5.11. On the very surface of the tool tip, there is mostly a high amount of carbon because of the contamination. More interestingly, the highest amount of indium, 7% was detected on the surface. This shows that the indium was traceable after first quarter of cutting operation. Because In was detected after some machining, one can say that In contributed to the tribological interactions at least for the first quarter of the machining operation. As etching continued, the concentration of indium decreased and could not be detected after 9 min. etching. After this depth Ti and N started to be detectable and their quantity increased substantially after 24 min. etching, where other elements had their lowest amounts. Iron transfer to the tool surface was detected as iron content was recorded on the surface and near surface regions. The amount of iron is comparable to indium at the surface, but into the surface the iron content increases substantially, becoming 50% after an etching time of 9 min; further etching revealed that this trend is decreasing after 9 min.

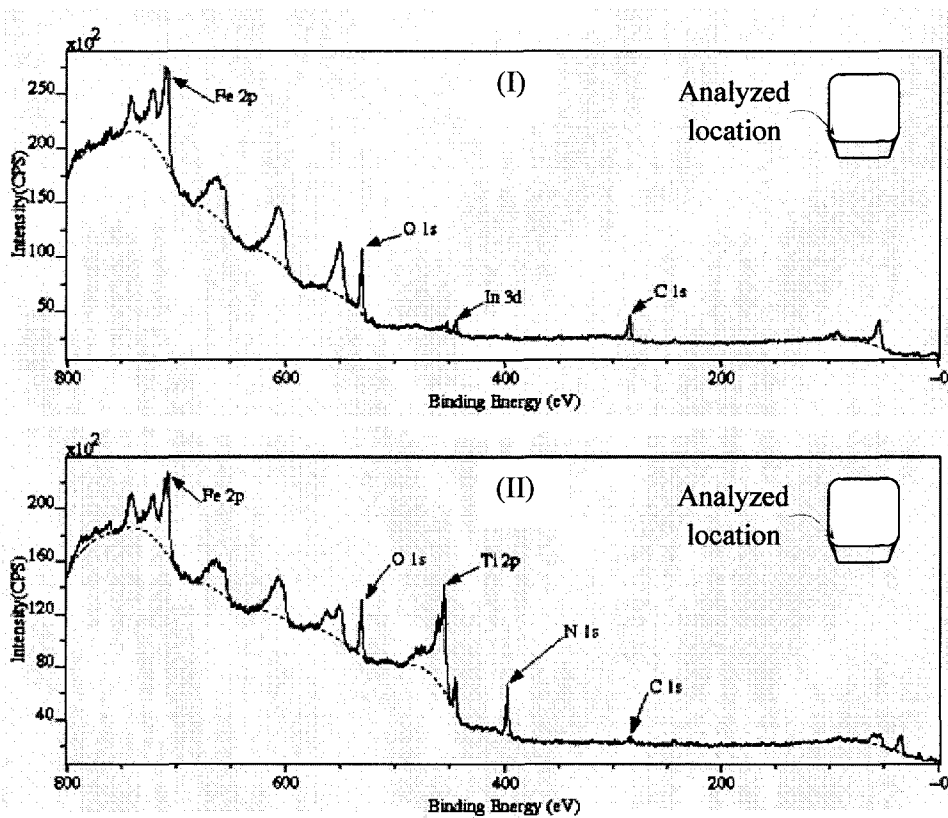


Figure 5.10. XPS outputs from a region near cutting edge of tool insert that were tested in dry machining: (I) is after 4 min. etching, (II) is after 14 min. etching.

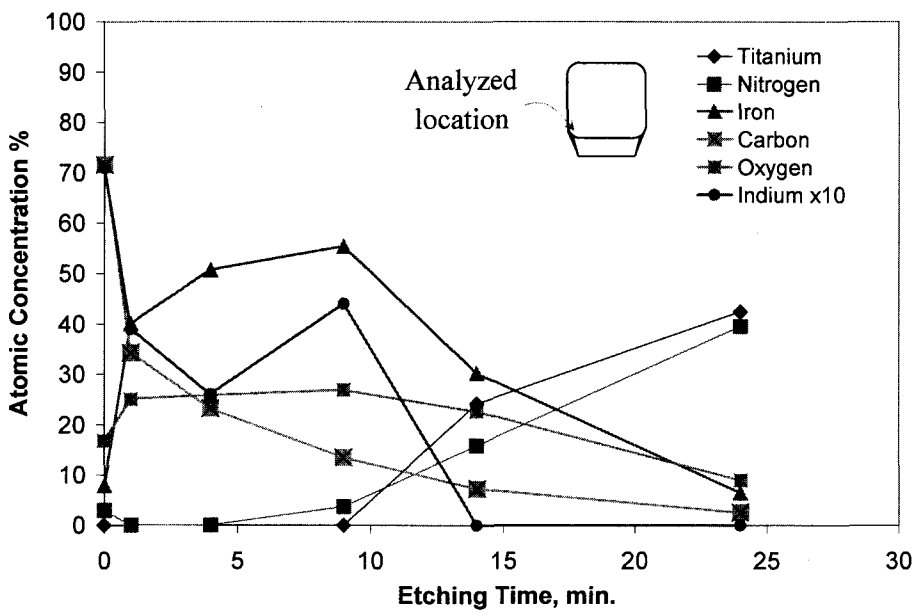


Figure 5.11. Atomic concentration changes through depth of surface layers of dry machined insert coated by indium layer on TiN with 5 μm reservoirs.

According to Trent [46] there is intensive interaction between tool and workpiece during cutting, which results in formation of seizure zone. This leads to very unfavorable frictional conditions and very intensive wear rate that is typical for cutting. These frictional conditions are typical first of all for continuous cutting conditions, i.e. turning operations. A way to improve frictional conditions is to use lubricant that can sustain heavy load/temperature conditions under operation. In this part of the study, we have examined the use of indium as a lubricant, as well as the effects of microreservoirs within the TiN coating. Micro-reservoirs that are filled with indium can supply solid lubricant to the frictional surface and in this way isolate (fully or partially) the workpiece and tool surface. The results presented here for wet machining demonstrate an increased tool life in samples incorporating indium. However, we did not observe a substantial difference in flank wear between the samples with microreservoirs vs. those without. This can be attributed to the fact that the flank face was not fabricated with microreservoirs, only the rake face. For dry machining, the microreservoir-coated sample did show some initial reduction in flank wear, but overall the flank wear rates for dry machining were greater than wet machining. The damage to the rake face was reduced for samples incorporating the microreservoirs (Figure 5.7), indicating they can be beneficial in this manner. The presence of In, detected on the rake surface of sample TiNIn-5H in the XPS experiments, is also of note since the absence of the microreservoirs may impact the ability of In to remain on the surface during cutting. A more detailed examination of In-coated samples both with and without microreservoirs will be necessary to reach a final conclusion. However, even with effective operation of the microreservoirs, the primary limitation of indium is its thermal stability and likely transformation to In oxide. As can be seen from

CoF vs. temperature curves (Figure 5.9) at the temperature above 600°C, In-based tribo-films lose their stability and efficiency of the lubricant is strongly diminishing. It is obvious that this is a result of using indium as lubricant. Indium is not appropriate to high dry cutting temperatures.

V.3. Conclusion

1. In this part of research, microbeading method, was implemented on only rake face of turning tool inserts. Indium was used as the solid lubricant. TiN-In coated inserts were tested by measuring flank wear in wet machining, and showed up to 4 times longer wear life than a TiN coating without indium. Examination of chips taken during cutting showed a smoother surface, indicating lower wear at the cutting edge.
2. TiN, TiN with In and TiN with In and 5 μm microreservoirs were tested in dry machining, and the coating with the 5 μm microreservoirs exhibited the least wear for most of the test period. However, wear performance was still inferior when compared with wet machining. This behavior was explained by measuring coefficient of friction under simulation tests. Below 600°C, coatings incorporating In had a lower coefficient of friction, but at higher temperatures, the TiN coating had the lower CoF.
3. The tool tested run under dry machining conditions for a 1600 m cutting distance was further investigated after the test with XPS. The presence of the indium near the tool tip, where the chip flows on the rake face, was confirmed, indicating that indium may be a useful solid lubricant under certain limited conditions.

CHAPTER VI

CONCLUSIONS

In this research a new method to fabricate composite coatings incorporating micro-reservoirs has been developed, and experiments have been carried out to gain an improved understanding of how these coatings function. These micro-reservoirs can provide storage for solid lubricants and to replenish them during surface interaction and wear. To fabricate these coatings, ceramic/glass beads were used as placeholders during coating deposition and then subsequently removed. The success of the micro-reservoir function depending on size, distribution and area coverage. Agglomeration of beads was an important fabrication issue, because it affects reservoir size and distribution (by increasing inter-hole distance and areas without reservoirs). While agglomeration cause some initial coatings to perform poorly, this issue was overcome by improvements in the spray technique.

In the absence of a solid lubricant, the incorporation of micro-holes in the coatings resulted in rapid failure during pin-on-disc tests. When graphite was applied, the lowest friction coefficients (below 0.1) were obtained with 10 μm -sized-holes (over the tested range of 1.5 to 10 μm). To further understand coating behavior, plane strain finite elements models of coatings with 2, 5 and 10 μm -sized-holes were prepared. Coatings with the 10 μm -sized-holes had lowest stresses and calculated work done at the critical

location of a hole profile during surface interaction with a pin, which would reduce the probability of failure.

Hard incorporating micro-reservoirs and an indium topcoat as a solid lubricant were deposited on the rake face of tool inserts. During machining with cutting fluids, the flank wear was measured up to four times greater tool life was obtained for most of the tools with micro-reservoirs and the In topcoat. However, the coating with In topcoat and no microreservoirs also performed in a similar manner. In dry machining, TiN with 5 μm reservoirs and an In topcoat had slightly less flank wear for most of the test compared to TiN alone and TiN+In, however, overall, the composite coating with micro-reservoirs and an indium topcoat did not show an outstanding performance. This is attributed to instability of In above 600°C under adhesive wear conditions that was believed to control surface interactions between the tool and the workpiece. XPS analysis performed near the cutting tip of a sample tested under dry machining conditions for 1600 m indicated that there was indium still present on the surface. These results suggest that indium may only be useful for limited temperature applications during dry cutting.

To further understand the behavior of micro-reservoirs in hard coatings, homogeneously distributed micro-holes were fabricated on silicon substrates using photolithography. Samples with 9 μm holes spaced 25 μm apart (9-25 sample) demonstrated fastest transition to lower friction values (against and alumina pin) compared to samples with 4 μm holes/25 μm spacing (4-25 sample) or 4 μm holes/11 μm spacing (4-11). The microreservoirs in the 9-25 samples helped provide stable FCs for longer periods of time on the tests carried out with a 200 rpm speed and 1 N load. The 4-11 samples have the same area coverage with 9-25 samples, but they showed more scatter in friction

coefficients. Besides having highest scatter values in FCs, the 4-25 samples could not reach 2000 cycles without wearing through. This indicates that both reservoir size and area coverage of the 4-25 samples were not sufficient to provide a stable transfer layer and prevent excessive wear. Optical microscope evaluations revealed that 9 μm -sized-holes showed the best lubrication provided from the microreservoirs. When a steel counterfaces was used, which increases the interaction area of pin on the substrate, the effect of size and area coverage became more prominent. The 4-25 samples wore through quickly but micrographs of 9-25 samples showed a good spread of lubricant from reservoirs. When graphite lubrication was used, larger (9-10 μm) reservoir sizes functioned better in samples made using both the microbeading method and the photolithography method. Possible reasons include a better lubricant capturing capacity of the larger reservoirs, a higher lubricant storing capacity of the larger reservoirs, and the ease of reaching lubricant in reservoirs.

This work has shown that there can be a benefit to incorporating microreservoirs within hard coatings, as long as they have a sufficient size (9-10 μm -sized-holes are suggested here) and surface density. Used in conjunction with a solid lubricant, these coatings can result in decreased friction and extended wear lives. Lubricant choice is important, particularly for high-temperature applications, such as cutting tool inserts.

CHAPTER VII

FUTURE WORK

1. Microbeading method can be further improved and modified to control agglomeration and increase area coverage values.
2. Other soft metals such as silver could be future candidates for a better lubrication for both tool inserts and other coating applications. Silver is also frictionally compatible with iron. Therefore it can be a good choice for machining applications.
3. Microbeading method can be applied on other manufacturing tools with wide, flat surfaces such as mold components working under high friction and wear conditions. Surface interaction of composite coatings fabricated by microbeading with wide, flat surfaces may increase effect of replenishment from reservoirs.
4. Further investigations can be made on silicon samples patterned by photolithography on wider wear tracks provided by steel counterfaces.
5. Reservoirs bigger than 10 μm can be fabricated in coatings using photolithography. And there may be benefits of further increasing size of reservoirs.
6. Most of the coatings deposited by magnetron sputtering process have high amounts of residual stresses. Because a micro-reservoirs is a discontinuity in a coating structure, it may decrease residual stresses. The effect of micro-reservoirs on residual stresses can be investigated.

REFERENCES

1. E. Rabinowicz, *Friction and Wear of Materials*, Second Edition, John Wiley and Sons, Inc., 1995, p.5-8.
2. K. Holmberg, A. Matthews, *Coatings Tribology: Properties, Techniques and Applications in Surface Engineering*, Elsevier, 1998, p.1.
3. B. Bhushan, *Introduction to Tribology*, John Wiley & Sons, Inc., 2002, p.4.
4. J.A. Williams, *Engineering Tribology*, Oxford University Press, 1994, p.1-2.
5. K. Miyoshi, *Solid Lubrication Fundamentals and Applications*, Marcel and Dekker, Inc., 2001, p.4-6.
6. D.R. Askeland, *The Science and Engineering of Materials*, 3rd Edition, PWS Publishing Company, 1994, p.721.
7. A.A. Voevodin, J. Bultman, J.S. Zabinski, "Investigation into three-dimensional laser processing of tribological coatings", *Surface and Coatings Technology* 107 (1998) 12.
8. C. Donnet, A. Erdemir, "Historical developments and new trends in tribological and solid lubricant coatings", *Surface and Coatings Technology* 180-181 (2004) 76.
9. Jehn, H.A., "Multicomponent and multiphase hard coatings for tribological applications", *Surface and Coatings Technology* 131 (2000) 433.
10. A. Savan, E. Pflüger, R. Goller, W. Gissler, "Use of nanoscaled multilayer and compound films to realize a soft lubrication phase within a hard, wear-resistant matrix", *Surface Coatings and Technology* 126 (2000) 159.

11. J.E. Krzanowski, J.H. Zimmerman, "Fabrication and Tribological Properties of Hard Coatings with Embedded Solid Lubricant Phases" *Proceedings of the STLE/ASME Joint Tribology Conference*, October 22-25, Society of Tribologists and Lubrication Engineers, Saint Antonio, TX, 2006.
12. J.H. Zimmerman, C.G. Guleryuz, J.E. Krzanowski, "Fabrication and tribological properties of titanium nitride coatings incorporating solid lubricant microreservoirs", *Surface and Coatings Technology* 202 (2008) 2023.
13. J.E. Krzanowski, D.Nunna, "Tribological Properties of MoS₂ Films Containing Ti and Carbon" titled presentation given in *Materials Research Society Fall 2002 Conference*, Session Y9.3.
14. J.L. Endrino, J.J. Nainaparampil, J.E. Krzanowski, "Magnetron sputter deposition of WC-Ag and TiC-Ag coatings and their frictional properties in vacuum environments", *Scripta Materialia* 47 (2002) 613.
15. J.L. Endrino, J.J. Nainaparampil, J.E. Krzanowski, "Microstructure and vacuum tribology of TiC-Ag composite coatings deposited by magnetron sputtering-pulsed laser deposition" *Surface Coating and Technology* 157 (2002) 95.
16. C.P. Mulligan, T.A. Blanchet, D. Gall, "CrN-Ag nanocomposite coatings: Effect of growth temperature on the microstructure", *Surface and Coatings Technology*, Article in Press (2008).
17. Voevodin, Zabinski, "Laser surface texturing for adaptive solid lubrication" *Wear*, 261 (2006) 1285-1292.
18. L. Rapoport, A. Moshkovich, V. Perfilyev, I. Lapsker, G. Halperin, Y. Itovich, I. Etsion, "Friction and wear of MoS₂ films on laser textured steel surfaces" *Surface Coatings and Technology* 202 (2008) 3332.
19. P. Basnyat, B. Luster, C. Murattore, A.A. Voevodin, R. Haasch, R. Zakeri, P. Kohli, S.M. Aouadi, "Surface texturing for adaptive solid lubrication" *Surface Coating and Technology* 203 (2008) 73.

20. J.E. Krzanowski, J.L. Endrino, K. Hirschman, "Novel Composite Coatings With 3D Coating Architectures for Tribological Applications Fabricated Using Semiconductor Patterning Processes", *Materials Research Society Fall 2002 Conference Proceedings*, Vol.750, 2002, p.273.
21. B.C. Schramm, H. Scheerer, H. Hoche, E. Broszeit, E. Abele, C. Berger, "Tribological properties and dry machining characteristics of PVD-coated carbide inserts", *Surface and Coatings Technology* 188-189 (2004) 623.
22. V. Derflinger, H. Brandle, H. Zimmermann, "New hard/lubricant coating for dry machining", *Surface and Coatings Technology* 113 (1999) 286.
23. H.L. Coldwell, R.C. Dewes, D.K. Aspinwall, N.M. Renevier, D.G. Teer, "The use of soft/lubricating coatings when dry drilling BS L168 aluminium alloy", *Surface and Coatings Technology* 177-178 (2004) 716.
24. G.S. Fox-Rabinovich, N.A. Bushe, A.I. Kovalev, S.N. Korshunov, L.Sh.Shuster, G.K. Dosbaeva, "Impact of ion modification of HSS surfaces on the wear resistance of cutting tools with surface engineered coatings", *Wear* 249 (2001) 1051-1058.
25. K.Holmberg, A.Matthews, *Coatings Tribology, Properties, Mechanisms, Techniques and Applications in Surface Engineering*, Elsevier B.V., 2009, p.197.
26. I.M. Hutchings, *Tribology Friction and Wear of Engineering Materials*, p.205-208.
27. E. Rabinowicz, in: M.P. Peterson, W.Q. Winner (Eds.), *Wear Control Handbook*, ASME, New York, 1980, p. 475.
28. John H. Zimmerman, "Fabrication and tribological properties of hard thin films with solid lubricant microreservoirs", Master of Science Thesis, University of New Hampshire, 2006.
29. E. Rabinowicz, *Friction and Wear of Materials*, Second Edition, John Wiley and Sons, Inc., 1995, p.90-91.

30. B. Bhushan, *Introduction to Tribology*, John Wiley & Sons, Inc., 2002, p.267-274.
31. E.R. Booser, Editor, *Handbook of Lubrication, Vol II: Theory and Practice of Tribology*, 2000, CRC Press, Inc., sponsored by ASLE, p.269-272.
32. X.E. Gros (editor), *Applications of NDT (Non-Destructive Testing) Data Fusion*, Kluwer Academic Publishers, 2001, p.62.
33. S. Bahadur, J.H. Magee (editors), *Wear Processes in Manufacturing*, ASTM, 1998, p.60.
34. G.S. Fox-Rabinovich, G.E. Totten (editors), *Self-Organization During Friction*, CRC Press Taylor and Francis Group, 2007, p. 127-129.
35. G.S. Fox-Rabinovich, A.I. Kovalev, L.Sh. Shuster, Yu.F. Boki, G.K. Dosbayeva, D.L. Wainstein, V.P. Mishina, "Characteristic features of alloying HSS-based deformed compound powder materials with consideration for tool self organization at cutting. 1. Characteristic features of wear in HSS-based deformed compound materials in cutting", *Wear* 206 (1997) 214-220.
36. G.D. Parfitt, *Dispersion of Powders in Liquids*, 2nd Edition, Halsted Press (John Wiley & Sons), p.2-3 & 13-15.
37. Robert L. Fusaro, "Effect of Substrate Finish on the Lubrication and Failure Mechanisms of Molybdenum Disulfide Films", *ASLE Transactions*, Vol.25, Issue 2, 141-156.
38. E.W. Roberts, B.J. Williams, J.A. Ogilvy, *J.Phys., D, Appl. Phys.* 25 (1992) A65.
39. *ASM Metals Handbook*, 9th Edition, Vol.3, page 12.
40. K. Holmberg, A. Laukkanen, H. Ronkainen, K. Wallin, S. Varjus, J. Koskinen, "Tribological contact analysis of a rigid ball sliding on a hard coated surface Part I: Modelling stresses and strains", *Surface and Coating Technology* 200 (2006) 3793-3809.

41. I.M. Hutchings, *Tribology Friction and Wear of Engineering Materials*, p.49.
42. <http://www.microchem.com/products/pdf/PMGI-Resists-data-sheetV-rhcedit-102206.pdf>
43. <http://www.microchem.com/>
44. <http://www.microchem.com/products/pdf/removerpg.pdf>
45. C.G. Guleryuz, J.E. Krzanowski, Stephen C. Veldhuis, German S. Fox-Rabinovich, "Machining performance of TiN coatings incorporating indium as a solid lubricant", *Surface Coatings and Technology*, 203 (2009) 3370-3376.
46. Trent, E.M., Wright, P.K. *Metal Cutting*, 4th ed. Butterworth-Heinemann: Woburn, MA, 2000.